Master of Science Thesis

Flow Mock-Up

Feasibility and Method Analysis of the Flow Field Reproduction of an Open Cabriolet Vehicle in order to Subjectively Assess Draught Phenomena

Benjamin C. Gabriëlse

February 27, 2017

Porsche Engineering
driving technologies

Aerodynamics

TU Delft

Faculty of Aerospace Engineering

Delft University of Technology

Flow Mock-Up

Feasibility and Method Analysis of the Flow Field Reproduction of an Open Cabriolet Vehicle in order to Subjectively Assess Draught Phenomena

Master of Science Thesis

by

Benjamin C. Gabriëlse

for obtaining the degree of Master of Science in Aerospace Engineering
at the Delft University of Technology,
to be defended on Tuesday August 30, 2016 at 10:00 AM.

February 27, 2017

This thesis is confidential and cannot be made public until December 31, 2021.

Porsche Engineering Services GmbH
and
Faculty of Aerospace Engineering · Delft University of Technology

Confidential Clause

This master thesis is based on internal, confidential data and information. All rights to the master thesis including the distribution on electronic media are owned by Porsche Engineering Services GmbH.

Deviating from this, the content of the thesis can be passed during a locking period of 5 years from the date of submission with the explicit written consent of Porsche Engineering Services GmbH to third parties.

Once the locking period has passed the consent is no longer required.

PORSCHE

Delft University of Technology

Delft University of Technology
Department of Aerodynamics

The undersigned hereby certify that they have read and recommend to the Faculty of Aerospace Engineering for acceptance the thesis entitled **"Flow Mock-Up"** by **Benjamin C. Gabriëlse** in fulfillment of the requirements for the degree of **Master of Science**.

Dated: February 27, 2017

Prof.dr. S. Hickel

Dr.ir. M.I. Gerritsma

Dr.ir. M. Voskuijl

Dr.ir. G.M.R. van Raemdonck

Preface

During my studies of Aerospace Engineering I developed the interest in the aerodynamics of vehicles, which is why I have chosen to complete an internship at the Aerodynamics and Thermodynamics department of Porsche Engineering Services GmbH. This confirmed my interest even more and thus I realized to follow up my internship with this thesis. This thesis is the result of an intensive 9 months of hard work and it concludes my Master of Science Degree in Aerospace Engineering.

The topic of my thesis was a very challenging and interesting topic, which was the reason that I accepted this assignment. I had to structure the high amount of literature that I needed to conduct my research which was very challenging. Overall the assignment was a very broad interpretable topic, where I had room to determine the path. This was not always very easy as there were no real expectations of the results, which had to be achieved.

I like to thank the Porsche Engineering Services GmbH, especially Björn Pehnert and Marcel Straub, for believing in me and giving me this opportunity. I learned a lot from them as they have two different point of views. We have had some long and intensive discussions which were very instructive and which will surely help me in my future career. Furthermore, I like to thank Marc Gerritsma for his supervision and feedback given. I always gained a lot of energy from our discussions, which encouraged me to go on. Last but not least I like to thank all the people that supported me during the final phase of my studies.

Abstract

In the automotive industry the development process is driven by a highly competitive market, calling for shorter and more cost-efficient development procedures. Computer aided engineering (CAE) is one possibility to achieve these reductions and becomes an inevitable tool in the development process. However, CAE does not provide the subjective evaluation, which still have to be conducted. In the development of the thermal comfort of open cabriolets, the subjective evaluation is dependent on expensive experimental methods and can only be conducted in a late phase of the development process, at which freedom of decision is low. Especially the thermal comfort in open cabriolets is very challenging as the passengers are surrounded by a turbulent flow field, exposing the passengers to velocities up to 40% of the driving speed.

This leaves room for optimization, which is why the idea of a flow mock-up is investigated. The procedure of a flow mock-up is a combination of digital development and physical simulation. A flow mock-up should simulate the flow field inside a passenger compartment of an open cabriolet from the results obtained from CFD simulations.

The research objective is to concretise the idea of a flow mock-up by identifying the requirements a flow mock-up has to fulfil in order to be advantageous for the development process as well as to be able to replicate the flow field of an open cabriolet. This is done by analysing the actual development process and proposing a modified development process, which includes the use of a flow mock-up. Furthermore, the characteristic factors, which influence the human perception while driving an open cabriolet, are identified from researches found in literature and analysis of measurement data. Finally, to investigate the technical practicability of a flow mock-up, a preliminary CFD investigation is conducted to investigate the possibility of replicating the flow field, which is present inside the passenger compartment of an open cabriolet. The flow field simulation should be replicated in a closed space and without the dependency on the vehicle geometry.

A modified development process has been proposed showing how the development process would look like when a flow mock-up is used. The subjective assessment of the thermal comfort in open cabriolets can be shifted forward in the development process by performing CFD simulations and simulating the flow field in the flow mock-up. The use of experimental testing in a windtunnel can be significantly reduced, leading to a more cost-efficient development. The results of thermal comfort evaluation in the flow mock-up can be used to influence the packaging of the base model with respect to thermal comfort in open cabriolet. Furthermore, the combination of digital development and flow mock-up increases flexibility as no physical components have to be produced. To realise the proposed modified development process, the flow mock-up is required to be independent of the vehicle's geometry, and the flow field should be controlled individually.

The second point of investigation was the identification of the characteristic factors, which influence the human perception while driving in an open cabriolet. These influence factors have been split into the human and the physical influence factors. The human factors include the factors, which influence how the human subjective perception is formed, while the physical influence factors identify the physical phenomena a human is exposed to, when driving in an open cabriolet. The human influence factors mainly require that the appearance of the flow mock-up should be very

similar to a real cabriolet. This is important for the psychological perception, because the subject should be able to associate the experience in the flow mock-up with that of an open cabriolet ride in order to evaluate the replicated thermal comfort similarly in the flow mock-up as the subject would in the real cabriolet.

The physical factors, which influence the perception of draught, are the velocity, pressure, temperature and air humidity. Especially the fluctuations of the velocity and the pressure characterize the perception of draught in an open cabriolet. Therefore, the flow mock-up is required to control these factors.

The CFD analysis is conducted with a simplified cabriolet model, with the configuration windows up and no wind-break. The aim is to replicate the flow field, which is obtained from a reference simulation with the simplified cabriolet model, in a constrained, reduced domain and without the dependency of the vehicle geometry. In the replicated flow field similar flow velocities at local body positions to the reference simulation have been obtained. However, a major difference has been identified, which is why optimizations are needed to improve the replication of the flow field.

In this thesis all the factors have been identified, which have to be considered when replicating the flow field inside the passenger compartment of an open cabriolet with the use of a flow mock-up. This research shows the theoretical possibility of a flow mock-up from which multiple further points of investigation have emerged. It serves as a basis for the detailed development of the flow mock-up.

Table of Contents

List of Figures

List of Tables

List of Symbols

Abbreviations

BFS	Backward Facing-Step
CAD	Computer Aided Design
CAE	Computer Aided Engineering
CFD	Computational Fluid Dynamics
DD	Design Decision
DES	Detached Eddy Simulation
DF	Design Freeze
DNS	Direct Numerical Simulations
FEA	Finite Elements Analysis
HIF	Human Influence Factors
HVAC	Heating, ventilation and air conditioning
LES	Large Eddy Simulation
MY	Model year
NS	Navier-Stokes
OS	Operating System
PackFreeze	Package Freeze
PD	Project Definition
PEP	Product evolution process
PIF	Physical Influence Factors
PM	Project Mission
PPD	Predicted Percentage Dissatisfied
RANS	Reynolds Averaged Navier Stokes
SOP	Start Of Production
WB	Wind-break

Greek Symbols

Symbol	Description	Units
ϵ	Rate of dissipation of turbulent kinetic energy	$[m^2 s^{-3}]$
μ	Dynamic viscosity	$[kgm^{-1}s^{-1}]$
ν	Kinematic viscosity	$[m^2 s^{-1}]$
ϕ_m	Model windscreen angle	$[deg]$
ρ_∞	Ambient air density	$[kgm^{-3}]$
τ_w	Wall shear stress	$[Pa]$

Latin Symbols

Symbol	Description	Units
$\overline{u_i' u_j'}$	Reynolds stress term	$[ms^{-2}]$
A	Cross-sectional area	$[m^2]$
a	Variable coefficient for curve fitting	$[-]$
b	Variable coefficient for curve fitting	$[-]$
c_f	Friction coefficient	$[-]$
C_p	Pressure coefficient	$[-]$
$C_{\pm 5\%}$	Confidence bound with $\pm 5\%$ PPD_l	$[-]$
d_m	Manikin head clearance	$[mm]$
h_m	Model height	$[mm]$
h_r	Model ride height	$[mm]$
k	Turbulent kinetic energy	$[m^2 s^{-2}]$
l_m	Model length	$[mm]$
n_p	Number of prism layers	$[-]$
p	Local pressure	$[Pa]$
p_s	Static pressure	$[Pa]$
p_t	Total pressure	$[Pa]$
p_∞	Ambient pressure	$[Pa]$
P_{infl}	Inflection point	$[-]$
PD_l	Local Percentage Dissatisfied	$[\%]$
$PPD_{l,lb}$	Local Predicted Percentage Dissatisfied at lower boundary	$[\%]$
$PPD_{l,ub}$	Local Predicted Percentage Dissatisfied at upper boundary	$[\%]$
PPD_l	Local Predicted Percentage Dissatisfied	$[\%]$
r_b	Rear edge radius	$[mm]$
r_f	Front edge radius	$[mm]$
Re	Reynolds number	$[-]$
Re_x	Reynolds number based on the characteristic length along a surface	$[-]$
s	Prism layer stretching coefficient	$[-]$
T	Temperature	$[K]$
t_{prism}	Prism layer thickness	$[mm]$
u_τ	Friction velocity	$[ms^{-1}]$
V	Air velocity	$[ms^{-1}]$
V_∞	Ambient air velocity	$[ms^{-1}]$
$V_{inboard}$	Velocity at the inboard position	$[ms^{-1}]$
V_{infl}	Velocity at inflection point	$[ms^{-1}]$
V_{lb}	Velocity at lower boundary	$[ms^{-1}]$
V_{max}	Maximum velocity	$[ms^{-1}]$
V_{min}	Minimum velocity	$[ms^{-1}]$
$V_{outboard}$	Velocity at the outboard position	$[ms^{-1}]$
V_{ub}	Velocity at upper boundary	$[ms^{-1}]$
w_m	Model width	$[mm]$

y^+	Dimensionless distance from the wall	$[-]$
y_1	Height of the first prism cell	$[mm]$
$y_{1/2}$	Half height of the first cell in the surface	$[m]$

Chapter 1

Introduction

The automotive industry is a highly competitive market, requiring the development process to become shorter while cost pressure is increased. One way to reduce these is by means of Computer Aided Design (CAD) and Computer Aided Engineering (CAE), which are becoming inevitable tools in the development process of automotive vehicles. 2D or 3D digital models are created with CAD programs and CAE software is used to perform the analysis of the vehicle properties. Among the CAE-methods are numerical simulations, which are used in the early development phase of a vehicle in almost every engineering department. Structural components are for example analysed using Finite Elements Analysis (FEA) while in the field of aerodynamics the flow around an object is simulated with the use of Computational Fluid Dynamics (CFD). These CAE-methods enable the possibility of identifying conflicts of objectives in the early development phase, in which changes can be made easily as the freedom of decisions is high and changes are related to lower costs than in a later phase when most decisions are taken, see Figure 1.1. Numerical simulations replace the need for detailed physical testing, therefore reducing the number of prototypes, leading to more cost-effective and shorter development cycles [1].

Most of the structural properties of the vehicle can be expressed in quantitative values, which can be processed by engineers, and therefore these can be simulated with CAE software [3]. However, properties related to the human perception are very difficult to express in quantitative values, because how a human feels is usually not expressed in numbers and the perception of humans depends on many individual properties. The subjective perception of the human has to be felt and experienced in order to be evaluated. Especially thermal comfort is one of the human perception properties in the development of an automotive vehicle which has to be evaluated through experimental testing. As the overall vehicle comfort is one of the most important decision criteria of purchasing a vehicle [4], thermal comfort has a high priority in the customer-oriented automotive development. Thermal comfort is defined as *"that condition of mind which expresses satisfaction with the thermal environment and is assessed by subjective evaluation"* [5]. The definition is very general and not straight forward, because thermal comfort not only depends on the given situation, i.e. the thermal environment, but thermal comfort also changes from person to person, i.e. the subjective evaluation. One of the main disturbances of thermal comfort is draught [6]. According to [5] draught is defined as *"an unwanted local cooling of the body caused by air movements"*. Thermal comfort and draught in the passenger compartment is the main topic of investigation of engineers in the field of heating, ventilation and air conditioning (HVAC) . In order to evaluate the thermal comfort of a

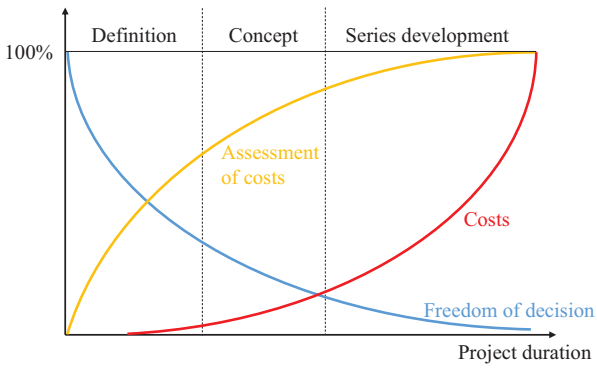

Figure 1.1: Variation of costs, assessment of costs and freedom of decision with the project duration [2]

new vehicle, analytical models to correlate the subjective evaluation with physical properties of the surrounding have been developed by conducting many experimental studies with predecessors and other vehicles [7]. The origin of analytic thermal comfort models date back to 1970 from Povl Ole Fanger, which is one of the most fundamental model [8], and has been mainly conducted for closed spaces, like buildings, especially office spaces. With these thermal comfort models the predicted percentage dissatisfied (PPD) can be determined, which expresses the percentage of people which are dissatisfied to the given thermal environment.

While these thermal comfort models are quite advanced for closed spaces, in which the environmental conditions are very moderate, such thermal comfort models are also desired for the evaluation of thermal comfort in open cabriolets with a retracted rooftop [10]. In contrast to the air flow in the passenger compartment of an open cabriolet, the air movements in closed spaces range from 0.05 m/s to 0.4 m/s [11]. In the case the rooftop of a cabriolet is retracted, the air flow influences the flow around the passengers significantly. A cabriolet, also known as a convertible, can come as a two or four seater sports car or as a roadster, occupying two seats. When the roof is retracted, the passenger compartment is dominated by a turbulent flow field which is created by the velocity difference between the surrounding air flow and the flow in the passenger compartment. During this situation the velocities surrounding the passengers are significantly higher, up to 40% of the driving speed [12], compared to the closed roof variant. With higher driving speeds the velocities in the passenger compartment increase as well and thus the level of comfort decreases as these flow phenomena negatively influence the comfort perception [13, 14]. Therefore, it is critical to evaluate the human perception in the development of a cabriolet vehicle. However, the thermal comfort models of closed spaces cannot be applied onto the thermal comfort evaluation of an open cabriolet. Very few investigations have been conducted about the thermal comfort in the passenger compartment of an open cabriolet passengers or have not been publicised. In the research of [12] an analytic model for cabriolets has been developed and further optimized in [15] and [16]. Although, these analytic models help the engineers to rate the thermal comfort, such a analytic model still relies on experimental windtunnel or road testing with a measurement manikin, see Figure 1.2, in a modified predecessor or a prototype. However, such a modified predecessor - if it exists - or prototypes are only available in later stages of the development process. As can be seen in Figure 1.1, the later the development phase, the higher the costs. Design changes stemming from the test results are very costly and risk the postponement of the planned start of production. Furthermore, a prototype is one of the major costs factors in the vehicle development as it can cost up to 1 million Euros. Furthermore, the time allocation of prototypes is strictly scheduled as they are used by multiple engineering departments [17]. The short amount of available testing time with a prototype, the high costs related to design changes in this phase as well as the high costs for using a prototype, limit the development of the thermal comfort of open cabriolets significantly.

Figure 1.2: Measurement manikin to evaluate the thermal comfort in open cabriolets [9]

In order to improve the development process related to thermal comfort of open cabriolets, the concept of a flow mock-up is proposed in this thesis. A flow mock-up should combine the quantitative values obtained from CFD simulations with the use of a physical simulator and enable the possibility of assessing thermal comfort in the early development phase. In the physical simulator,

representing the flow mock-up, the flow field, which is obtained from CFD simulation of the open cabriolet, is replicated and can be perceived by a subject. Simply said, the general idea of a flow mock-up is to place a person on a seat in a chamber, in which flow generators generate such an air flow, that the person gets the perception that he is seated in an open cabriolet. Consequently, the person inside the flow mock-up has the possibility to assess the comfort level of the cabriolet. This assessment can be further used to evaluate and improve the comfort of open cabriolets. The experience with physical simulators in other areas has shown that simulators are highly flexible, cost- and time-efficient and an early assessment can be performed [18].

Compared to the actual development process of thermal comfort of open cabriolets, the thermal comfort could be assessed in the early development phase, where the costs for design changes is low and the freedom of decisions is high. The reason for this is because CFD simulations dominate the early aerodynamic development process, which can be used as an advantage by replicating the flow field in a flow mock-up. With the use of a flow mock-up it is the aim to omit the use of experimental testing in a windtunnel with a modified predecessor or a prototype, thereby reducing the development costs significantly.

The general purpose of a flow mock-up can be defined as:

The possibility to subjectively assess a ride in an open cabriolet in a cost-effective way and in the early phase of the vehicle development

To the present day, there exist no record of any research involving a flow simulator that especially deals with the comfort development of open cabriolet vehicles.

Thesis Scope and Objective

In order to find a way of improving and facilitating the development process with respect to thermal comfort in an open cabriolet, this thesis aims to concretise the idea of a flow mock-up and to investigate the following research question:

Which factors influence the possibility to experimentally replicate the flow field of an open cabriolet in a flow mock-up in the early development phase, addressing thermal comfort, especially draught phenomena and how can this flow around a cabriolet passenger be replicated?

This includes to determine

1. what is the **additional benefit** of a flow mock-up,
2. what does the flow mock-up has to **fulfil** in order to generate this additional benefit and
3. what does the flow mock-up has to **look like** in order to generate this additional benefit?

These questions are answered by the approach, which has be schematically visualized in Figure 1.3. First, the actual *development process* with the focus on how could a flow mock-up be implemented and how would the flow mock-up improve this process is analysed. This has to be done first because the automotive development process thrives to develop and innovate a vehicle in the shortest amount of time, as efficient as possible. The further development of the concept of the flow mock-up therefore depends on whether the actual development would benefit from the implementation of a flow mock-up or not. From this analysis, requirements on the flow mock-up can be derived, which describe what a flow mock-up should fulfil in order to be beneficial for the development process. Thereafter, the factors which influence and characterise the experience of driving in an open cabriolet have to be identified. To find these *influence factors*, the human physiology, describing what factors make a human perceive the simulation to be comparable with an open roof cabriolet ride, has to be analysed as well as the physical factors, which are present in

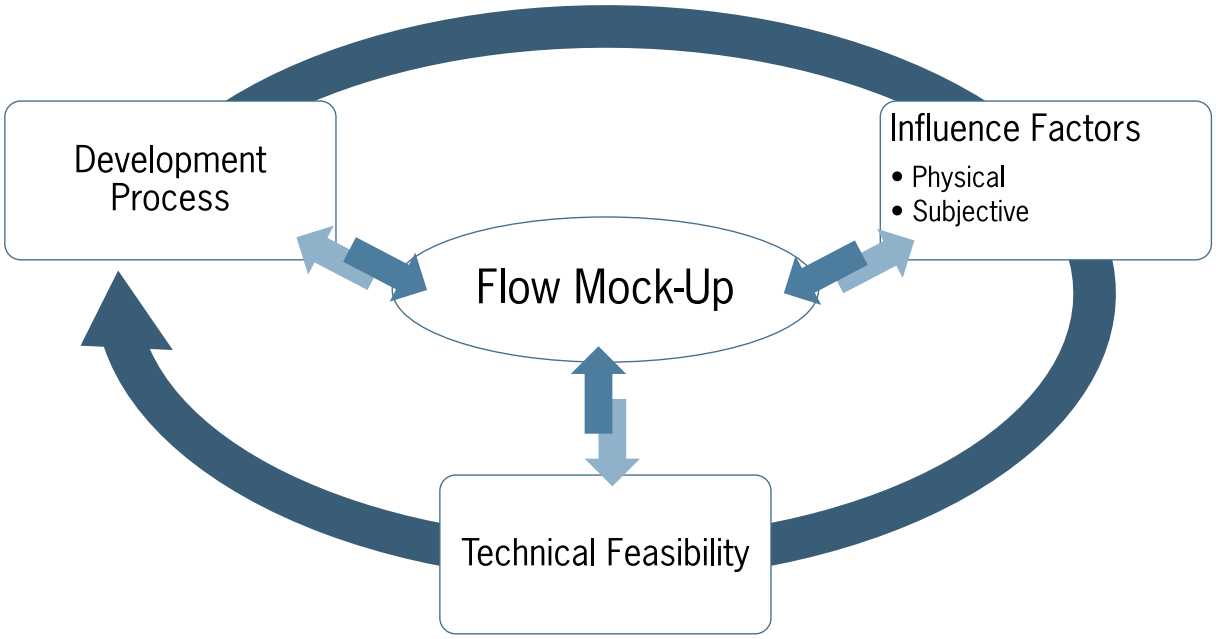

Figure 1.3: Overview of topics

the passenger compartment of an open cabriolet. These factors not only characterize the experience but also determine the set-up of a possible flow mock-up. Consequently, these influence factors prescribe the tasks, a flow mock-up should be able to replicate in order to simulate a realistic experience in an open cabriolet. After the influence factors have been identified, it has to be investigated how these factors are replicated, describing the *technical feasibility* of a flow mock-up. The first step to investigate the technical feasibility is by analysing if it is possible to replicate the flow field of an open cabriolet without the need of the physical vehicle, which is the idea of a flow mock-up. This is done by means of a CFD analysis by first simulating the flow around the total cabriolet vehicle and then in a reduced computational domain, which only surrounds the passenger and which would represent a possible set-up of a physical flow mock-up. It is the aim to reproduce the same flow field in the reduced computational domain as is given by the reference simulation of the total vehicle. From this, the reproducibility of the flow field without the main influencing geometry can be investigated as well as to find possible positions of flow generators where boundary conditions have to be set to produce a similar flow field for the actual physical set-up of a flow mock-up.

The overall process is an iterating process, which is indicated in Figure 1.3 by the arrows from the three topics of investigation towards the flow mock-up and back. While the individual topics prescribe requirements on the flow mock-up, the individual topics can also limit the requirements, which are prescribed on the flow mock-up from the respective other topic. For example, the technical feasibility can limit the possibilities which are prescribed by the requirements of the development process as well as the requirements, which results from the influence factors.

Thesis Organization

The thesis is set up as follows. First, in Chapter 2 the fundamental theory needed for this research is given. In Chapter 3 the actual cabriolet development process is analysed in order to be able to place the concept of a flow mock-up for open cabriolets into the context of the overall development process. Thereafter, Chapter 4 elaborates on the influence factors concerning the human's per-

ception as well as factors characterizing the physical flow field of an open cabriolet. In Chapter 5 measurement data is analysed in detail, in order to develop technical requirements on the flow mock-up. The functional requirements of a flow mock-up, resulting from the previous chapters, are summarized in Chapter 6 in order to sketch a picture of the flow mock-up. These functional requirements prescribe the technical feasibility of which the possibility of replicating the flow field of an open cabriolet in a closed space, independently of the vehicle geometry, is investigated in Chapter 7 with a CFD analysis. The conclusion of this research and further recommendations are finally described in Chapter 8.

Chapter 2

Fundamental Theory

This chapter includes the essential fundamental theory which is needed throughout this master thesis.

2.1 Aerodynamic Fundamentals

In this section the important aerodynamic fundamentals, which are relevant for this research, are elaborated on. For further detailed aerodynamic background and derivations it is referred to textbooks like [19, 20].

The aerodynamics in the automotive sector can be considered as *incompressible*, as the velocity is below a Mach number of $M < 0.3$ ($\approx 100m/s$) [19]. Therefore, the stated equations are given for incompressible flow. This assumption implies that the density ρ can be considered constant, when treating the fluid flow around commercial passenger street vehicles. Furthermore, the flow further away from the vehicle surface can be generally regarded as *inviscid* as the viscosity of air is in the order of $10^{-}5$ and thus the viscous forces can be assumed to be negligible except close to the fluid boundary, where the boundary layer plays a significant role.

2.1.1 Aerodynamic Flow Equations

The aerodynamic flow equations, also known as the governing equations of fluid dynamics, consist of the momentum equation, the continuity equation and the energy equation. The **momentum equations** for fluid flows, also called Navier-Stokes (NS) equation, are derived from Newton's second law of motion applied to a fluid flow and relates pressure, momentum and viscous forces with each other. It states that *the rate of change of momentum of a fluid particle equals the sum of the forces acting upon it.* The **continuity equation** states that *mass can be neither created nor destroyed*, i.e. mass is conserved. Furthermore, the **energy equation** is obtained from the first law of thermodynamics and the physical principle is that *energy can be neither created nor destroyed, it can only change form.* In the context of this thesis only the three-dimensional, unsteady and incompressible continuity equation and NS-equations are of interest and are given by:

$$Conservation\ of\ Mass: \qquad \frac{\partial u_i}{\partial x_i} = 0. \tag{2.1}$$

$$Conservation\ of\ Momentum: \qquad \frac{\partial u_i}{\partial t} + u_j \frac{\partial u_i}{\partial x_j} = -\frac{1}{\rho}\frac{\partial p}{\partial x_i} + \nu \frac{\partial^2 u_i}{\partial x_j^2}. \tag{2.2}$$

$$\tag{2.3}$$

Here the Einstein summation convention has been used.

2.1.2 Reynolds Number

The Reynolds number is an important dimensionless similarity parameter that describes the influence of the viscous forces on the fluid flow. It allows to classify the flow regime and to compare different types of flow experiments with each other. The Reynolds number is defined as the dimensionless ratio of the inertial forces to viscous forces and quantifies their relevance for the prescribed flow condition:

$$Re = \frac{\rho_\infty U_\infty L}{\mu} = \frac{U_\infty L}{\nu}. \tag{2.4}$$

The aerodynamics of commercial passenger vehicles deal within a Reynolds number range of $Re = 10^5 - 10^8$ due to the low kinematic viscosity of air $\nu_{air} = 1.48 \times 10^{-5}\,\mathrm{m}^2/\mathrm{s}$ (at $15°C$), indicating that the inertial forces dominate in the flow field. Considering a passenger vehicle of $4\ m$, driving at $30m/s$ a Reynolds number of 8.1×10^6. According to [19] a flow can be regarded as *inviscid* if the local Reynolds number exceeds 1×10^7.

2.1.3 Bernoulli's Equation

Bernoulli's equation relates pressure and velocity to each other. It can be applied throughout the flow in the case of a steady, incompressible and irrotational flow or along individual streamlines, when the flow is steady, incompressible and the effects of shear stress are negligible. The equation is derived from the momentum equation, Equation (2.2), and is given by Equation (2.5).

$$p_s + \frac{1}{2}\rho_\infty V_\infty^2 = p_t = constant. \tag{2.5}$$

It states that the total pressure in a fluid always stays the same and that either the static pressure or the dynamic pressure changes. With the use of this relation the fluid can be described in a very efficient way.

2.1.4 Pressure

Pressure is an important parameter in the field of aerodynamics. Due to pressure, which is created by the air flow around the body, drag and lift are created, depending on the form of the body. In order to be able to compare different flow situations with each other, the pressure coefficient is used. The pressure coefficient is a dimensionless number that describes the pressure difference between the local pressure p and the ambient pressure p_∞ and it is normalized by the dynamic pressure. It is given by Equation (2.6).

$$C_p = \frac{p - p_\infty}{\frac{1}{2}\rho_\infty V_\infty^2}. \tag{2.6}$$

Considering the pressure in an in the use of Bernoulli's equation, Equation (2.5), the pressure coefficient can be expressed in terms of the local velocity, given by:

$$C_p = 1 - \frac{V^2}{V_\infty^2}. \tag{2.7}$$

2.1.5 Continuity Equation

A useful relation is the quasi-one-dimensional continuity equation for incompressible flow flow, which is given by Equation (2.8).

$$AV = constant, \tag{2.8}$$

With this relation the flow through a converging-diverging channel can be very easily described and derived. For the complete derivation of this equation it is referred to [19].

2.2 Aerodynamics of a Passenger Vehicle

In order to be able to evaluate the situation the driver and the passengers are exposed to when driving in a cabriolet vehicle, the flow phenomena around a cabriolet have to be identified. First, the general flow field around a conventional vehicle with a closed roof is described in Section 2.3. Section 2.4 elaborates on the flow field around a cabriolet and in Section 2.4 the measures to prevent draught phenomena in cabriolets are presented.

Aerodynamic Flow Phenomena around Vehicles

The aerodynamics around passenger vehicles is characterised by specific flow phenomena. Drag is the most common aerodynamic characteristic for which the aerodynamics are optimised and it is the result of multiple flow phenomena around the vehicle. However, in the present thesis the drag of the vehicle is of lesser importance as the focus is on the thermal comfort of an open cabriolet. Additionally, it is generally known, that the drag coefficient of cabriolets are worse compared to their closed roof version [13], because of the high turbulence flow which is created by removing the roof. This is further explained in Section 2.4.

Boundary layer In aerodynamics the flow around a solid body is investigated and one of the most fundamental phenomenon is the development of a boundary layer adjacent to the solid body's surface. The boundary layer is formed on the surfaces due to viscous forces, where the velocities are lower and the reference scales are smaller. Figure 2.1 illustrates the development of a boundary layer due to the difference in velocity directly on the surface and the undisturbed air with the freestream velocity U_{inf}, flowing around the solid body. The velocity gradient indicates a zero velocity at the surface, the so called *no-slip* condition, which gradually increases due to the process of shearing of adjacent layers of air [21]. The boundary layer is said to be laminar, when the velocity component is parallel to the surface and turbulent when there is also a perpendicular velocity component. Between these two types of boundary layer is the transition point. The thickness of the boundary layer, which is smaller for laminar flow and higher for turbulent flow, is dependent on the roughness of the surface as well as the velocity of the surrounding flow. The boundary layer also thickens with the length of the surface and with it the pressure drops.

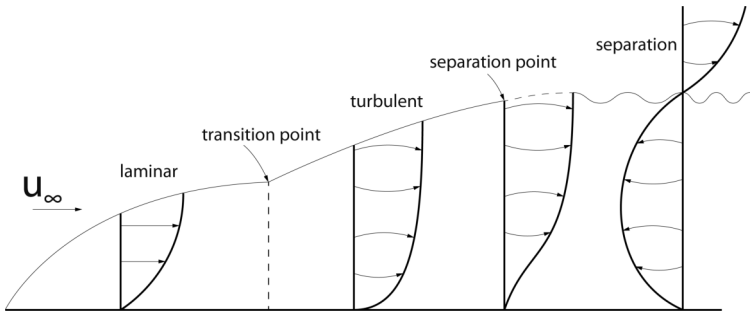

Figure 2.1: Laminar, turbulent and separated boundary layer [22]

Flow Separation Separated flow starts to develop after the separation point, see Figure 2.1, when the gradient of the velocity profile is zero and the pressure gradient is greater than zero,

i.e. an adverse pressure gradient. Thus, the mathematical description of the point of separation is given, when

$$\frac{\partial p}{\partial x} > 0, \tag{2.9}$$

$$\left(\frac{\partial u}{\partial y}\right)_{y=0} = 0, \tag{2.10}$$

$$\tau_w = 0. \tag{2.11}$$

After the separation point, the fluid flow separates and the velocity gradient becomes negative, $\frac{\partial u}{\partial x} < 0$, indicating the occurrence of backflow.

Separation occurs mostly due to sudden changes in surface shape. Common regions of separated flow on road vehicles are

1. just beyond the leading edge at the bonnet of the vehicle (A),
2. the transition from the bonnet and the windscreen (B),
3. the transition region from the roof and the rear window (C),
4. beyond the rear trailing edge of the vehicle, the wake (D),
5. at both front corners to the side of the vehicle,
6. in the wheel houses with the interaction of the wheels and
7. the A-pillars.

The letters indicate the position in Figure 2.3. For an open cabriolet, a special kind of separation occurs at the windscreen header, which especially affects the thermal comfort in the passenger compartment and is further explained in Section 2.5.

2.3 Aerodynamics Around a Conventional Passenger Car

One way to describe the flow around a vehicle is done by considering the vehicle to be stationary while the air is considered to flow around the vehicle. In reality this is the other way around, but like this it is easier to explain the flow properties. The flow around a passenger car is three-dimensional and dominated by viscous effects, like the boundary layer and multiple regions of flow separation. However, to explain the flow properties like velocity and pressure over the top and the bottom of a passenger car a simplified description of the flow around a passenger car is given by defining control volumes and considering the flow away from the boundary as two-dimensional and inviscid. In this way the pressure and velocity conditions can be explained by the principle of a converging-diverging duct, see Figure 2.2. Furthermore, the flow conditions can be determined by using the principle of Bernoulli along a streamline.Figure 2.3 shows the streamlines around a conventional notchback passenger car and its pressure distribution over the top and the bottom.

In front of the vehicle the air has the velocity V_∞, which is the equivalent velocity of the car, and atmospheric pressure p_∞. The first point of contact with the vehicle is the front spoiler, point A in Figure 2.3, where the air is slowed down from V_∞ to zero velocity resulting in a stagnation point. The velocity at this point is zero, thus the pressure coefficient C_p equals to 1. From this point the flow can pass below or above the vehicle. To explain the flow conditions, first the principle of a converging-diverging channel is explained.

As can be seen in Figure 2.2, the inlet area A_1 of a converging duct is bigger than the outlet area, thus $A_1 > A_2$. By the principle of continuity (Equation (2.8)), the velocity at the outlet

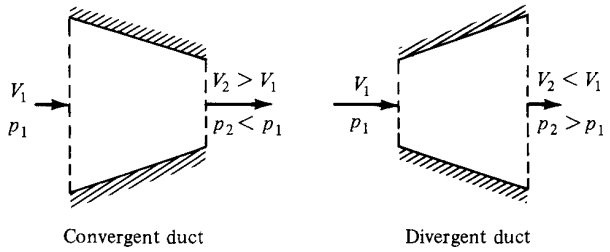

Figure 2.2: Incompressible flow in a converging-diverging duct [19]

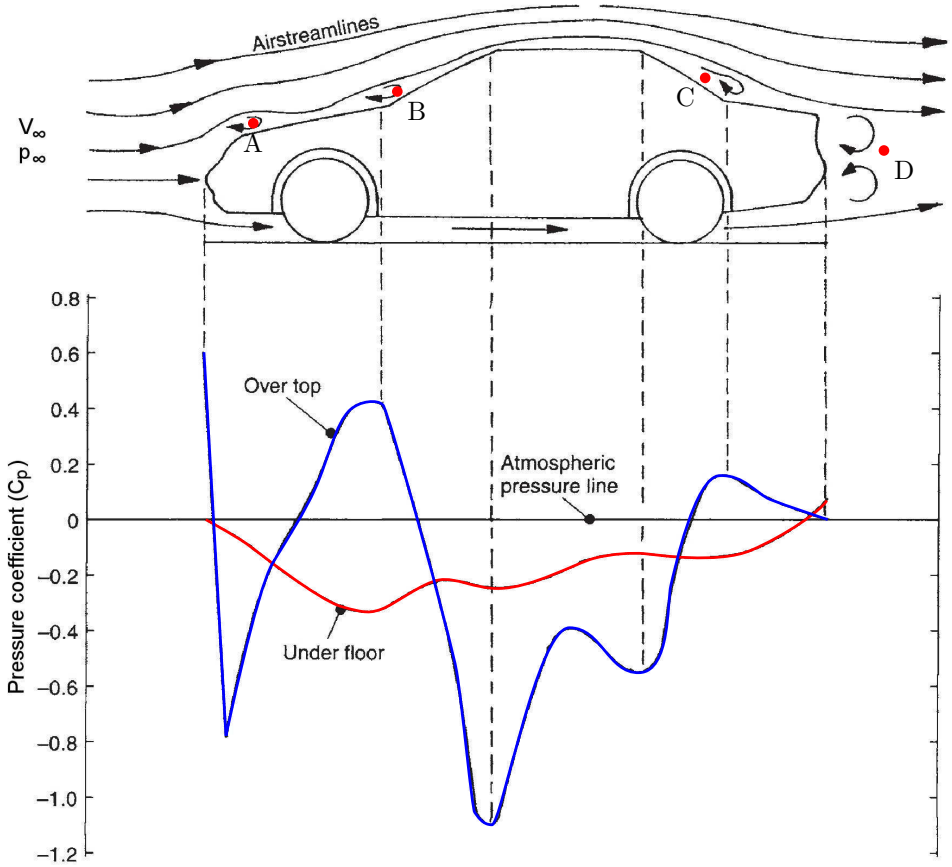

Figure 2.3: Streamlines around a conventional vehicle and pressure distribution over the top and bottom surface [21]

will be higher $V_1 < V_2$ and from Equation (2.7) it follows that the pressure coefficient becomes negative, i.e. $p_1 > p_2$. The opposite is given for a diverging channel, namely

$$\begin{aligned} A_1 &< A_2, \\ V_1 &> V_2, \\ p_{s_{in}} &< p_{s_{out}}. \end{aligned} \tag{2.12}$$

Applying this onto a vehicle, the flow underneath the vehicle can be explained straight forward. Defining a control volume below the car, a converging-diverging channel is obtained. In front of the car, i.e. at the inlet, velocity V_∞ and pressure p_∞ are present. Then the cross-sectional area converges, consequently, the pressure is lower than the ambient pressure p_∞ $(= p_1)$ and the

air velocity underneath the vehicle accelerates. Thus, as Figure 2.3 shows, a negative pressure coefficient is present along the underbody. Whereas at the outlet, the air expands, hence the air velocity decelerates and the pressure coefficient increases.

To explain the air flow above the vehicle, it is split into five sectional control volumes, visualized in Figure 2.4:

1. From the front of the vehicle (A) to the transition point of the bonnet and the windscreen (B)
2. From the transition point of the bonnet (B) and the windscreen to the windscreen header (C)
3. From the windscreen header (C) to the rear point of the roof (D)
4. From the rear point of the roof (D) to the transition point of the rear window and the trunk (E)
5. From the transition point of the rear window and the trunk (E) to the rear of the vehicle (F)

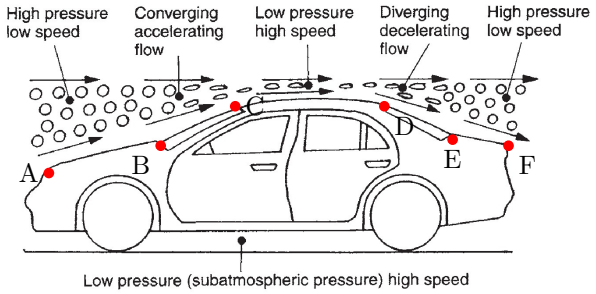

Figure 2.4: Relative air speed and pressure conditions over the upper profile of a moving car [21]

Section 1 and section 2 can be considered as converging channels, while section 4 and 5 as diverging channels. Due to the transition point between the bonnet and the windscreen, a separation bubble is created. Separation bubbles are enclosed spaces that are occupied by circulating air, trapping the air resulting a reduction of velocity, i.e. into a positive pressure coefficient. Thereafter, the air flow contracts again, increasing the velocity and decreasing the pressure. Over the roof the airspeed is at its highest and has a negative pressure value. From the roof's trailing edge to the rear of the vehicle the air flow is able to expand, therefore the pressure increases again. Additionally, due to the high velocity flow over the roof, separation at the roof rear edge occurs, resulting in a separation bubble behind the rear window, which causes a positive pressure coefficient. The velocity distribution increases from section 1 to 3 due to the converging section and decreases again from section 3 to 5 due to expanding flow.

2.4 Aerodynamics of an Open Cabriolet

The flow field around an open cabriolet differs from a conventional closed roof vehicle due to the absence of the roof after the windscreen header. Considering the simplified description of the flow as described above for the conventional passenger vehicle, the flow conditions around a cabriolet until the windscreen header are the same. After the windscreen header, see point A in Figure 2.5, the high velocity flow abruptly detaches and separation occurs. At this point the flow detaches and is decelerated by the low velocity flow inside the passenger compartment. This results in an unsteady shear layer above the passengers, which creates vortices and extracts fluid from the passenger compartment, as indicated in Figure 2.5. Due to the extraction of fluid, the pressure inside the passenger compartment decreases. The low pressure drives the shear layer downwards until it attaches again at the rear trunk of the cabriolet. At this reattachment point the pressure coefficient equals to one, thus this point is a stagnation point. Additionally, from the CFD simulation conducted in [23], shown in Figure 2.6, it can be observed that the flow at the rear of the side windows, point A, is driven towards the symmetry line of the vehicle. This flow

is the result of the flow over the A-pillar along the side windows and a detachment from the rear of the side windows. The underpressure inside the passenger compartment drives the flow from the outboard to the inboard and encloses the passenger compartment from the side. The shear layer over the top and the flow from the sides meet at a stagnation point at the middle of the rear trunk. The combination of low pressure, instationary shear layer and flow from the side drives the replenishment of air from the stagnation point on the trunk, which is called backflow. The passenger compartment is thus enclosed, forming a so called separation bubble inside which the flow is recirculating due to the combination of the shear layer and low pressure.

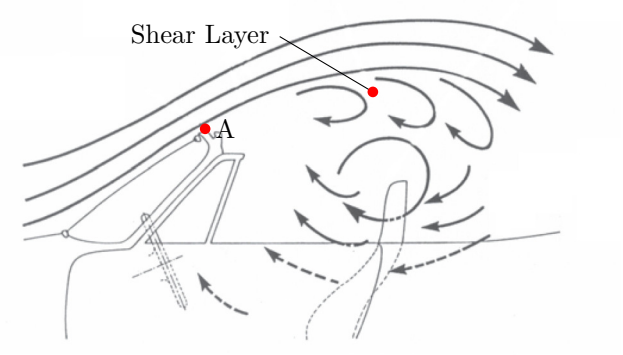

Figure 2.5: Flow field around an open-roof cabriolet

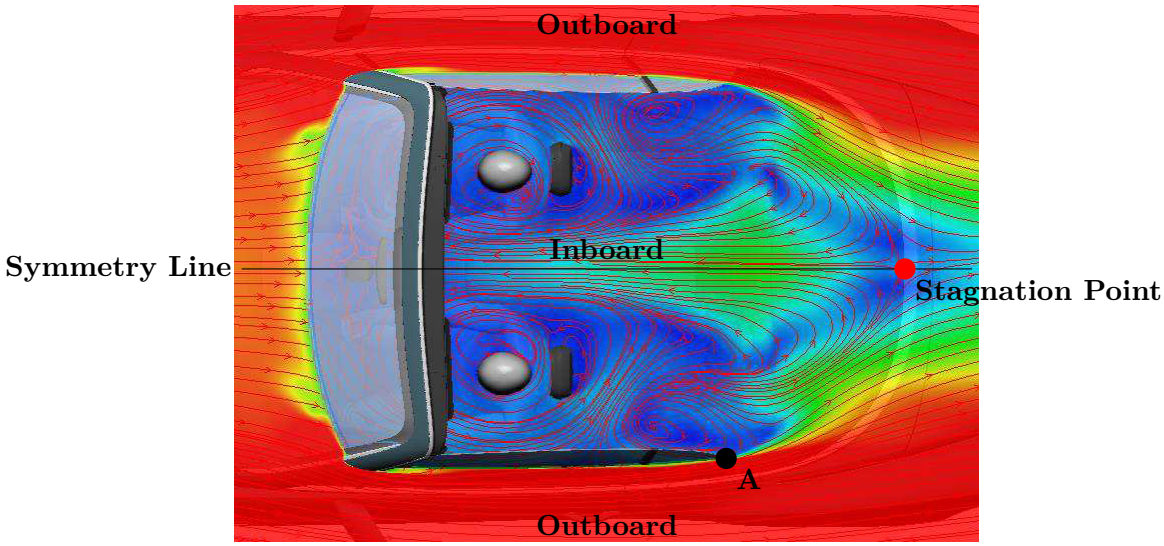

Figure 2.6: XY-plane from CFD simulation of a Bentley Continental GTC cabriolet [23] showing the velocity distribution (from red = high V to blue = low V) with indicated terminology

The main geometries, which influence the flow field of the passenger compartment of a cabriolet, identified by the experimental investigations of [13] and [24] are

- the windscreen slant angle,
- the inward sloping of A-pillars and side windows,
- the height of the trunk,
- central roll bar (if present).

Thermal comfort The thermal comfort of the passengers is influenced by the unsteady shear layer and the backflow. The unsteady shear layer periodically bursts and vents, resulting in pressure and velocity fluctuations. The backflow exposes the passengers to velocities up to 40% of the driving speed [12], which are the highest at the inboard upper body. Both phenomena cause the passenger to feel draught and make the passenger feel uncomfortable.

Draught Reduction Measures

Several measures for the improvement of the passenger comfort in an open cabriolet have been developed. The most common draught reduction component is the wind-break or draft stop, see Figure 2.7. The wind-break is either made of a permeable fabric or glass. Both prevent backflow and consequently the formation of recirculation. Multiple studies [12, 14] have shown the advantage of a wind-break on the thermal comfort, because it significantly reduces the air velocity around the passenger.

Figure 2.7: Wind-break

The fabric wind-break is permeable thus it does not block the pressure, which is the case for non-permeable wind-breaks like glass. For the latter the gradients between the surrounding and the passenger compartment are higher compared to the permeable wind-break, where a better equilibrium is present. The non-permeable wind-breaks often have higher wind noise, but their advantage is a better visibility to the rear [20].

An expendable spoiler at the windscreen header is a device to mainly improve the comfort for passenger in the back of a four-seater cabriolet. Such a device can be seen in Figure 2.8a. The basic idea is that the profile directs the the flow upwards, such that the shear layer between the surrounding flow and the flow in the passenger compartment shifts upwards as well [25].

Another device for thermal comfort improvement is Daimler's AirScarf, see Figure 2.8b. An AirScarf is mounted on the head rest of the seat and blows warm air into the neck of the passenger. Although the device increases the local velocity at the neck, the high temperature air improves the comfort level. This device is intended for the use on cold sunny days, as a low outside temperature influences the perception of draught.

(a) Spoiler at the windscreen header

(b) Daimler's AirScarf

Figure 2.8: Two different draught reduction components

2.5 Flow over a backward-facing step

A simplified description of the flow over an open cabriolet, especially the aerodynamic behaviour after the windscreen header, is given by the flow over a backward-facing step (BFS). A two-dimensional visualization indicating the main flow characteristics is shown in Figure 2.9. The BFS is characterized by a sudden discontinuity in the surface, i.e. a step, at which the flow detaches.

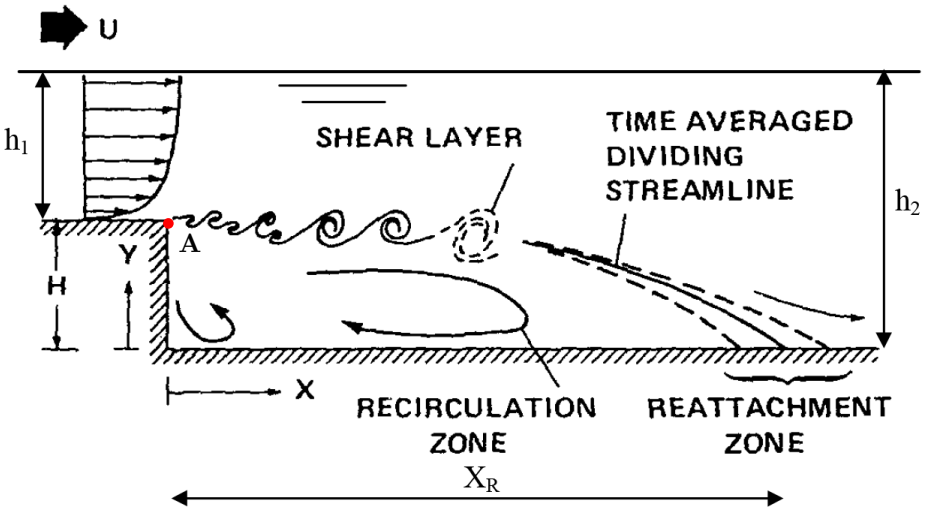

Figure 2.9: Schematic overview of a two-dimensional flow over a BFS, indicating the characteristic flow structures [26]

Due to the difference in velocity between the high velocity flow over the top and the basically stationary flow behind the step, free-shear of fluids occurs, resulting in a shear layer, that mixes the low-momentum fluid behind the step with the high momentum flow over the top. The shear layer reattaches after a specific reattachment length, denoted by X_R in Figure 2.11. At the point of reattachment the surface velocity equals to zero, resulting in a stagnation point at the point of reattachment. The shear layer thus encloses the space behind the step. Within this enclosed region, recirculation occurs due to the rotational movement of the shear-layer vortices impinging on the lower channel wall, with negative horizontal velocities near the bottom surface [27, 28]. Thus, the velocity profiles are S-shaped within the recirculation zone, indicating an adverse pressure gradient [28]. As the pressure gradient is positive, it is given, that the pressure within the recirculation region is lower than ambient pressure, resulting in a negative pressure coefficient. A typical pressure distribution along the surface behind the BFS can be seen in Figure 2.10.

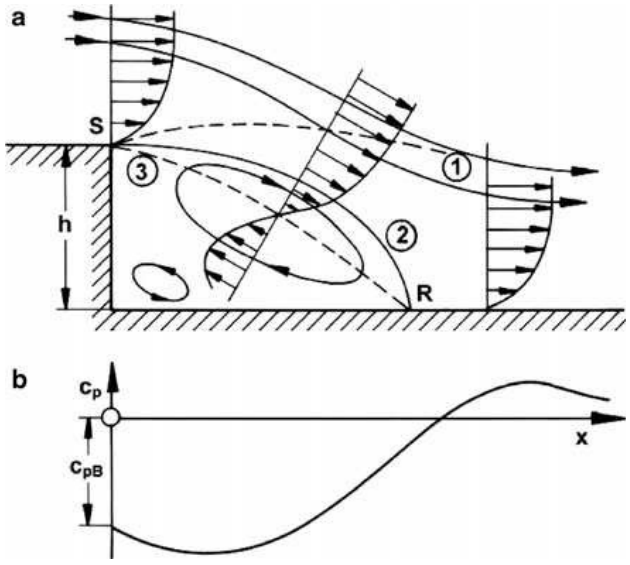

Figure 2.10: Flow over a two-dimensional BFS (a) and the respective distribution of the pressure coefficient [20]

The three-dimensional flow over a BFS shows the same flow characteristics as the two dimensional flow, which has been described above. A topological visualization of the three-dimensional flow over a BFS is given in Figure 2.11. As can be seen, additional three-dimensional effects are

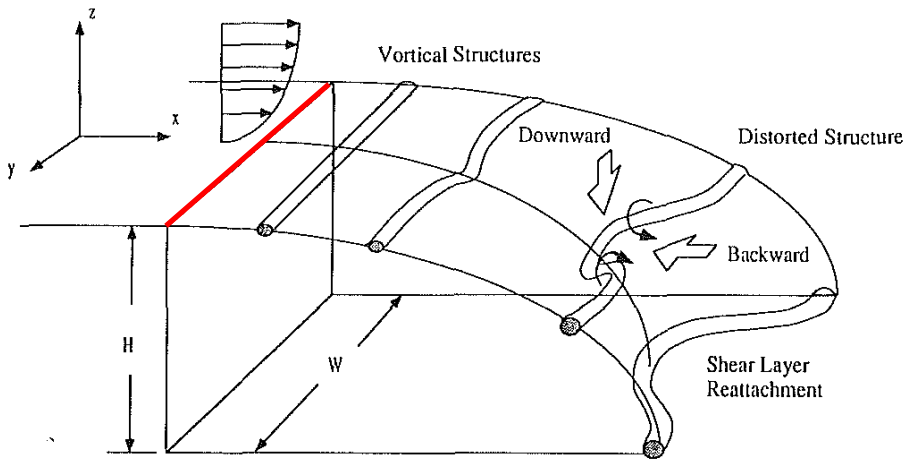

Figure 2.11: Topological sketch of the three-dimensional separation region [29]

the backward and downward deformation of the vortical structures near the centerline. *The vorticity redistribution spreads toward the wall and greatly increases the spanwise entrainment near the center of the step*, resulting in an earlier reattachment of the separated shear layer at the centerline compared to the reattachment towards the outside. The spanwise entrainment near the centerline from the walls induces movement from the wall toward the center. The entrained fluid near the center line is directed upstream again inside the recirculation region toward the wall. Most of this recirculating fluid moves backward and upward and is entrained again by the shear layer [29].

Comparing the flow over a BFS to the flow over an open cabriolet, the point of detachment, indicated by the red line in Figure 2.11, represents the windscreen header of an open cabriolet. As can be seen in Figure 2.6 the effect of deformation of the vortical structures from the outboard towards inboard is increased due to the flow around the sides of the vehicle. The reattachment zone is indicated by the stagnation point at the trunk.

2.6 Computational Fluid Dynamics

In the field of fluid dynamics Computational Fluid Dynamics (CFD) is used to solve and analyse the aerodynamic behaviour around a certain object. This is done by discretizing the physical domain into small finite volume elements, where the aerodynamic flow equations, given in Section 2.1.1, are solved numerically. For the analysis conducted in Chapter 7 the CFD solver StarCCM+ from CD Adapco has been used. In this section the basic CFD equations are given as well as the settings of the solver, which were used during the analysis.

2.6.1 Turbulence modelling

In order to solve the aerodynamic flow equations, different mathematical models can be used. The main difference of the mathematical models is how the turbulence flow is resolved. The Direct Numerical Simulation (DNS) model fully resolves all the physical scales of the flow and is therefore the most accurate. However, the simulation of flow problems at Reynolds Numbers as high as for road vehicles would exceed the computational capabilities, which are currently available, by far. In order to reduce the computational power demand the turbulence has to be modelled. Therefore,

other mathematical models have been developed, namely Large Eddy Simulation (LES), Detached Eddy Simulation (DES) and Reynolds Averaged Navier Stokes (RANS). LES resolves the large eddies and filters out the small eddies, which are removed and modelled. The approach of the RANS is to decompose the NS-equations into time-averaged and fluctuating components in order to solve the mean flow and model the effects of the turbulence on the mean flow. DES is a hybrid model that usually uses LES while RANS is used in the boundary layers. The forfeit from LES to RANS is that a lot of information about the turbulent structures, especially the large eddies which transport momentum and energy, is lost as they are averaged over time in RANS simulations. LES and DES do still require high computational power and thus time, which is why the RANS has been chosen to be used in the framework of this thesis.

The RANS-equations are obtained by decomposing the velocity component into the mean and the fluctuating components and substituting it into the governing equations Equation (2.1) and Equation (2.2). These equations are given in Equation (2.13).

$$\begin{aligned} \frac{\partial \bar{u}_i}{\partial x_i} &= 0, \\ \rho\left(\frac{\partial \bar{u}_i}{\partial t} + \bar{u}_j\frac{\partial \bar{u}_i}{\partial x_j}\right) &= -\frac{\partial}{\partial x_j}\left[\bar{p}\delta_{ij} - \mu\left(\frac{\partial \bar{u}_i}{\partial x_j} + \frac{\partial \bar{u}_j}{\partial x_i}\right) + \rho\overline{u_i' u_j'}\right]. \end{aligned} \tag{2.13}$$

The first two terms in the square bracket on the right hand side are the mean molecular stress and the third term the Reynolds stress or turbulent stress, $\overline{u_i' u_j'}$. This additional term leads to the so called closure problem and needs to be modelled.

In order to achieve closure for all the unknowns, turbulence models are used. Multiple turbulence models exists among which the $k-\epsilon$ turbulence model is widely used in the industry of vehicle aerodynamics. The reason for this is not only because of its good agreement with reality also because of its robustness and the fast convergence [30]. The $k-\epsilon$ turbulence model is a two-equation model, in which the turbulent kinetic energy k and the small eddy energy dissipation rate ϵ are modelled.

One version of the $k-\epsilon$ turbulence model is the *realizable* $k-\epsilon$ turbulence model. This model is a newer version of the *standard* $k-\epsilon$ turbulence model and according to [31] the *realizable* $k-\epsilon$ "differs from the standard $k-\epsilon$ model in two important ways:

- The realizable *realizable* $k-\epsilon$ model contains a new formulation for the turbulent viscosity.
- A new transport equation for the dissipation rate, ϵ, has been derived from an exact equation for the transport of the mean-square vorticity fluctuation.

The term "realizable" means that the model satisfies certain mathematical constraints on the Reynolds stresses, consistent with the physics of turbulent flows. Neither the standard $k-\epsilon$ model nor the RNG $k-\epsilon$ model is realizable." Furthermore, the realizable $k-\epsilon$ turbulence model is better suited in "flows involving rotation, boundary layers under strong adverse pressure gradients, separation and recirculation" [31]. Therefore, this model has been chosen for the CFD analysis in Chapter 7. For detailed information about the different turbulence models it is referred to [32].

When choosing the constant density, turbulent flow and the $k-\epsilon$ turbulence model, StarCCM+ recommends and automatically chooses the $k-\epsilon$ two layer turbulence model. This model *combines the realizable $k-\epsilon$ model with the two-layer approach in which the computation is divided into two layers. In the layer next to the wall, the turbulent dissipation rate and the turbulent viscosity are specified as functions of wall distance. The values of specified in the near-wall layer are blended smoothly with the values computed from solving the transport equation far from the wall. The equation for the turbulent kinetic energy is solved in the entire flow.* [33].

2.6.2 Boundary layer modelling

A boundary layer is formed over an object when air flows over it, which is described above in Section 2.2. In order to analytically describe development of the boundary layer it has been divided into three regions: the *viscous sublayer*, the *buffer layer* and the fully turbulent *log-law region*. Within the viscous sublayer the turbulence is negligible while the viscous effects are small in log-law region. In the buffer layer both the turbulence and viscous effects are dominant. The regions can be distinguished with the use of the dimensionless wall coordinate y^+, which can be calculated with use of the following equations [32, 33].

$$c_f = 0.0576 \cdot Re_x^{1/7} \quad for\ 5 \times 10^5 < Re_x < 10^7, \tag{2.14}$$

$$\tau_w = c_f \frac{1}{2} \rho U_\infty^2, \tag{2.15}$$

$$u_\tau = \sqrt{\frac{\tau_w}{\rho}}, \tag{2.16}$$

$$y^+ = \frac{y_{1/2}}{\delta_\nu} = \frac{u_\tau y_{1/2}}{\nu}, \tag{2.17}$$

where c_f is the friction coefficient, τ the wall shear stress, u_τ the friction velocity, $y_{1/2}$ the half height of the first cell in the surface and Re_x the Reynolds number based on the characteristic length along a surface. The y^+-value is a measure of the distance between the wall and the centroid of the first adjacent cell, evaluated as function of the computed velocity field. It determines whether the influences in the wall-adjacent cells are laminar or turbulent, hence indicating the part of the turbulent boundary layer that they resolve [34]. The respective y^+-values for the different regions are:

- Viscous sublayer: $0 < y^+ < 5$
- Buffer sublayer: $5 < y^+ < 30$
- Log-law region: $y^+ > 30$

The different scaling regions are sketched in Figure 2.12.

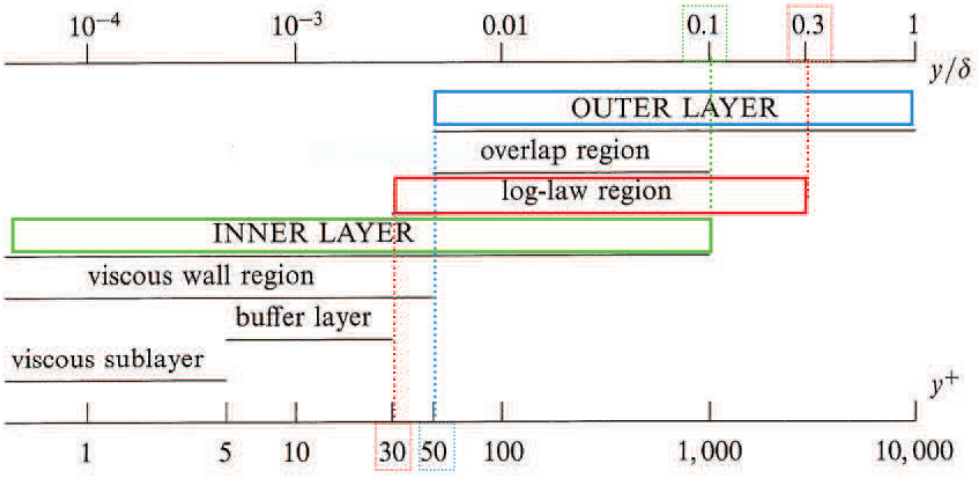

Figure 2.12: A sketch showing the various wall regions and layers defined in terms of $y^+ = y/\delta_\mu$ and y/δm for turbulent channel flow at high Reynolds Number ($Re_\tau = 10^4$) [32]

In order to resolve the boundary layer in detail, low y^+-values are needed. This implies that the generated mesh of the domain has to be very fine and consequently increases computational time. However, for high Reynolds number flows the low viscosity affected near wall region does not

need to be resolved [31]. Therefore, wall treatment models exist, which model near-wall turbulence quantities such as wall shear stress, turbulent production and turbulent dissipation. StarCCM+ offers the possibility to choose three different wall treatment methods: *Low y+, High y+* and *All y+*. The *Low y+* wall treatment resolves the entire boundary layer and is recommended for low Reynolds number flows, while the *High y+* wall treatment is for high Reynolds number [33]. The *All y+* wall treatment is a combination of the other two models. According to [33] the *All y+* wall treatment *"seeks to represent the behaviours of the previous two wall treatments in the limit of very fine or very coarse meshes. It is a design goal that this wall treatment should give results similar to the low-y+ treatment as* $y+ \to 0$ *and to the high-y+ treatment for* $y+ > 30$*. It will also give reasonable results for intermediate meshes where the cell centroid falls in the buffer layer. However, the aim should be to have either* $y+ < 1$ *including a well resolved viscous sublayer or* $30<y+<50$*."*. It is recommended to use this model, which is why this model has been chosen.

In order to obtain the desired y^+-values, prism layers on the model boundaries have to be defined when the domain is meshed. Prism layers are adjacent to the solid surfaces and they cover the boundary layer on the wall to ensure that the boundary layer is resolved correctly. In StarCCM+ different prism layer properties can be chosen for the model boundaries. These properties consist of the prism layer thickness, the number of prism layers and the prism layer stretching. These three parameters are connected by

$$t_{prism} = y_1 \cdot (1 + s^{n_p - 1}), \tag{2.18}$$

where t_{prism} is the prism layer thickness, y_1 the height of the first prism cell, s the prism layer stretching and n the number of prism layers. The thickness of the prism layer has to be chosen such that it lies within the respective region, to obtain the desired y^+-value.

Solver The solver determines how the governing equations are solved. StarCCM+ offers to choose a *coupled flow solver* or a *segregated flow solver* for the numerical setup setting three dimensional, steady and the material gas. The segregated solver solves the governing equations sequentially (i.e., segregated from one another), while the coupled solver solves them simultaneously (i.e., coupled together) [31]. Generally, the coupled flow solver is used for high-speed compressible flows while the segregated solver is intended for incompressible and mildly compressible flows. Therefore, the segregated flow solver has been chosen for the CFD analysis in this research.

Chapter 3

Project Related Requirements

The automotive development process is the most important and confidential process of the automotive companies. The development process has several milestones, which are strictly timed in order to ensure an orderly cooperation between the different departments. For the flow mock-up to be successful and to be interesting to be developed further, the development process has to be analysed on the possibility to implement the flow mock-up as well as the potential of the flow mock-up. This leads to requirements a flow mock-up has to fulfil to improve the development process.

This chapter discusses the development process in the automotive industry and how the cabriolet development is considered. Furthermore, a modified development process is presented, which considers the use of a flow mock-up. Thereafter, the resulting requirements for the flow mock-up are summarized by sketching two specific scenarios of the application of a flow mock-up in the development process.

3.1 Development Process

The industrial development of automobiles follows a specific Product Evolution Process (PEP), also known as *time-to-market process* [17]. It describes the whole process from the definition of the vehicle mission, the strategy and its variants to the vehicle design and development to the production of the first customer vehicle. The general PEP set-up is similar for every car manufacturer, however, they differ in the details due to different core competences as well as their time schedule [35]. It should serve as guidance for every project as well as for the collaboration between the departments of different disciplines. Due to a lot of dependencies between the departments multiple milestones are defined, which serve also as deadlines for data exchange. The discussion of all the processes is beyond the scope of this research and for further information it is referred to [36]. In the following only the relevant steps with respect to the aerodynamic design of a cabriolet are discussed.

Generally, the PEP is characterised by four main chronological phases: the definition, the concept, the series development and the series preparation phase. These are visualized in Figure 3.1 together with the most important milestones: project mission (PM), project definition (PD), package freeze (PackFreeze), design decision (DD), design freeze (DF) and start of production (SOP).

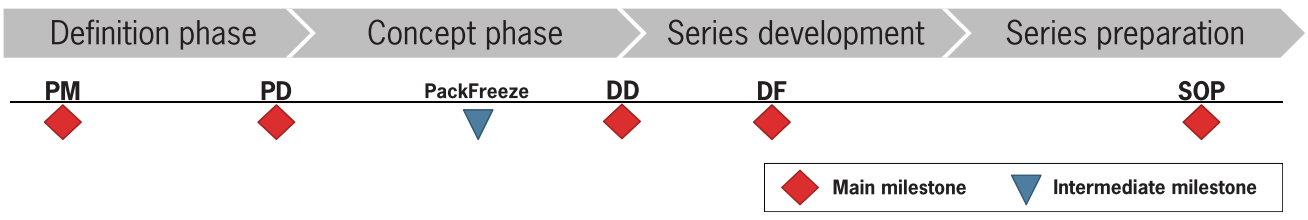

Figure 3.1: Four main phases of the PEP with relevant milestones

At the beginning of the definition phase the project mission is defined after which the top level requirements are determined by conducting a detailed analysis of the competitors, market, customers, etc., resulting in the project definition. The PD states next to many other vehicle properties whether the project consists of the development of a solitary model, a new vehicle model line with multiple variants and derivatives, a facelift or a complete redesign. A cabriolet can be either a solitary model, such as the Porsche Boxster, or a variant of the base model. In most cases the latter applies to a cabriolet and therefore the design is pre-set by its closed version.

In the concept phase the top level requirements are concretised into the functional concept, multiple design studies and technical feasibility. During this phase the packaging of the vehicle is defined as well. The packaging includes next to the packaging of the base model, all the components needed for a cabriolet or other variants and is fixed with the package freeze. The concept phase is concluded with the final design decision of one vehicle design.

The series development phase deals with the realization of the vehicle so that it can be produced by a manufacturing plant. This includes the detailed component design, optimization processes, production processes etc. Furthermore, this phase consists of the design freeze of the vehicle, after which the development moves into the detailed phase. At this stage the development costs are the highest because most of the vehicle properties have been fixed. During the definition and the concept phase the development costs are relatively low and gradually increase with the project duration. How the costs are assessed throughout the project is mainly done in the definition phase of the project. The freedom of decision however has the opposite trend, as more and more vehicles are fixed to the end of the project duration. This is illustrated in Figure 3.2.

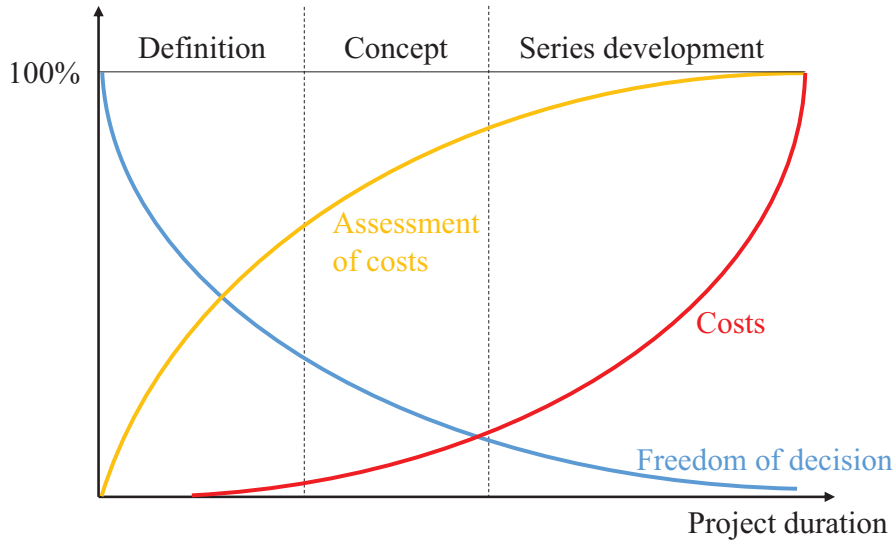

Figure 3.2: Variation of costs, assessment of costs and freedom of decision with the project duration [2]

The aerodynamic development starts as soon as the product mission is defined with the determination of the target drag coefficient and the initialization of the CFD computation of the first design models. At first multiple models with different designs are aerodynamically evaluated and in close cooperation with the styling department reduced to two models during the concept phase [37, 38, 39]. At this instance the first windtunnel measurements are started. On a scaled model different influences are tested while a 1:1 clay model will be produced as soon as the general proportions are fixed. The relevant aspects of development process of the base model are shown in Figure 3.3 with a schematically placement of the cabriolet development process to the PEP of the base model. The upper part of the figure shows the aerodynamic development of the base model. The lower part of the figure represents the cabriolet aerodynamic and comfort development

which is postponed by 4 months. For a cabriolet the aerodynamic development consists of form optimization of the closed roof variant with the use of CFD and in a scaled wind tunnel. The drag coefficient is optimized for the base-model or with a closed rooftop. Generally it is known that the cabriolet has a higher drag coefficient when the roof is open. Therefore, the design and the aerodynamics are mainly dependent on the development of the base model. An important aspect of the aerodynamic design of a cabriolet with an open roof is the lift balance of the car due to separation at the windscreen header.

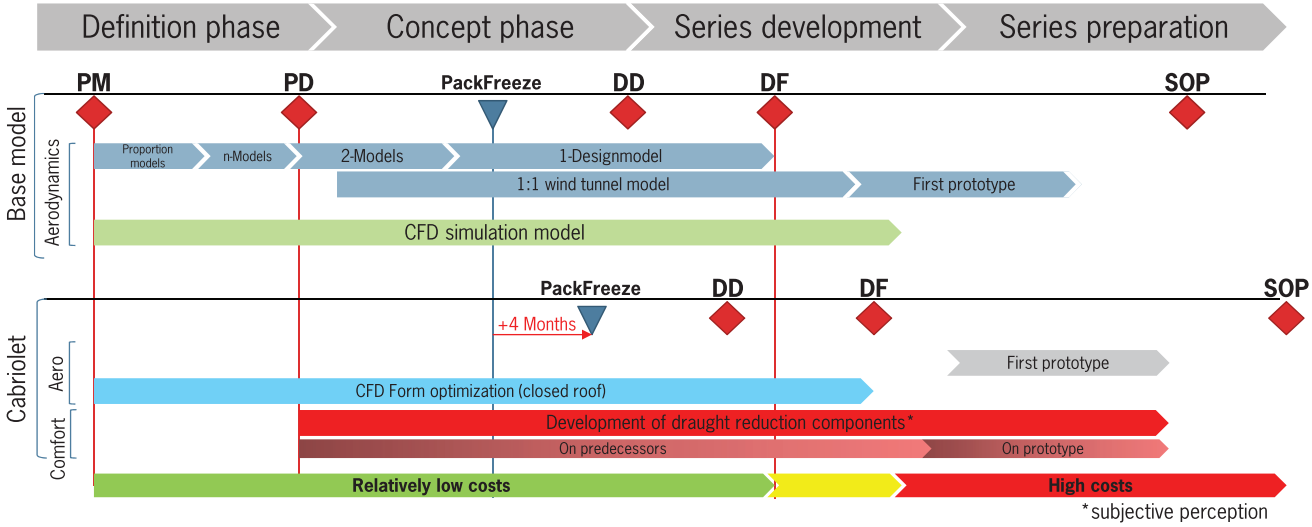

Figure 3.3: Aerodynamic development process of a base model and cabriolet

Next to the aerodynamic balance of the vehicle the optimization of the passenger comfort is important during the development of the cabriolet. Cabriolets are driven at velocities above 200 km/h and the passenger comfort should ideally be provided for almost the whole velocity range. In order to optimize the passenger comfort of a cabriolet, draught reduction components can be implemented, see Section 2.4 for more information. However, the influence of these components can only be tested on a full-scale model as the human perception plays a major role in the evaluation. Therefore, the development and investigation of these components is additionally done with the use of either their predecessor or only with a prototype near the end of the series development phase. In the case a predecessor is available, it has to be modified and tested. This results in high costs due to the production of components and the possible reconstruction of the windscreen or other redesigned parts influencing the flow field. Furthermore, the packaging of the base model defines the majority of the packaging while the package freeze of the cabriolet contains the detailed packaging of the foldable rooftop. Therefore, due to the already fixed packaging, no major components can be implemented anymore. Only improvements of components that are accounted for in the package freeze and small components, with a low influence on the comfort, can be implemented. If no predecessor exists the driving comfort development can only be conducted on the prototype, which is limited to a short amount of time, related to high costs as well as limited possibilities for the addition of new components. If a predecessor of a cabriolet is available, the evaluation of draught reduction components can not be done right from the start. Next to the modifications that have to be made on the vehicle according to the changes of the new design, the draught reduction components have to be engineered with a high level of detail, as they have to be produced and mounted to the vehicle. At the time it is possible to subjectively evaluate these components, the package freeze of the base model has already been determined. Furthermore, the modified vehicle has to be tested in a wind tunnel or on the road. While one wind tunnel session of 8 hours costs around 20.000 €, road testing on open roads has the additional risk for car manufacturers that

they are seen and photographed as well as the possibility of accidents. For manufacturers that do not own a wind tunnel these costs are even higher.

As well as the package freeze, the design decision and the design freeze of the cabriolet are mostly determined by the base model. For the cabriolet these milestones mainly concern the design of the foldable rooftop and the rear part of the vehicle.

All in all the following disadvantages of the actual cabriolet development process regarding passenger comfort development can be summarised:

- Low flexibility, due to dependency on predecessor and prototype
- High costs, because of windtunnel use
- Low influence or no possibility to influence the packaging of the base model
- Short development time if no predecessor exists

3.2 Modified Cabriolet Development Process

The above mentioned disadvantages can be improved by investigating the passenger comfort in the early development phase. This can be done by developing a method which can reproduce the flow field around the passenger compartment such that the human perception can be evaluated. Such a flow mock-up should be able to replicate the influence of different components without the use of a predecessor or a prototype. Use can be made of the already available CFD simulation model, which should provide the details of the flow field in the passenger compartment. Furthermore, it would be advantageous to have the opportunity to influence the packaging of the base model. In this way, new concepts that are proven to improve passenger comfort can be implemented into the packaging and refined in the prototyping phase. This can accelerate the development process of passenger compartment comfort, reduce costs due to fewer prototype-production and modification on predecessors, increase the flexibility as well as reallocate or even reduce development time. Such a modified comfort development process can be seen in Figure 3.4.

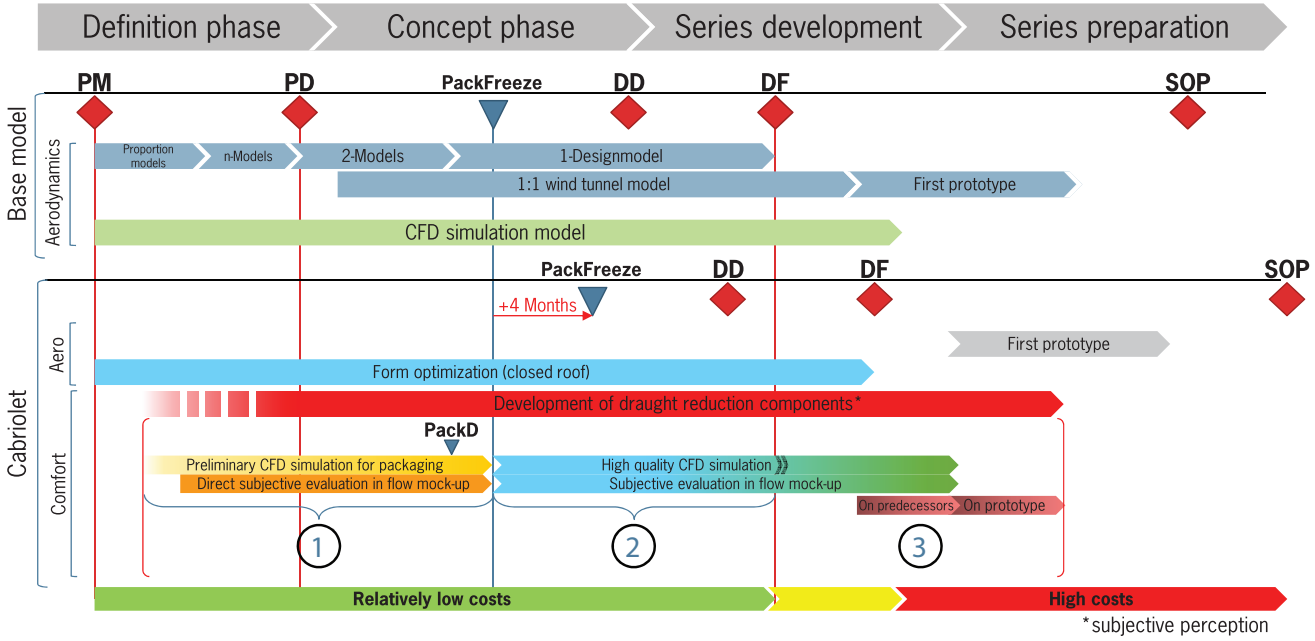

Figure 3.4: Modified aerodynamic development process of a base model and cabriolet

The figure shows again the usual development process of the base model at the upper part as well as the modified comfort development of the cabriolet. First of all, the development of the draught

reduction components can be shifted forward by starting with preliminary CFD simulations and replicating this flow field with the use of the flow mock-up, indicated in the figure as bright and dark orange. This opens the opportunity to directly evaluate the human subjective perception in response to the newly developed components and to have influence on the important milestone package freeze (PackFreeze) of the base model. The CFD simulations should be preliminary, thus no high quality calculations are needed. This is because only bigger components have to be investigated as they have to be considered in the overall packaging and a low detailed CFD simulation gives enough information to evaluate their influence on the flow field in the passenger compartment. The intermediate milestone *PackD* in the figure indicates the point, where a decision regarding the packaging has to be made and has to be communicated to the department responsible for the packaging of the base model.

After the package freeze of the base model, the details of the draught reduction components have to be worked out. The quality of the CFD simulations has to increase and the subjective evaluation can be done in the flow mock-up. Additionally, influence of the proposed form optimization for the base model can be can be simultaneously investigated and evaluated in the flow mock-up. Thus, it can deliver additional criteria to decide upon certain form optimizations before the design freeze of the base model is reached. In order to be able to subjectively evaluate this, the flock mock-up should be able to replicate the changes on the flow field. This phase is illustrated in the figure as bright blue as it focuses on the aerodynamic form optimizations.

Finally, indicated in green and red, the development can be focused on the cabriolet only. The details and design of the draught reduction components can be finalized and validated with the use of the prototype.

This can be summarized into three phases, as have been indicated by the numbers and the color in Figure 3.4:

(1) The package relevant phase - orange

- Preliminary CFD simulations
- Direct subjective evaluation of the influence of the big components, which have to be considered for the packaging, in the flow mock-up
- Focus: Influence packaging of the base model
- Time available: 9-12 months

(2) The base model relevant phase - blue

- CFD simulations with high quality needed
- Direct subjective evaluations of the optimized draught reduction components as well as design changes of the base model in the flow mock-up
- Focus: Evaluation of design changes of the base model
- Time available: 11 months

(3) The highly detailed & verification phase - green and red

- Finalization of draught reduction component design
- Verification of the draught reduction components with the use of predecessor or prototype
- Focus: Elaboration and verification of draught reduction components
- Time available: 14 months

The combination of CFD simulations and flow mock-up increases the flexibility significantly as no components have to be produced and high variety of components can be simulated and directly

evaluated in the flow mock-up. Furthermore, the testing with the use of the predecessor can be reduced significantly or even skipped. This results in significantly lower costs, which are due to modifications on the predecessors as well as wind tunnel costs. There will be almost no extra costs due to the CFD simulations, as data is already available from the base model, which have to be slightly modified. Development on the prototype can then serve as validation/optimization, resulting in further cost reductions as well as reduction in time.

The main results that will provide the flow mock-up with information of the flow properties should be delivered from CFD Simulations.

3.3 Requirements resulting from the PEP

In the ideal situation the flow mock-up is able to replicate the flow field of an open cabriolet, the flow mock-up should fulfil certain requirements in order for the flow mock-up to be advantageous for the development process. The main goals of the flow mock-up can be summarized as

- increasing the flexibility for the development of comfort related components,
- making it possible to assess open cabriolet comfort in the early development phase, and
- influencing the packaging of the base model.

To achieve these goals, two possible scenarios are defined, which describe the tasks a flow mock-up should fulfil.

Scenario 1: Direct comparison of before and after The first scenario includes the replication of the flow field in such a way, that it is possible to compare the perception of different flow fields with each other. This ability would enable the comparison of the flow field perception of different design models in the concept phase, of the geometry changes made from the package freeze to the design freeze of the base model as well as different draught reduction components. Furthermore, the flow field can be benchmarked with the flow field of other cabriolets. Additionally, it offers the possibility of giving project managers and decision-makers the opportunity to perceive the influence of newly designed draught reduction components themselves. This could help to make well-founded decisions based on the results of the flow mock-up without the need of a windtunnel.

For this scenario, the flow mock-up should be able to replicate and switch between different flow fields in a short amount time, because in that case the differences can be noticed in the best way. This implies that the replication of the flow field should be *independent of the vehicle geometry*. If the generated flow field is dependent on geometries of the vehicle, reconstructions would be needed to replicate a different flow field, which in turn would counteract the requirement to switch between flow field in a short amount of time.

This scenario would make the development process more flexible as multiple components can be tested and evaluated in a short amount of time. The independency on vehicle geometries would reduce the costs, as no components would have to be manufactured. Consequently, no predecessor would be needed to evaluate the flow field as well as no windtunnel time is required.

CFD simulations would have to be conducted in the early development phase in order to perform this before the packaging of the base model. The approximate amount of time for the execution of these simulations would be 9-12 months.

Scenario 2: Reverse Engineering In the second scenario the flow mock-up would be used to determine the optimal thermal comfort situation, which is translated to CAD. The idea is to place a subject into the flow mock-up and giving him the task, to determine the positions at which an

uncomfortable perception is present. Then the flow properties at this position are adapted until an optimal situation is created. With the use of these settings the information is transferred back to CAD and the resulting geometry is given.

This enables it in the development to improve the thermal comfort at specific location and adapt the geometry in such a way, that the optimal solution is achieved.

For this scenario a reference simulation would have to be generated, which has to be adapted. For this to be possible, a tool is needed, which adapts the geometry of the reference simulation in such a way, that the subjectively determined optimal flow situation is found. These kind of optimisations are already done by improving geometry with respect to drag or lift, for example CFD optimization with adjoint gradient methods [40, 41].

Furthermore, this would require the flow field to be controllable individually. Therefore, multiple flow generators would have to be used which can be regulated independently to influence the flow field. The extent of this method would determine in which phase, and how much time has to be allocated for this scenario. If big geometry changes are needed, this would have to be conducted before the package freeze, otherwise the newly developed geometries cannot be implemented. For small geometry changes this could be performed in phase 2 or phase 3, which have been described above, to optimize the details of the draught reduction components.

General requirements As is mentioned in the previous section, the high costs during the actual development process are generated due to experiments conducted in the windtunnel as well as to the modification of the predecessor and testing with the prototype. For the flow mock-up to replace these conventional development procedures it should be less expensive to operate than the conventional methods.

Chapter 4

Factors of Influence

The test subject should get the subjective feeling of driving in an open cabriolet when seated in a flow mock-up. Therefore, the factors, which influence this experience have to be identified. These factors of influence can be split into two main groups: the Human Influence factors (HIF), which describe the human physiology, e.g. what influences the subjective feeling of a human and how is the subjective assessment of a human formed and the Physical Influence factors (PIF), which deal with the flow field around an open cabriolet.

This chapter elaborates on all identified factors. The factors are explained and their importance is put in relation to the flow mock-up.

4.1 Human Influence Factors

Every car manufacturer has the goal to sell as much cars as possible. The manufacturers offer different types of cars and different types of luxury. The latter includes the level of comfort which is hard to define in general, because humans are individuals and not everybody has the same idea about comfort. According to [5] the definition of *thermal comfort* is given by *"that condition of mind which expresses satisfaction with the thermal environment and is assessed by subjective evaluation"*. It is a phenomenon that is not experienced the same way by every human being. A situation that has been called comfortable by a person, can be rated differently by the same person due to influences as health, mood, etc. According to [20] these two facts have been defined as *interindividual* and *intraindividual*, respectively. For example, some humans feel comfortable in a vehicle which is sportive, meaning it is good to control, which comes with a direct steering and a hard suspension. Others however, like to have a vehicle which has a soft suspension and is isolated and quiet. Therefore, it is very difficult for an engineer to quantify comfort and to design a vehicle based upon calculations and numbers. This is the reason, why the subjective perception still plays a very important role in the development of a vehicle.

The most studies on human sensitivity to draught phenomena are conducted within closed spaces or office spaces. The ambient conditions of these environments differ significantly from the environment a passenger of an open cabriolet is situated, because the evaluated velocities are only up to 0.4 m/s. The essential difference between draught phenomena in closed spaces and an open cabriolet is that the people in a closed space do not expect these phenomena, thus they react more sensible to low air velocities, while in a cabriolet the passengers expect to be exposed to high air velocities and draught phenomena, thus they accept higher velocities. Therefore, the conducted studies are only conditionally applicable to the investigation of open cabriolet vehicle [20]. However, a general behaviour and sensitivity of the subjects can be derived from these studies in order to describe the conditions a subject is exposed to when experiencing an open cabriolet ride.

The human influence factors, which influence the perception of driving in a cabriolet, are given in Table 4.1. They have also been categorized into three groups.

Table 4.1: Categorized human influence factors

Basic factors	Influenceable factors	Non-influenceable factors
Smell	Metabolism	Mood
Light	Clothing/Isolation	Health
Vibrations	Expectation	
Noise		
Climate		
Anthropometry		

4.1.1 Basic Factors

As mentioned before, thermal comfort is hard to define, because it is a human perception resulting from a sum of multiple sense organs. The factors which address these senses are the basic factors. They include the five traditional human senses, which are sight, hearing, taste, smell and touch. In studies with test subjects these factors are often not mentioned directly as most common disturbing factors, because they are unnoticeable, i.e. neutral. However, these human senses are very sensible in case of any deviation from the neutral state and a deviation can quickly lead to distraction and consequently to discomfort [42].

Smell One of the most sensible organ of humans is the sense of smell [4]. If the smell is disturbing, it can divert the test-subject and the test-subject can feel uncomfortable right from the start. Therefore, the source has to be identified and if possible eliminated or active air fresheners have to be used to neutralise the smell. A too aromatic smell would also not be appropriate for a cabriolet.

Light This factor addresses the sense of sight. An open cabriolet ride is associated with a sunny day, thus this has to be considered in the design of a flow mock-up. A bright/daylight light source can be used to simulate the the condition of a sunny day. Furthermore, illuminated objects attract the attention of a subject. This effect can be used to focus the attention of the test-subject to a specific direction, away from unexpected components, which have to be used to replicate the flow field. For example, a screen can be used to show a road simulation, which is also done with full vehicle simulators.

Vibrations A vehicle is often exposed to mechanical vibrations due to the engine and road irregularities, which are mostly absorbed by the suspension. The vibrations are translated to the passengers over the vehicle bottom, steering wheel and mainly over the seat, which can be cushioned to absorb vibrations as well. Common vibrations, which are present in a vehicle, range from frequencies of 0.5 Hz and 80 Hz [43], while a human is able to perceive vibrations up to 500 Hz [44]. Vibrational motions consist of up- and down-movement, pitching left right and rolling to the front and back. Vibrations can also be heard, when the vibration is in the in the audible frequency range of 20 Hz to $20,000$ Hz. One of the properties of a *comfortable* car is, if no vibrations can be felt or heard, when driving the car.

Simulating realistic vibrations could enhance the driving experience. However, unwanted or unusual vibrations can distract the test-subject from the actual focus of the simulation. Furthermore, vibrations of the vehicle are not the focus of the flow mock-up and these could mislead the test-subjects as they do not focus on the actual experimental object, which is the perception of the flow field. Additionally, vibrations from components used in the design of the flow mock-up should be eliminated.

Noise Noise is considered as an unwanted sound and disturbs people. Anything from quiet but annoying to loud and harmful can be considered as noise. Sound is measured in decibel [dB]. A sound of 0 dB is the threshold of the human hearing. A noise of sound pressure of 100 Pa at a frequency of 1 kHz is considered as pain threshold, corresponding to 134 dB. Common values are 30 dB equivalent to whisper, 60 dB to conversational speech and 160 dB to the volume of a jet transport aircraft.

When driving a cabriolet the noise level is considerably higher compared to closed passenger vehicle. At velocities of 90 km/h up to 120 km/h a sound level of 82 dB to 92 dB have been measured in open cabriolets [45, 46]. While at lower driving velocities the engine sound is dominant, the noise generated due to turbulent air flow around the car becomes dominant at higher velocities. For a closed passenger car wind noise becomes dominant at velocities between 80 km/h to 100 km/h [44]. Therefore, the wind noise for cabriolet is already dominant at lower velocities.

Typical driving velocities in the evaluation of thermal comfort of open cabriolet are above 60 km/h. Therefore, the noise level in a flow mock-up should be similar to the real situation, as the flow field of a cabriolet is to be replicated. However, in order to reproduce the flow field, flow generators have to be used, which could produce an unusual noise. Such a noise can influence the perception of a test-subject in a negative way, as these noises are unexpected, when driving in a cabriolet. In the design of a flow mock-up this should be considered. Flow generators could be placed outside of the room and the air flow can be guided into the room from the outside.

In order to enhance the experience of driving in a cabriolet for the test-subjects, it can be considered to play an engine sound.

Climate The climate describes the environmental conditions surrounding the passenger, such as temperature, humidity, and air velocity. While the climate inside a closed roofed passenger vehicle can be regulated and kept constant due to the closed space, the climate inside the passenger compartment of an open cabriolet is highly dependent on the weather conditions and the season of the year. Furthermore, the exposure to these conditions is enhanced by the turbulent flow field inside the passenger compartment of an open cabriolet, as described in Section 2.4. It is generally known, that a cabriolet is driven with an open roof when it is sunny. From a survey in [12] the temperature is one of the main criteria to open the roof or not. The temperatures a cabriolet is driven with an open roof ranges from 10°C to 35°C.

The study of [11] investigated the perception of draught phenomena in ventilated spaces and concluded that draught phenomena are more significant at lower temperatures and higher turbulence intensity. Although, this study only considers draught phenomena in ventilated spaces, where both the velocity and the turbulence intensity are much lower compared to the situation in an open cabriolet, the essential conclusions on the human sensitivity to draught phenomena due to temperature and turbulence intensity can be mapped onto the situation of an open cabriolet. Thus the climate has a big impact on the overall experience, because an open cabriolet is exposed to extreme conditions due to the turbulent flow field.

For a flow mock-up it is one of the main objects to replicate the climate that is present inside the passenger compartment of an open cabriolet. To replicate a sunny day, a bright light source would be sufficient, as already described with the factor light. Because the temperature, air velocity and the turbulence intensity have a significant influence on the thermal comfort, these factors have to be controlled. This is further elaborated in Section 4.2 separately for the factors temperature, air velocity and turbulence.

Anthropometry This factor deals with the comparative study of sizes and proportions of the human body. The engineering standard of the ergonomics of seated body dimensions have been defined in DIN 33402 [47] and ISO 7250 [48]. The seating position in a cabriolet is especially

important for the comfort. For example, the upper part of the head of a tall person can stick over the windscreen header and thus high velocity flow directly hits the forehead. This is highly uncomfortable especially at high driving velocities. Furthermore, the size of the passenger also has an influence on the overall flow field and consequently the local velocities at different body parts.

In [15] the difference in flow velocities at different body parts of 5th, 50th, 75th and 95th percentile man have been investigated. The results show, that the worst condition, i.e. the highest velocities, is present for 95th percentile men, except at the inboard forehead and inboard shoulder. Velocity differences up to 1 m/s have been measured between the different percentile men. Therefore, it can be concluded that the anthropometry has a noticeable influence on the flow field. To make the measurements comparable and reproducible, they have been limited to a specific group of percentile men.

The investigation clearly shows a difference in velocities for different body heights, therefore it is an important aspect which has to be considered, when designing the flow mock-up. Either the flow mock-up or simulated flow field should be optimized for a specific group of body height or the velocity reproduction has to be adaptable. CFD investigations can identify the worst case scenario, which then has to be reproduced in the flow mock-up with the same group of percentile men. Another option would be, to have an adjustable seat, which can be set for every subject such that every subject's upper body is positioned at the same height.

These basic factors have been put into a so called climate comfort pyramid by [42], as illustrated in Figure 4.1. It shows the basic factors on top of each other and indicates, the lower the factor the higher its importance. If the one at the bottom is satisfactory or unnoticeable, the next higher factor is considered [4]. Although, these factors are satisfactory most of the time due to the overall design, they do not have to be underestimated, as disturbance can quickly divert the test-subject.

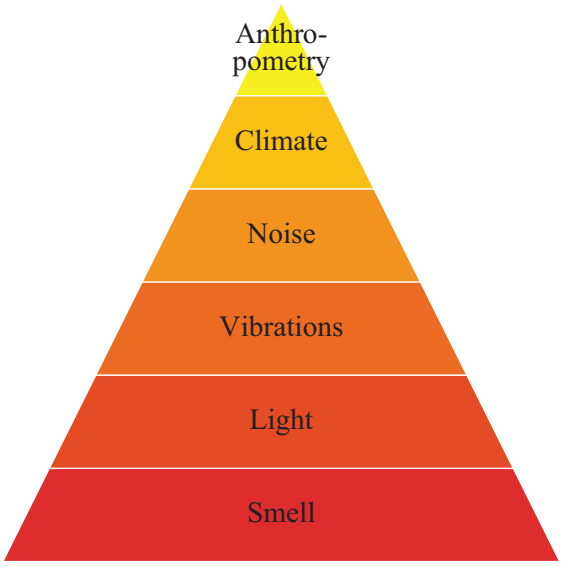

Figure 4.1: Comfort pyramid according to [42]

4.1.2 Influenceable Factors

The factors which are not considered as basic factors are put in the second category. This category includes the factors, which can be actively influenced by the design of the flow mock-up and the way the experiment is conducted.

Metabolism With metabolism it is referred to the processing of chemical energy into heat and mechanical work of metabolic activity within the organisms of the human body. This includes

the processing of food, exchange of heat with the environment by radiation and convection, and heat loss by evaporation of body fluids. The average vital organ temperature of a human body is $37°C$. Metabolism tries to maintain this body temperature, when thermal disturbances occur [49]. Furthermore, metabolism is measured in metabolic rate, which is expressed in terms of the transformation of chemical energy into heat and mechanical work by metabolic activities within an organism per unit area of the total body surface $[W/m^2]$. It is also expressed in $[met]$, where 1 met is equivalent to 58.2 W/m^2 [5].

The metabolism influences sensitivity to temperature. The metabolic rate increases with workload. The higher the metabolic rate, the higher the heat produced by the organism, thus the higher the body temperature. Therefore, a higher metabolic rate makes it possible to sustain lower temperatures, which is also confirmed by [50]. Furthermore, elderly people are less active thus they produce less metabolic heat, apart from that age has no direct effect on the perception of draught [51].

The metabolic rate in the flow mock-up can be influenced by setting up a driving simulation, which is connected to the steering wheel and the pedals of the flow mock-up. The more demanding it is, e.g. racing, the higher the metabolic rate, thus the test-subject is more resistive to lower temperatures. The metabolic rate for driving is between $60-115$ W/m^2, or equivalent to $1-2$ met, as can be found in [5]. In order not to focus the attention of the subject too much onto the driving simulation, a simple driving simulation like a ride on a country road should be sufficient for the flow mock-up.

Clothing/Isolation In an open cabriolet the passenger is exposed to the outside weather conditions. Passengers adapt their clothing to the present weather conditions and in an open cabriolet a scarf is considered to protect the neck from draught phenomena.

Clothing protects and isolates the human skin from thermal disturbances. The more the human skin is covered with clothes, the less sensitive is the to changes of the flow. Typical isolation values of different clothing can be found in [5].

When performing the experiments with the flow mock-up the test-subject has to be informed about the tested climate and wear appropriate clothes. Furthermore, in the experimental study of [52] the subjects have been given the opportunity to modify their clothing in the beginning of the experiment, such that they felt thermally neutral. Thereafter, the clothing has been kept constant and other experimental conditions have been tested. This can be applied also when placing subjects into the flow mock-up. In this way, every subject is given a starting point to which the different tested conditions can be compared. Any deviation from this can then be evaluated as more comfortable of less comfortable. The test conditions should be the same for every test subject, therefore, they have to be monitored and controlled.

Expectation The expectation determines, how a person adjust to a situation. For example, in closed spaces, like offices, velocities up to 0.4 m/s can cause draught and can be perceived as highly uncomfortable [53]. However, in an open cabriolet significant higher velocities are accepted [20]. The passenger expects to be exposed to air flow in an open cabriolet and thus he adjusts himself to the situation. Therefore, the expectation has an influence on the sensitivity of the person.

The expectation can be influenced by the appearance of the flow mock-up. Furthermore, the subjects have to be clarified about the tested conditions and what to expect.

4.1.3 Non-Influenceable Factors

The factors which cannot be influenced by the design of a flow mock-up are the **mood** and the **health** of the test-subject. Both factors can influence the way subjects react, e.g. when the subject is in a bad mood or ill, the subject can react more sensible.

These two factors can be considered in the evaluation by asking the subjects about their current mood and health and if the subject thinks that it has any effect on their perception. Furthermore, the impact of these factors can be reduced by performing the tests on multiple days and with multiple test-subjects.

4.2 Physical Influence Factors

In an open cabriolet the passenger are exposed to the flow field as described in Section 2.4. The different physical factors, which act on the passengers and consequently influence the perception of the experience, can be split into the properties of the flow field, which are the velocity and the pressure, and the properties of the environmental conditions, including temperature, air humidity and solar radiation.

Flow velocity From the measurements conducted in [12, 15, 16], which are analysed in depth in Chapter 5, the averaged local velocities around the passenger in the front range from 0.5 m/s to 12.6 m/s for driving velocities of 60 km/h to 120 km/h depending on the body position, which is 3% to 40% of the driving speed. This can be confirmed by the conducted measurements as described in Section 5.1. In [23] velocities up to 15 m/s are measured for passengers in the back of a four seater cabriolet. Subjects perceive velocities above 6 m/s as highly uncomfortable, as is the result of a survey from [12, 15]. Furthermore, these velocities are not uniform but fluctuating due to the turbulence created by the shear layer, which is considered to be more uncomfortable than uniform flow [6, 11, 52]. The turbulence intensity increases with the driving speed [15], consequently the thermal comfort at higher driving speeds decreases. The uncomfortable feeling due to the flow velocity is because the flow velocity cools down the exposed human skin due to heat dissipation.

The reason velocity fluctuations are felt even more uncomfortable is, because of the alternating temperature sensed at the skin as lower velocities dissipate lesser heat than higher velocities [11]. The velocity fluctuates in an open cabriolet for example at the drivers head between 4.5 m/s and 10 m/s at a driving speed of 100 km/h and between 5 m/s and 15 m/s at a driving speed of 130 km/h [10]. According to [54] frequencies between 0.08 Hz and 2.1 Hz are felt by the human as fluctuations, while higher frequencies are felt as uniform fluctuations. Frequencies of 0.3 Hz and 0.5 Hz at air velocities between 0.05 m/s to 0.4 m/s have been identified as maximum discomfort levels [53, 55]. Investigations of what kind of air velocity fluctuation frequencies are present in cabriolets have not been found.

Pressure The pressure inside the passenger compartment is lower than the ambient pressure, as a result of the separation bubble as described in Section 2.4. In [23] pressure coefficient values have been measured around the passengers at the front seat, ranging from -0.36 to -0.4, which is a pressure reduction of 245 Pa to 272 Pa from the atmospheric pressure of $101,325$ kPa, depending on the body part. At the rear seats the pressure coefficient ranges from -0.3 to -0.5, equivalent to 204 Pa to 340 Pa. As a consequence of the velocity fluctuations dynamic pressure fluctuations are also present. These pressure fluctuations influence the thermal comfort as well and are also sensible for a human in the frequency range from 0 Hz to 10 Hz [15]. In the study of [11] dynamic pressure fluctuations are already sensed at low velocities of 0.4 m/s, while these increase at higher velocities. No exact measurements of pressure fluctuations inside the passenger compartment of an open cabriolet have been found. Unsteady CFD simulations in [23] indicated pressure fluctuations between C_p-values of -0.47 and -0.55 for the inboard ear when no draft stop is present, which is equivalent to absolute pressure difference of 37 Pa. In A constant pressure drop of 235 Pa is not

perceived as uncomfortable by the passengers, however, the fluctuations is the factor described as uncomfortable.

Because the underpressure and pressure fluctuations are the result of the generated flow field, the flow mock-up should not actively be able to influence the pressure. However, it is a factor which influences the perception of an open cabriolet ride, which therefore has to be verified.

Temperature In combination with the air velocity the temperature is a crucial part of causing draught. In the study of [56] a group of subjects have been exposed to air velocities ranging from 0.05 m/s and 0.4 m/s at temperatures of 11°C and 17°C while performing a task with an estimated metabolic rate of 90 W/m^2, which is equivalent to the metabolic rate when driving a car. The study shows that at lower temperatures subjects are more sensitive to draught than at higher temperatures, which is also verified by multiple other studies [11, 50]. The reason for this perception is that the temperature of the skin, which is exposed to the low temperature air velocity, cools down due to convection of heat. The study of [57] shows that a deviation of ±1.5°C from the ideal skin temperature of 33.4°C leads to dissatisfaction. Furthermore, fluctuating air velocities cause the skin temperature to fluctuate as well, which is registered by thermoreceptors in the skin and is felt more uncomfortable than uniform air flow. For further explanation of the function of thermoreceptors it is referred to [4, 58]. This effect of discomfort at low temperatures is also the a reason why cabriolets are mainly driven in periods of higher temperature. In closed spaces people tend to complain about draught at low temperatures up to 23°C already at low air velocities up to 0.25 m/s. At temperatures above 30°C draught phenomena of air velocities around 1.6 m/s are considered to be acceptable and comfortable, although pressure fluctuations due to the higher velocities may be felt as unacceptable [59].

The temperature therefore is an important factor for the flow mock-up as it is a driving factor for the perception of draught, especially for extreme conditions which are present in an open cabriolet. It is directly related to the climate conditions, which are desired to be replicated. The temperature can be influenced by a heating or cooling system. One option would be to place the whole flow mock-up into the climate chamber or connect the two systems with each other. If the flow mock-up has to be placed into a climate chamber, the flow mock-up needs to be mobile and the size should be such that it can be fitted into existing climate chambers.

Air humidity The way how the ambient temperature dissipates heat from the skin is also related to the humidity of the air. The air humidity influences the transfer of heat between skin and surrounding air, as water droplets dissipate heat faster. The engineering standard of ASHRAE Standard 55 [5] defines relative humidity as *the ratio of the partial pressure of water vapour in a gaseous mixture of air and water vapour to the saturated vapour pressure of water at a prescribed temperature*. With respect to draught phenomena air humidity between 30% to 70% is considered to have low influence. Above 70% air humidity in combination with temperatures above neutral temperature the air is considered as sultry, increasing the discomfort level. Values lower than 30% cause dry sensation which can irritate bronchial ways and thus to discomfort [60]. For the flow mock-up the air humidity thus has to be monitored and adjusted to the desired climate conditions.

Solar radiation In [10, 14] the solar radiation has been mentioned to play a major role on the thermal comfort in open cabriolets, as direct insolation of certain body parts causes discomfort. However, no direct measurements have been found of the insolation while driving in an open cabriolet. Furthermore, the solar radiation does not have a direct influence on the draught phenomena. The simulation of solar radiation could enhance the experience of the simulated climate, but does not affect the perception of the flow field.

4.3 Draught-sensitive Body Parts

The most common body part at which the human is sensitive to draught phenomena when driving an open cabriolet has been identified to be the upper body, including the head, neck and shoulders [12]. These are also the most common position, which are investigated in the studies of draught in closed spaces [6, 11, 52, 53]. The reason for this is that the skin of these body parts are exposed to the air flow while the other body parts are usually covered and isolated by clothes. Especially in the passenger compartment of an open cabriolet, the velocities at the upper body are significantly higher, compared to the velocities near the lower body, which is why the upper body is mentioned the most by the passengers [12].

The sensitivity of the different body parts when driving in an open cabriolet are analysed in depth in Chapter 5.

Chapter 5

Analysis of Measurement Data

In this chapter measurements conducted on cabriolets are analysed in detail. First, in Section 5.1 measurements are conducted on an open road in order to measure the changes in velocity in an open cabriolet due to different draught reduction components. Thereafter, in Appendix A.1 measurement data from [12, 15, 16] are analysed in detail to determine sensitivity requirements on the accuracy of the flow mock-up.

5.1 Measurements

In order to get acquainted with the velocity field and its flow phenomena of an open cabriolet, as well as which component has what kind of influence velocity measurements are conducted. For these measurements a Porsche 911 Carrera Cabriolet (991-1) is used and the velocity measurements are taken with a hand-held low-speed vane anemometer at the positions indicated in Figure 5.1. The velocities at these positions are measured for multiple configurations, see Table 5.1, and at driving speeds of $50km/h$ and $120km/h$. The results are plotted in Figure 5.2 and Figure 5.3, respectively. The measurements are taken on the open road, thus they are influenced by surrounding conditions. The conditions on that day are recorded with a northern wind of $11 - 15\ km/h$, a temperature between $17°C$ and $19°C$ and an air humidity between $56 - 60\%$.

Table 5.1: Tested cabriolet configurations

	Wind break	Side windows up	Rear triangle windows up
Config A	✓	✓	✓
Config B		✓	✓
Config C		✓	
Config D			
Config E	✓		

These measurement positions have been chosen in analogy to the described flow field and should be an indication of the main flow phenomena that surround the passenger. Position 1 is an indication of the velocity magnitude of the backflow into the passenger cabin, while position 2 shows the influence of the vertical position at the inside position. Position 3 points out how far the flow propagates into the passenger cabin. Position 4 has been chosen to demonstrate how the flow behaves near the windscreen. From position 5 an impression of the flow that returns to the back is obtained, while position 6 should indicate the condition at the head of the passenger.

The figures indicate the average velocity and the highest and lowest measured velocity for the respective configuration and for the respective position. In both Figure 5.2 and Figure 5.3 a similar trend line from position 1 to 6 can be noticed. This trend line is proportional to the driving speed as well as to the configuration. Take for example configuration D, where all the windows

Figure 5.1: Positions of the measurements taken in a Porsche 911 (991-1) Cabriolet

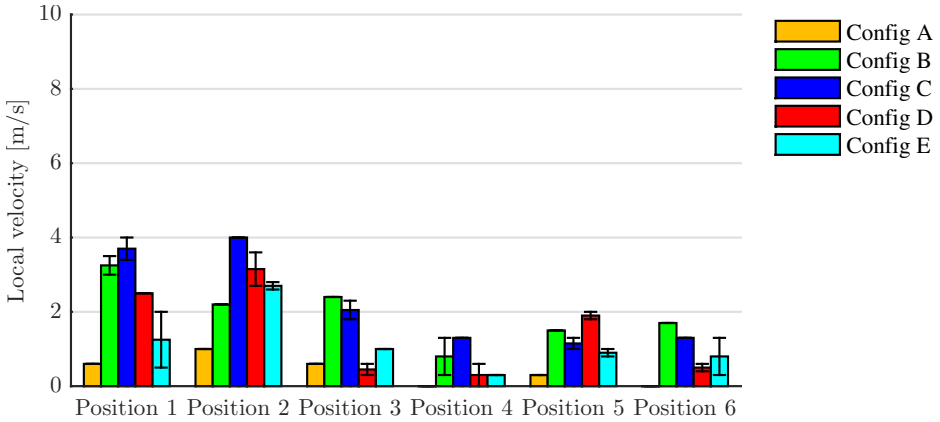

Figure 5.2: Measurements taken in a Porsche 911 (991-1) Cabriolet at driving speed of 50 km/h

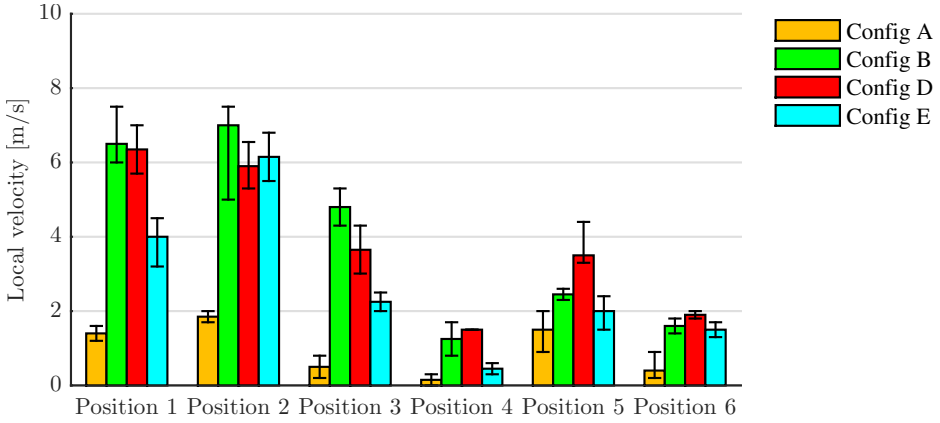

Figure 5.3: Measurements taken in a Porsche 911 (991-1) Cabriolet at driving speed of 120 km/h

are retracted, and no wind break is used. As for configuration A, where every components is used, the velocity magnitude measured for both configurations at position 2 is higher than the velocity measured at position 1 and 3. Every position for every configuration behaves the same to each other. This can also be confirmed in the research of [12, 15, 23].

Furthermore, one would expect, that configuration D would show the highest velocity magnitudes, because this is the configuration with the least restrictions. The only component that is in between the high velocity flow and the passenger cabin is the windscreen. The flow is not restricted to flow along the side windows. However, configuration C has been the configuration with the highest velocities at driving speed of 50 km/h and configuration B for driving speed of 120 km/h. Due to limited time configuration C could not be measured at driving speed of 120 km/h.

The influence of the wind break as draught reduction component shows significant improvement. This can be seen when comparing configuration B with configuration A. However, the influence is only given in combination with all windows up, as can be seen by comparing configuration E - only with a wind break - with configuration D.

When comparing positions 1 to 3 with position 5 a significant difference can be noticed. This is the difference between the inboard and the outboard position. This is confirmed by the findings from [12, 15, 23], which shows that for every different vehicles the the inboard velocity is always bigger than the outboard velocity.

The following insights from this measurement series can be concluded:

1. the velocity magnitude inside the passenger cabin is proportional to the vehicle configuration as well as to the driving speed
2. the advantage of draught reduction component like the wind break is only employed in combination with the windows up
3. the inboard velocity magnitudes are bigger compared to the outboard velocity magnitudes

5.2 Sensitivity Analysis of Reference Measurement Data

The research of [12, 15, 16] have produced valuable measurement data which can be used to find the sensitivity of different body parts to flow velocity as well as the velocity range which is present in the passenger compartment of an open cabriolet. These properties can be interpreted to set physical requirements for the flow mock-up. The aim of these research papers has been to formulate a mathematical model, which can be used to determine a comfort number for a vehicle only with the use of measurements conducted with a manikin. This has been done by correlating measured velocities at specific body position with subjective perception of test subjects. The measurements have been conducted at 11 measurement points for each cabriolet at three different velocities, 60 km/h, 90 km/h and 120 km/h, as well as with and without a windbreak. A total of 600 questionnaires have been evaluated and summarized in a value called the local Percentage Dissatisfied (PD_l) for every body position, as well as every driving speed and configuration. This results in 1056 values or 48 velocity magnitudes with their respective subjective evaluation for every measurement points which can be interpreted. The vehicles used for the experiment can be found in Appendix A.

5.2.1 Determination of Body Part Sensitivity & Flow Mock-Up Accuracy

In order to be able to determine the accuracy a flock mock-up should have, a general sensitivity criterion for every respective body part needs to be formulated. For this a curve is fitted through all measurement data of every vehicle, every configuration and every driving speed. The best curve fitting type was determined in [12] and equals to:

$$PPD_l = \frac{100}{1 + (a/V_l)^b} \tag{5.1}$$

where $PPD_l\%$ is the local Predicted Percentage Dissatisfied and $V_l\%$ the local velocity, while the coefficients a and b are fitted to the respective measurement data. This equation has been chosen according to [12], because of two reasons:

1. it guarantees a starting point in the origin as it is assumed that for a velocity of $0m/s$ the percentage dissatisfied due to draught is also equal to zero
2. it does not exceed a value of 100 as it is not possible to have more than 100% dissatisfied people

As an example, the results of the inboard neck and the outboard shoulder are depicted in Figure 5.4. From the plots a high variation in measurement data can be observed, which is because the measurement data for all vehicles, all configurations and all driving velocities have been summarized in the plot. This variation perfectly reflects the *inter-* and *intraindividual* behaviour. While in [12, 15, 16] further measurement data, like the local velocity, local acceleration and local number of gusts, have been used to deal with the variation and improve the correlation, this is not done for this research, as it is desired to have a value that represents the velocity margin instead of a value that is dependent on multiple variables.

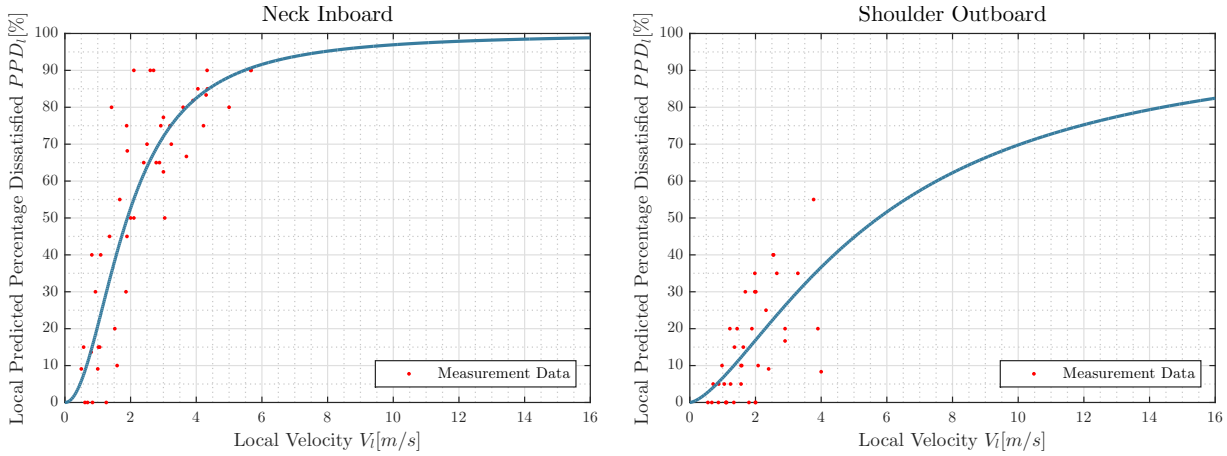

(a) Inboard neck **(b)** Inboard forehead

Figure 5.4: Velocity magnitude versus the respective local percentage dissatisfied for the inboard neck and the outboard shoulder

The coefficients a and b for every curve a given in Table 5.2.

To find the sensitivity, the slope of the fitted curve can be analysed. The slope in Figure 5.4a is noticeably steeper compared to the slope in Figure 5.4b. Taking for example PPD_l of 50% and 80% these correspond to a velocity magnitude of 2 m/s and 3.6 m/s, respectively, in Figure 5.4a, while in Figure 5.4b the corresponding velocity magnitudes are 5.6 m/s and 14 m/s, respectively. This means, the same percentage dissatisfied for the inboard neck rate a lower velocity as uncomfortable, while for the outboard shoulder the same percentage rate a more than two times higher velocity as uncomfortable. Thus a steep curve indicates a high sensitivity, while a flat curve indicates a low sensitivity. In order to compare the sensitivity of different body parts based on a general value, the slope at the at the inflection point can be used. This location indicates the point with the highest slope, thus the point of the highest sensitivity.

Furthermore, the curve can be generally divided into three section of different slopes, two outer sections and one middle section. The slopes in the outer sections are considerably flatter compared

Table 5.2: Coefficients for Equation (5.1) for the respective body part

Position	a	b
Head	3.8513	2.9327
Forehead Inboard	3.6922	2.2999
Forehead Outboard	4.1316	1.9594
Back of the Head Inboard	2.5900	2.9858
Back of the Head Outboard	2.6528	2.4425
Cheek Inboard	2.4070	2.3733
Cheek Outboard	4.1110	2.4722
Neck Inboard	1.9026	2.0819
Neck Outboard	2.2986	1.9985
Shoulder Inboard	5.2810	1.6027
Shoulder Outboard	5.7464	1.5110

to the slope in the middle section. While the first section is small, the 3rd section is the biggest. In order to define a general criterion to divide these sections, the first derivative of the curve can be used as it is an indication of the slope in every point of the curve. A good division of the regions has been achieved by defining the boundaries at the points indicating the boundary of 25% of the maximum slope. These points are located at the transition of the steepest part of the curve to a flatter region. Thus the middle section represents 75% of the sensitivity, while the two outer sections together represent 25%.

Additionally, the points indicating ±5% from the inflection point are defined as a general deviation from velocity at the inflection point.

The final graph of the inboard neck with the these boundaries as well as the inflection point is given in Figure 5.5. The other plots can found in Appendix A.1. The results for every body part are summarized in Table 5.3.

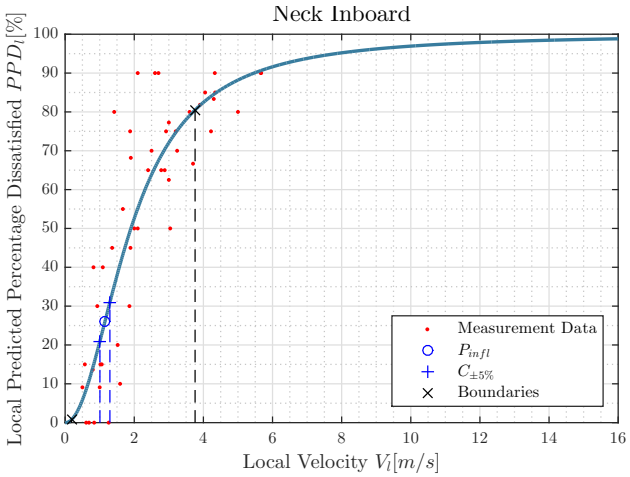

Figure 5.5: Velocity magnitude versus the local percentage dissatisfied for the inboard neck

Table 5.3: Summarized results from graphs for all body parts

Position	Slope at P_{infl}	V_{infl} $[m/s]$	$C_{\pm 5\%}$ $[m/s]$	V_{lb} $[m/s]$	V_{ub} $[m/s]$	$PPD_{l,lb}$ [%]	$PPD_{l,ub}$ [%]
Head	21.43	3.02	±0.23	0.99	6.97	1.85	85.04
Forehead Inboard	18.94	2.46	±0.27	0.52	7.15	1.07	82.07
Forehead Outboard	15.58	2.33	±0.32	0.31	8.23	0.61	79.41
Back of the Head Inboard	32.31	2.05	±0.16	0.69	4.66	1.90	85.22
Back of the Head Outboard	27.36	1.86	±0.18	0.44	5.06	1.26	82.91
Cheek Inboard	29.61	1.65	±0.17	0.37	4.63	1.17	82.51
Cheek Outboard	17.79	2.91	±0.28	0.71	7.82	1.30	83.06
Neck Inboard	34.79	1.15	±0.14	0.19	3.76	0.78	80.50
Neck Outboard	28.25	1.33	±0.18	0.19	4.57	0.67	79.78
Shoulder Inboard	11.54	2.12	±0.44	0.11	10.45	0.19	74.90
Shoulder Outboard	10.60	2.00	±0.47	0.06	11.18	0.11	73.23

These results show the following:

- The slope at the inflection point is an indication for sensitivity - a higher value indicates a higher sensitivity.
- The confidence bound can be used as a velocity range which deviates 5% from the PPD_l at the inflection point, thus from the worst case scenario. It indicates that if the accuracy of the flow mock-up deviates for example ±0.23 m/s from the average velocity of 3.02 m/s at the inflection point, the percentage of dissatisfied has a variation of 10%.
- The inner section indicates the velocity margin in which the respective body part is the most sensitive.
- The upper bound tells us the velocity after which a higher value would have no big influence on the perception of the velocity.
- The lower bound tells us below which values are considered as unnoticed.

From the slope at the inflection point the following order of sensitivity can be determined:

1. Neck inboard
2. Back of the head inboard
3. Cheek inboard
4. Neck outboard
5. Back of the head outboard
6. Head
7. Forehead inboard
8. Cheek outboard
9. Forehead outboard
10. Shoulder inboard
11. Shoulder outboard

It can be noticed that in all cases the inboard position has a higher sensitivity compared to the outboard position. This can be related to the fact that the velocity at the outboard position with respect to the inboard position is lower or more generally that the flow phenomena at the inboard position have a bigger influence on the perception of comfort than the flow phenomena at the outboard position. Additionally, the test-subjects always rate the local situation in comparison to the total situation. This means, that the test-subject is always most influenced by the most uncomfortable body part and rates the other body parts with respect to the most uncomfortable body part.

5.2.2 Flow Mock-Up Velocity Range

The measurement data can be further used to determine the velocity range in which a flow mock-up has to operate as well as to be able to replicate the flow field of different vehicles. Therefore, the measured velocities at every body part are plotted for every configuration and for every vehicle. The plot of the head is given below in Figure 5.6 and the plots of the other body parts can be found in Appendix A.2.

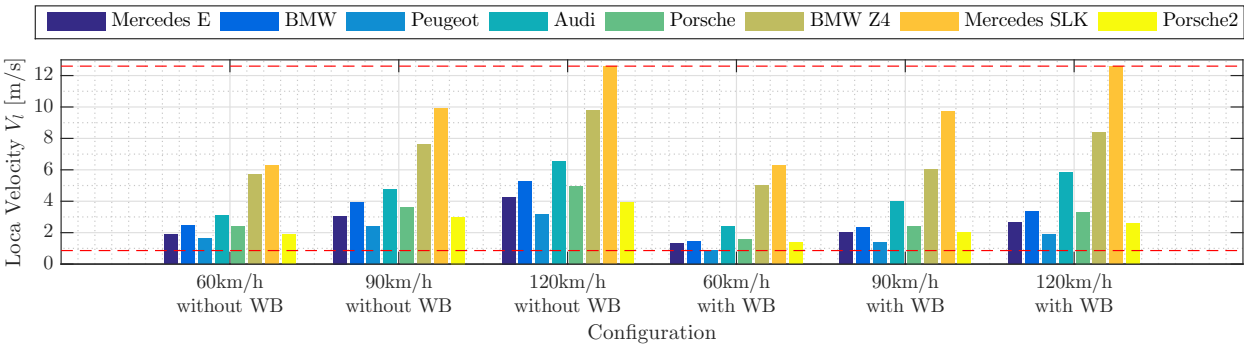

Figure 5.6: Measured average velocities at the head for every vehicle at every velocity and every configuration

In the plots the overall minimum and maximum are both marked with a horizontal line. These minima and maxima are summarized for every body part in Table 5.4.

Table 5.4: Minimum and maximum velocity measured for every vehicle and every configuration

Position	V_{min} [m/s]	V_{max} [m/s]
Head	0.86	12.60
Forehead Inboard	0.80	9.61
Forehead Outboard	0.60	7.35
Back of the Head Inboard	0.70	7.78
Back of the Head Outboard	0.70	4.40
Cheek Inboard	0.50	6.12
Cheek Outboard	0.51	3.50
Neck Inboard	0.50	5.67
Neck Outboard	0.54	4.39
Shoulder Inboard	0.50	6.77
Shoulder Outboard	0.55	4.00

The highest velocity is measured at the head, which seems logical as it is the closest to the high velocity flow and the shear layer that flows over the vehicle and the lower the body part the lower

the measured velocity. From the values of Table 5.4 follows the velocity range a flow mock-up has to be able to replicate if driving speeds of 60 km/h, 90 km/h and 120 km/h should be simulated. Although, other vehicles, which have not been measured, could exceed these velocities, it can be expected that the maximum velocity will not be exceeded, due to the development of the comfort in cabriolets.

These values can be compared with the upper and lower velocity bounds of the sensitivity of the respective body part from Table 5.3. For the outboard position of the forehead, back of the head, cheek, neck and shoulder as well as the inside shoulder the measured velocities fall inside the sensitivity range. For the head and inboard positions forehead, back of the head, cheek and neck the highest measured velocities are 1.5 m/s to 5.6 m/s higher than the upper sensitivity boundary. Thus the flow mock-up has to be accurate in the whole velocity range for replicating the flow around the outboard positions forehead, back of the head, cheek, neck and shoulder as well as the inside shoulder. For the positions head and inboard positions forehead, back of the head, cheek and neck the flow mock-up can become less accurate at the higher velocities, as beyond the upper sensitivity boundary test-subjects rated the perception as uncomfortable and small changes did not have a big influence, as can be seen in Figure 5.5 and Appendix A.1.

Furthermore, from the figures a linear increasing trend for every vehicle from 60 km/h to 120 km/h can be identified, for both configurations. This confirms the observation as described in Section 5.1.

From the measurement data no general characteristic of difference between the vehicles can be identified. The measured velocities for every vehicle do not indicate similar differences at different body positions. The velocities at the different body part are randomly distributed for different body parts as well as for the different configurations. For example, at the inboard forehead the highest velocities have been measured for every driving velocity and configuration in the Porsche. However, for the outboard forehead, the highest velocities have been measured in the Mercedes E-Class for the configuration without the wind-break, while the highest velocities with a wind-break have been measured in the Peugeot at the same body position. This can be extended to the other body positions. Thus, in order for the flow mock-up to be able to replicate different vehicles, the flow mock-up should be able to generate a flow field, which can be controlled individually. To achieve this, multiple flow generator have to be used, which have to be controlled independently to generate different velocities.

Inboard & Outboard Comparison As already mentioned before, the overall velocity at the inboard position is higher than the outboard position for all body positions. This difference between the inboard and outboard position can be further investigated by plotting it for every vehicle and every configuration. The plot for the shoulder is depicted in Figure 5.7 and the plots of the other four body parts can be found in Appendix A.3.

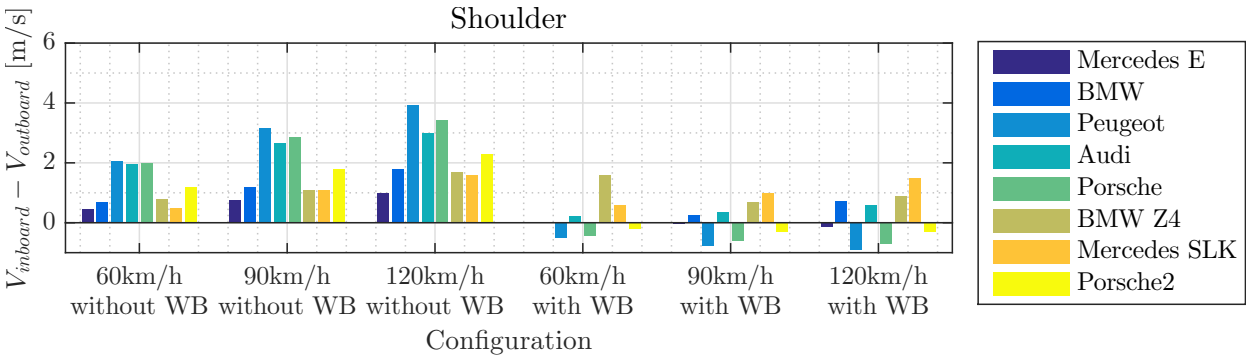

Figure 5.7: Velocity difference between inboard and outboard at the shoulder for every tested vehicles

A general observation is, that for the vehicle configuration with a wind-break the difference between the two sides is lower and the difference becomes bigger with increasing driving speed. For the vehicle configuration without a wind-break the plots indicate a higher velocity at the inboard position for every body part - with an exception at the neck in the case of the Mercedes E-Class - at every driving speed for every tested vehicle. In the case with a mounted windbreak however, the difference between inboard and outboard position varies between cars as well as body part. At the forehead, for two out of the eight vehicles, the inboard position is slightly lower than the outboard position. For the position at the back of the head the inboard position is still bigger than the outboard position, except for the Mercedes E-Class, for which the difference is even close to zero without a wind-break. The measurements at the cheek show a higher outboard velocity for two vehicles, while the neck position for six of the eight vehicles the outboard velocity magnitude is higher compared to the inboard position.

This difference in velocity between the inboard and outboard indicates, that the flow mock-up should distinguish the flow velocities at the inboard and the outboard. As described in Section 2.4, the air flows from the inside rear to the front inside, where it turns to the outboard and back again, where it starts to circulate.

Chapter 6

Functional Requirements of the Flow Mock-Up

The results of the previous chapters can be combined to generate a detailed picture of the flow mock-up. This includes the requirements, which have to be fulfilled by the flow mock-up in order to be advantageous for the development as well as to be able to replicate the flow field of a cabriolet and give the subject the impression to be seated in an open cabriolet.

The project related aim of the flow mock-up is to be able to take an early assessment of what is needed to improve the thermal comfort in an open cabriolet, such that it can be integrated into the packaging of the base model. In order to achieve this aim two scenarios are given, which are considered to be advantageous for the development process. The first scenario consists of the ability to directly compare different configurations and different vehicles with each other and to subjectively determine which is better. Therefore, the flow mock-up should be able to replicate multiple flow situations. For this the flow mock-up has to be *independent of the vehicle geometry*, such that no complicated reconstructions are needed for different configurations or vehicles. The latter is needed, because the best comparison can be made, if the flow mock-up can switch from a flow field of vehicle A to the flow field of vehicle B instantly.

The second scenario is the possibility of *reverse engineering*. The aim is to directly process the perception of discomfort at specific body parts and to modify the flow field accordingly. To achieve this, the flow mock-up should be able to be be controllable in such a way that velocities at certain positions can be adjusted independently. This scenario is a more advanced version of a flow mock-up.

Furthermore, the flow mock-up should reduce the demand on the experimental windtunnel testing in the development process of the cabriolet. Therefore, the flow mock-up needs to be competitive. Therefore, it not only should be possible to replicate the flow field with the flow mock-up, but the flow mock-up should also be less costly. Next to advantage of the flow mock-up that no windtunnel model is needed, i.e. less costs, the operation costs of the flow mock-up should be less. To achieve this, the flow mock-up should not be as big as a windtunnel. Since we are only interested in the flow inside the passenger compartment, where the velocities are between 3% to 40% of the driving velocity, the flow mock-up does not have to produce the same flow as a windtunnel. Therefore, the dimensions of a flow mock-up are set to the dimensions of a European garage for one car, which are 2.55 by 3 by 6 meters (HxWxL).

For the flow mock-up to satisfy the human influence factors, as described in Section 4.1, the essential task of the flow mock-up is that the test-subjects can associate the flow mock-up with a real cabriolet ride. The first impression of the test-subject is formed by the appearance of the flow mock-up. Therefore, the appearance should be very similar to a an open cabriolet. The most convenient option is to use a cut-out of a cockpit of an actual cabriolet. This can look similar as the simulator from Ansible Motion displayed in Figure 6.1 and is already common in a design of simulators, see for example the formula 1 vehicle simulator of Red Bull . Furthermore, to

enable benchmarking of different vehicle models and manufacturers, the cockpit design should be kept general, e.g. no specific manufacturer. Additionally, a screen can be placed in front of the

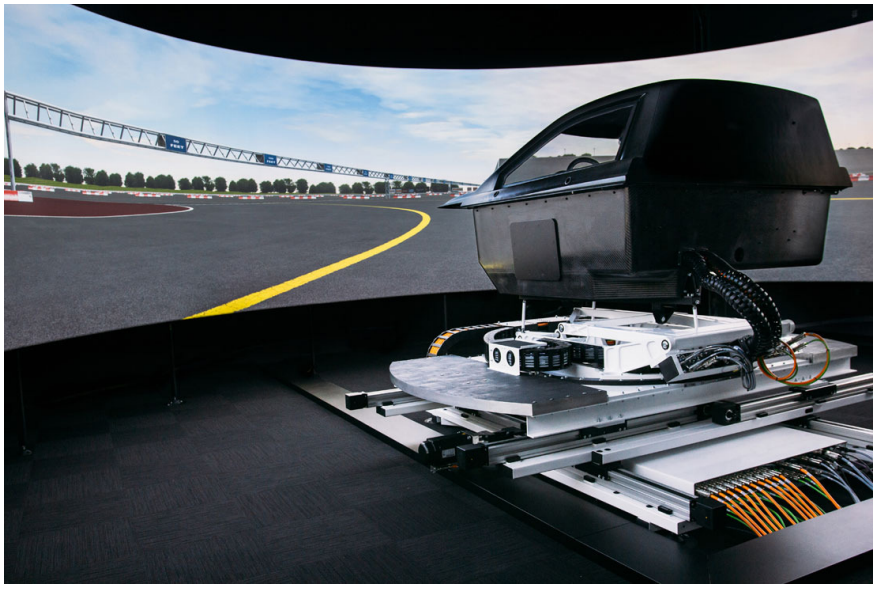

Figure 6.1: Simulator with a cut-out of the front vehicle from Ansible Motion [61]

vehicle, displaying a road simulation, which can be connected with an interactive action for the test-subject. This can be done with the use of a driving simulation or game that gives the subject the opportunity to steer and accelerate. This would also enable to regulate the metabolic rate, as it is directly connected to the activity of the subject.

Another option would be to use virtual reality, as can be seen in Figure 6.2. The design of the flow mock-up can be kept simple as can be seen on the left of the figure, while the virtual reality would give the subject the perception that he is situated in an open cabriolet. The advantage would be that components to replicate the flow field can be placed everywhere. However, subjects could keep the simplistic appearance of the flow mock-up in mind and can be misled by it as they cannot associate the situation with the experience of driving in an open cabriolet. Furthermore, the virtual reality headset would isolate the eye region from the air flow.

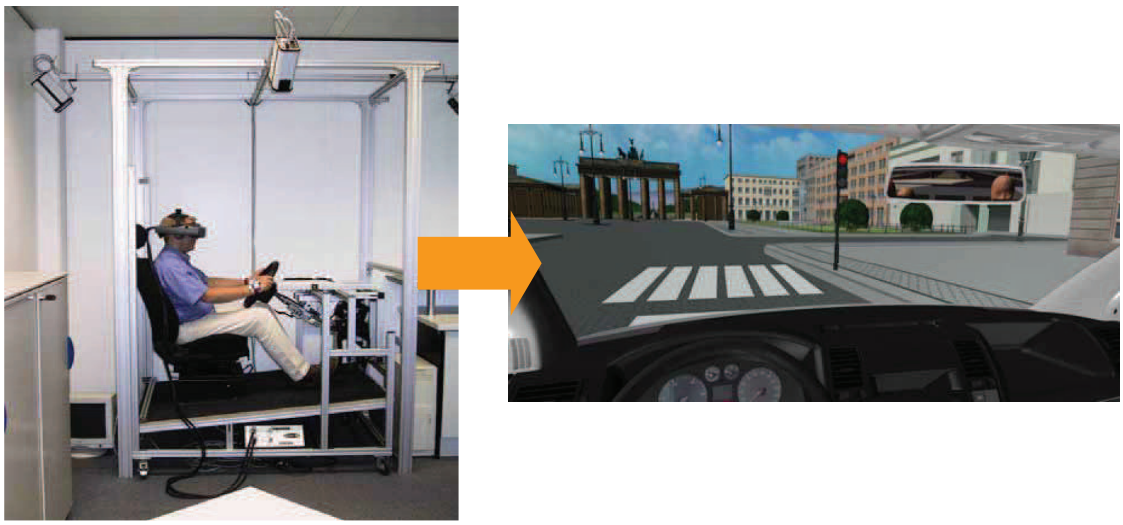

Figure 6.2: Use of a ergonomic mock-up with virtual reality [2]

The most challenging task of the flow mock-up is to replicate the physical phenomena, which are present when driving an open cabriolet, see Section 4.2. The environmental factors like temperature and humidity are directly related to the perception of draught while the solar radiation can be regarded as secondary, because it does not influence the perception of draught. Therefore, the temperature and air humidity in the room of the flow mock-up should be controllable and should represent the desired climate conditions, which are to be tested. Moreover, the flow mock-up should be able to replicate the flow-field, which is characterised by velocity and pressure fluctuations. Therefore, average velocities in the range of 3% to 40% of the driving velocity, e.g. from 1.67 m/s to 13.33 m/s at a driving velocity of 120 km/h, have to be replicated with velocity fluctuations of -2 m/s to $+3$ m/s from the average velocity. The fluctuations are the crucial part as they have been identified as the most influential factor of the thermal comfort inside the passenger compartment of an open cabriolet.

From the analysis of the measurement data from [12, 15, 16] in Chapter 5 the sensitivity of the different body parts have been determined, which determine the accuracy of the flow mock-up at specific body parts. At the most sensitive body part, which is the neck, the flow mock-up should be accurate within ± 0.14 m/s from the average velocity in order to be within a $\pm 5\%$ confident bound of the predicted percentage dissatisfied. The lowest accuracy of ± 0.47 m/s has been determined for the outboard shoulder. Furthermore, the analysis indicates, that in order to replicate different vehicles, the flow mock-up should be able to generate a flow field that can be controlled independently, as the measured velocities at the different body positions do not show characteristic differences between the vehicles. This requirement was also identified for the second scenario proposed for the development process.

Summarizing the functional requirements on the flow mock-up, it can be said that the flow mock up should

- be independent of the vehicle's geometry but give the impression to be seated in a cabriolet,
- be able to control the flow field individually, i.e. change velocities independently,
- fit in a room with the dimensions of 2.55 by 3 by 6 meters (HxWxL),
- replicate velocities from 3% to 40% of the driving velocity
- have an accuracy of ± 0.14 m/s from the average velocity in order to be within a $\pm 5\%$ confident bound of predicted percentage dissatisfied.

Chapter 7

CFD Analysis of the Flow Mock-Up

The idea of a flow mock-up is to give a test-subject the feeling to be seated in a driving and open cabriolet. This can be achieved by satisfying the human perception on one side and by replicating the physical conditions on the other side, as described in Chapter 6. The latter can be analysed with the use of Computational Fluid Dynamics (CFD). With CFD the flow around objects can be predicted by numerically solving simplified Navier-Stokes Equations. In this case, CFD can serve as a tool to investigate the possibility of replicating the surrounding flow field around a passenger of a cabriolet without the dependency of the vehicle geometry. Basically, in this analysis the computational domain is reduced from a windtunnel-like domain with the flow around the total cabriolet model to a domain, which only surrounds the passenger and which would represent a possible set-up of a physical flow mock-up. Next to the reproducibility of the flow field without the main influencing geometry, it is the aim to find possible positions of flow generators where boundary conditions have to be set to produce a similar flow field for the actual physical set-up of a flow mock-up.

First, in Section 7.1 the procedure is described, how this analysis is conducted. Section 7.2 provides the numerical set-up and Section 7.3 elaborates on a mesh sensitivity study. After the mesh is chosen for further analysis, Section 7.4 elaborates on an analysis of the important region to identify the key features that influence the flow field in the passenger compartment, such that a flow field can be replicated in a reduced domain, which is done in Section 7.5. In Section 7.7 the implications of the CFD results on the physical flow mock-up are drawn. Finally, in Section 7.6 the unsteady flow phenomena for a reduced domain are briefly reviewed.

7.1 Methodology

The aim of this analysis is to identify locations, where flow generators in the physical flow mock-up need to be placed in order to replicate the flow field of an open cabriolet ride. To achieve this, a simplified model of a cabriolet vehicle has been created with the use of Dassault Systems CatiaV5, as can be seen in Figure 7.1. The model has side windows, two seats and two manikins, representing 95 percentile males, which are placed at the driver and the passenger position. The edges of the model are rounded in order not to trigger flow separation due to sharp edges. The idea of the simplified model is that the general flow phenomena, as described in Section 2.4, can be reproduced and observed while keeping the computational costs low. Components such as the wheels, complex shaped underbody, side mirrors, etc. would increase the computational costs while they do not directly influence the flow in the passenger cabin, see Section 2.4. Thus, these components have been omitted to keep the simulation simple. Furthermore, the passenger cabin is simplified as no interior components are included and the area at the feet is filled, as velocities at this space are nearly zero and the feet are not sensitive to draught phenomena when driving an open cabriolet, compare Section 4.3. The model dimensions are in analogy with the Porsche 911 Carrera Cabriolet (991-2) [62] and are summarized in Table 7.1. The coordinate system related to

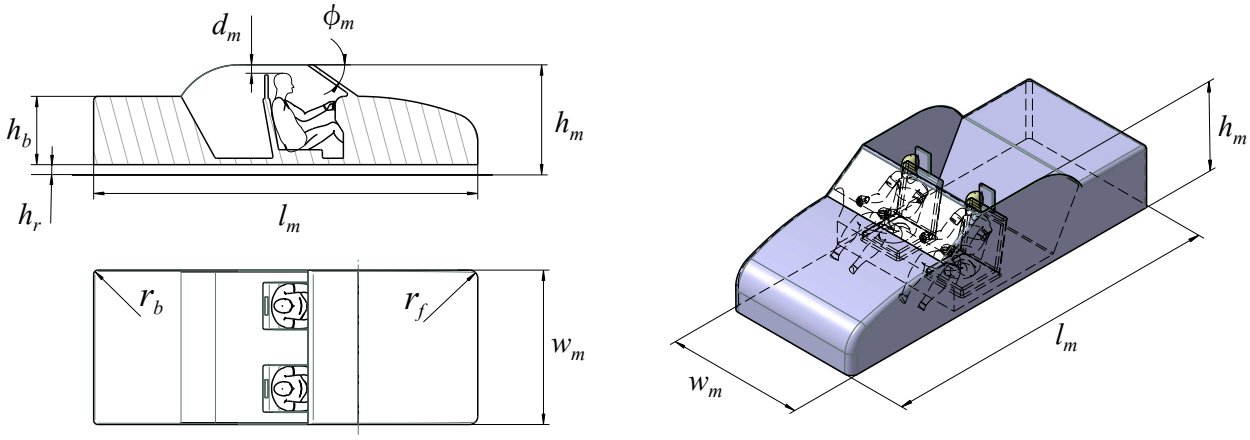

Figure 7.1: Side, top and isometric view of the simplified full cabriolet model used for CFD Analysis

this model is given in Appendix B.

Table 7.1: Dimensions of simplified CFD model

Dimension		Symbol	Value
Model length	$[mm]$	l_m	4499
Model height	$[mm]$	h_m	1289
Model width	$[mm]$	w_m	1808
Model windscreen angle	$[deg]$	ϕ_m	35
Model ride height	$[mm]$	h_r	120
Manikin head clearance	$[mm]$	d_m	95
Front edge radius distribution	$[mm]$	r_f	100 - 75 - 50
Rear edge radius	$[mm]$	r_b	50

This model is used for the computation of a reference simulation, which is compared and validated with verified results found in literature, refer to [10, 14, 63, 64]. The reference simulation is analysed with respect to the flow that influences the surroundings of the manikin and the identification of suitable locations for imposing the boundary conditions onto a reduced domain representing the physical flow mock-up. As described in Chapter 6, the flow mock-up should ideally be independent of the geometry of a specific vehicle, such that multiple vehicles can be replicated in the mock-up. Therefore, the reduced domain contains only the space around the manikin. Additionally, the requirement that the test-subject in the flow mock-up should be able to associate the situation in a flow mock-up with the experience in a cabriolet requires that the components of the vehicle, which directly surround the manikin and are in the field of vision, have to be considered as well. Thus the reduced domain contains the windscreen, the dashboard, side windows and the seat. Furthermore, the physical flow mock-up is limited by the size of the the intended space which is set to 2.55 by 3 by 6 meters (HxWxL).

An important aspect is to keep the mesh of the reduced domain the same as the reference simulation. This is done by subtracting the small domain from the reference domain while keeping the mesh properties the same. In this way it is assured that the conditions obtained from the reference simulation can be imposed onto the boundaries of the reduced domain.
Thus the following steps which are conducted can be summarized:

1. Generate the reference simulation

2. Investigate the target area flow field surrounding the manikin for pressure and velocity and identify the source which influences the surrounding flow field the most
3. Identification of inlet and outlet positions for the reduced region
4. Definition of the reduced region
5. Identification of quantitative and qualitative targets
6. Simulate reduced region with boundary conditions obtained from the reference simulation imposed on all boundaries of the reduced region
7. Approach a realistic set-up for the flow mock-up by reducing the imposed boundary conditions on the boundaries

7.2 Numerical Set-Up

Before the intended CFD analysis can be conducted, the simulation has to be set-up. The specifications of the used machine are summarized in Table 7.2 and the CFD program used is Star CCM+ from CD Adapco. Star CCM+ offers a lot of solution methods, therefore a numerical model has to be selected based on the required accuracy, available hardware resources and computational time. The latter was very limited leading to the decision, to use RANS with steady conditions (see Section 2.6.1 for further information). This is somewhat contradicting to the fact that the main factors, which influence the subjective feeling, are fluctuating phenomena, which are unsteady phenomena. However, the purpose of this CFD analysis is to show a general feasibility of the reproduction of the flow field with predetermined boundary conditions in a reduced domain as well as an indication of the locations where to initiate boundary conditions. Furthermore, multiple researches exist about the flow over an open cabriolet, which solve steady state equations like [10, 64, 65] and show that the obtained solutions are usable for the analysis of the flow field around a cabriolet.

Table 7.2: Machine specifications used for CFD simulations

Linux Workstation
OS: KDE 4.3.4 Intel Xeon CPU E5-2643 3.30 GHz (8 Cores) 128 GB of RAM

To reduce computational time even more, use is made of the symmetry of the model and the flow phenomena. That the flow is symmetrical has been demonstrated in the different research papers of [10, 14, 63, 64] and can also be observed for the initial simulations of this model. Therefore, only the flow around half the model is simulated. The model is placed in a computation domain with a symmetry plane, that represents a virtual windtunnel. The dimensions of the computation domain have been chosen such that the assumption can be made, that the flow the inlet conditions will not be effected by the flow around the model while at outlet the flow can be assumed to have uniform pressure. The dimensions are shown in Figure 7.2. The blockage ratio for this domain can be calculated with Equation (7.1) and is sufficiently small, according to [30].

$$BlockageRatio = \frac{A_{model}}{A_{domain}} = 0.83\%. \tag{7.1}$$

The settings for the conducted CFD simulations are summarized in Table 7.3. The reasoning for the choice as well as the explanation of these settings are given in Section 2.6. The initial conditions of the numerical simulation are given in Table 7.4.

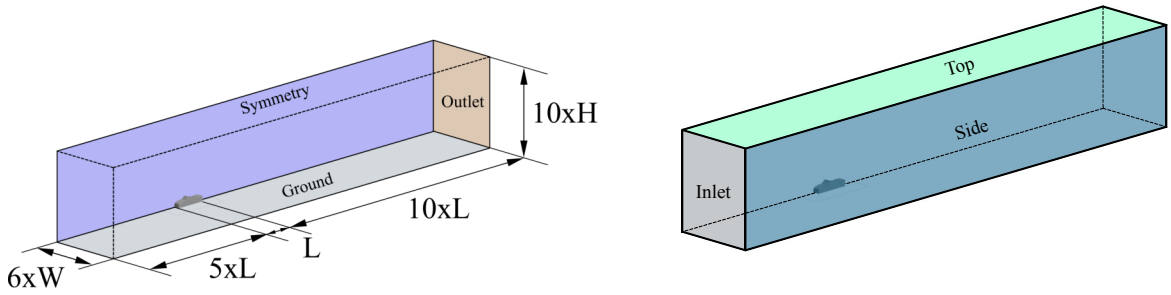

(a) Dimensions and outlet, ground and symmetry planes

(b) Computation domain planes inlet, top and side

Figure 7.2: Dimensions of the symmetrical computation domain of the CFD Analysis

Table 7.3: Numerical set-up summary

Model	Symmetrical
Numerical Equations	RANS
Turbulence Model	Realizable two layer $k-\epsilon$
Flow type	Constant density & incompressible
Time modelling	Steady flow
Wall treatment	All y+
Solver	Segregated flow

Table 7.4: Initial conditions of the numerical simulation

Velocity	$[m/s]$	33.33
Kinetic energy, k	$[J/kg]$	0.001
Static Pressure, p	$[Pa]$	101,325
Air density, ρ	$[kg/m^3]$	1.18415
Dynamic viscosity, μ	$[kg/(m\ s)]$	$1.855\,08 \times 10^{-5}$
Temperature, T	$[K]$	288.15

Mesh

Another important aspect of the numerical set-up before starting the simulation is the mesh. In StarCCM+ the meshing is done with the use of defining a *base size*. The base size defines the size of a cell and is given in $[mm]$. It is used as a characteristic dimension for flexibility to define certain regions relative to this base size. Increasing the base size makes the mesh of the dependent regions coarser while decreasing it makes the mesh finer. Additionally, an absolute cell size can be set for regions, where the resolution of the mesh should be kept the same when changing the base size.

Certain regions of the computational domain are refined as at these regions flow phenomena occur, that have a main influence on the overall solution. Therefore, refinement boxes are defined at these regions to capture these relevant flow phenomena, e.g. flow separation, vortices or areas which are of importance for the research - in this case the whole passenger cabin. Figure 7.3 shows all of the refinement boxes and their properties are summarized in Table 7.5. Near the model, the mesh has to be fine due to flow interactions, while in the far field the mesh can be coarse, as it can be assumed that the flow is not influenced any more. Important regions due to flow separation are the windscreen header (*Windscreen_Edge*) and the rear edge of the model (*Rear_Detachment_*-

Edge), red in Figure 7.3a. Furthermore, as mentioned earlier, the focus of this analysis is the flow inside the passenger cabin, thus the mesh of this region has been resolved finer compared to other regions, see Table 7.5. The cabin contains the *Cabin_fine* refinement box (red in Figure 7.3b), which includes the surroundings of the manikin, and *Cabin* refinement box which also includes the area above the trunk of the model. An additional refinement box has been defined around the whole windscreen including the A-pillars (*Windscreen*), because at these locations important flow interactions occur as the flow, which propagates from this region, influences the flow field in the passenger cabin. A final refinement box is set around the whole model (*CarBox*). The *Windtunnel* is the remainder of the domain shown in Figure 7.2.

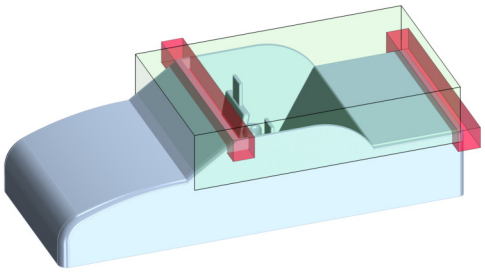

(a) Refinement boxes: Cabin_fine, Windscreen_Edge & Rear_Detachment_Edge

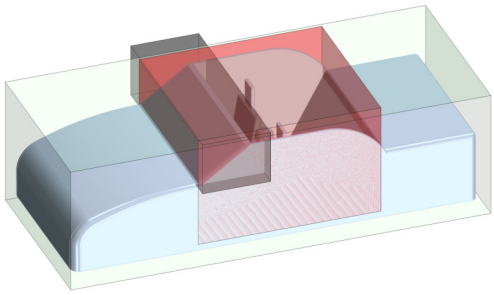

(b) Refinement boxes: CarBox, Cabin & Windscreen

Figure 7.3: Refinement boxes around the CFD model

Table 7.5: Definition of the refinement boxes

Refinement box	Percentage of Base [%]
CarBox	9
Cabin	7.5
Cabin_fine	2.75
Windscreen	4.5
Rear_Detachment_Edge	2.75
Windscreen_Edge	2.5
Windtunnel	100

Boundary layer modelling Next to the regional refinement of the surrounding mesh, the boundary layer on the model has to be resolved as well. For this a wall treatment model has to be chosen in StarCCM+. The *All y+* wall treatment model has been chosen, which is explained in Section 2.6. Additionally, prism layer properties have to be defined on the model boundaries. For the boundaries in the computational domain these parameters are given in Table 7.6. The Box_-Inlet, Box_Outlet, Box_Side and Box_Top do not have prism layers, because at these boundaries no boundary layer is present, as these are an inlet, an outlet and two symmetry-planes, respectively.

In order to optimize this prism mesh, the y^+-values have been analysed. When using the *All y+* wall treatment model a y^+-value between 30 and 50 is recommended [33]. Therefore, regions with higher y^+-values than 50 and lower than 30 have been resolved higher or lower, respectively. Important surface boundaries are all model edges, e.g. the A-pillar, windscreen header, the windscreen top surface as well as the rear of the vehicle and the back of the passenger cabin. At these surface boundaries the flow separates from the surface and therefore they need to have a high resolution as they influence the flow significantly.

Table 7.6: Surface boundary mesh properties

	Number of Prism Layers	Prism Layer Stretching	Prism Layer Thickness [mm]	Surface Size [%]
Body	7	1.25	15	3
Manikin	5	1.3	18	6
Radius1	10	1.2	15	1.5
Radius2	9	1.25	15	1.5
Radius3	8	1.25	15	1.5
Box_Floor	5	1.3	5	15
Floor_Big	4	1.3	4	100
Box_Inlet	-	-	-	100
Box_Outlet	-	-	-	100
Box_Side	-	-	-	100
Box_Top	-	-	-	100

7.3 Mesh Analysis

In order to investigate the dependency of the flow field on the resolution of the computational domain as well as to optimize for computation time for further analysis, a mesh analysis is done. From this analysis the coarsest acceptable mesh, which is used for the model reduction analysis, is obtained.

As mentioned in the previous section, the mesh can be controlled with the *base size*, which defines the basic cell size of the mesh. The defined refinement boxes are given as a percentage of this base size, thus when the base size is reduced, the cell size in the refinement boxes is reduced. Six different meshes with decreasing base size have been generated and investigated. The resulting meshes and their base sizes are given in Table 7.7.

Table 7.7: Mesh properties

	Base Size [mm]	Cell Count
Mesh 1	750	1 823 542
Mesh 2	550	3 178 241
Mesh 3	400	5 854 292
Mesh 4	350	7 498 160
Mesh 5	300	10 591 883
Mesh 6	250	15 741 870

The CFD simulations can be validated qualitatively with the results obtained in [14, 23, 63, 64] as well as with the conducted measurements as described in Section 5.1.

Velocity field Looking at the XY- and XZ-section planes of the simulations with different meshes it can be confirmed, that the main flow phenomena, such as the high inboard velocity, the shear layer, the vortex between the shear layer and the fluid of the passenger compartment are present for all the investigated meshes.

Pressure field For all the investigated meshes the pressure in the passenger compartment is lower than the ambient pressure. This is in accordance with the experimental results from [10, 14, 23].

Convergence Before the simulations can be analysed they have to be checked for convergence. This is done by monitoring the velocities at the defined measurement probes as well as the drag coefficient over the number of iterations, of which the latter is plotted in Figure 7.4a. The figure shows that for every simulation the drag coefficient converged to a discrete value. The obtained drag coefficients are similar to drag coefficients of present cabriolets, which have a $\Delta C_D \approx= 0.015-0.050$ higher drag when its roof is open compared to its closed version [13, 20], ranging from 0.33 to 0.46 [20, 65].

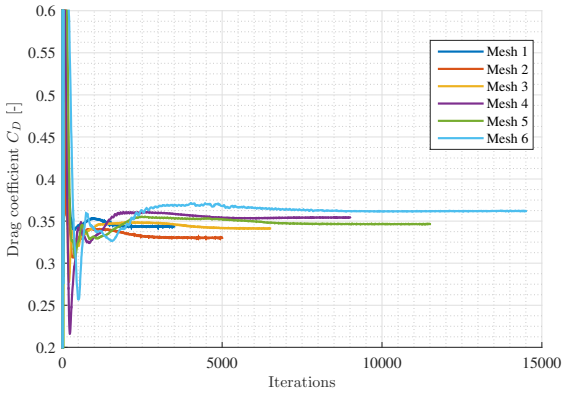

(a) Drag coefficient convergence residuals of the different meshes

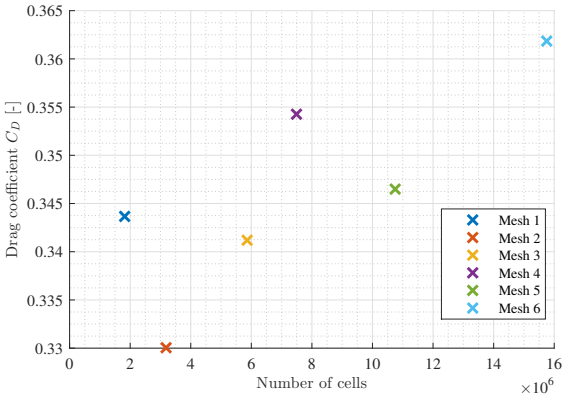

(b) Drag coefficient

Figure 7.4: Results from CFD Simulations for different meshes

In Figure 7.4b the final drag coefficient values of the different simulations are plotted. It is expected, that the drag coefficient converges to a specific value, the finer the mesh becomes. However, no direct asymptotic behaviour in the drag coefficient can be observed. Especially mesh 4 and 6 show significant differences. An explanation why these two meshes have such a difference cannot be given, as the mesh settings have not been changed. The only difference between the meshes is the cell base size, as given in Table 7.7, while the resolution of the refinement boxes are given as a percentage of the cell base size.

Analysing the flow field at the symmetry plane, the differences between the two mentioned meshes compared to the other meshes become visible. In Figure 7.5 the section cuts at the symmetry plane of mesh 1, 3, 5 and 6 have been depicted. In Figure 7.5d the difference between mesh 6 and the others is indicated by the rectangle. It can be noticed, the flow, which propagates from the stagnation point over the edge into the passenger cabin, does not propagate downwards into the bottom of the passenger cabin. This is the case for the other three depicted figures. For mesh 4 the same behaviour as in Figure 7.5d can be observed, while mesh 2 has a similar flow field as Figure 7.5a, Figure 7.5b and Figure 7.5c.

By comparing these flow fields with the simulations obtained in [23] qualitative similarities to meshes 1, 2, 3 and 5 can be observed. In this research different cabin configurations have been investigated for cabin comfort by windtunnel measurements and CFD simulations. The results from the CFD simulations are confirmed by the measurement conducted in the windtunnel. The CFD simulations are conducted with a mesh of 172 million voxels and unsteady conditions. Figure 7.6 shows the XZ-symmetry plane of a steady and an unsteady simulation as well as the XY-plane from this research. It is noticeable that the main flow phenomena of the unsteady simulation can be recognized in the flow field of the steady simulation. Among these are

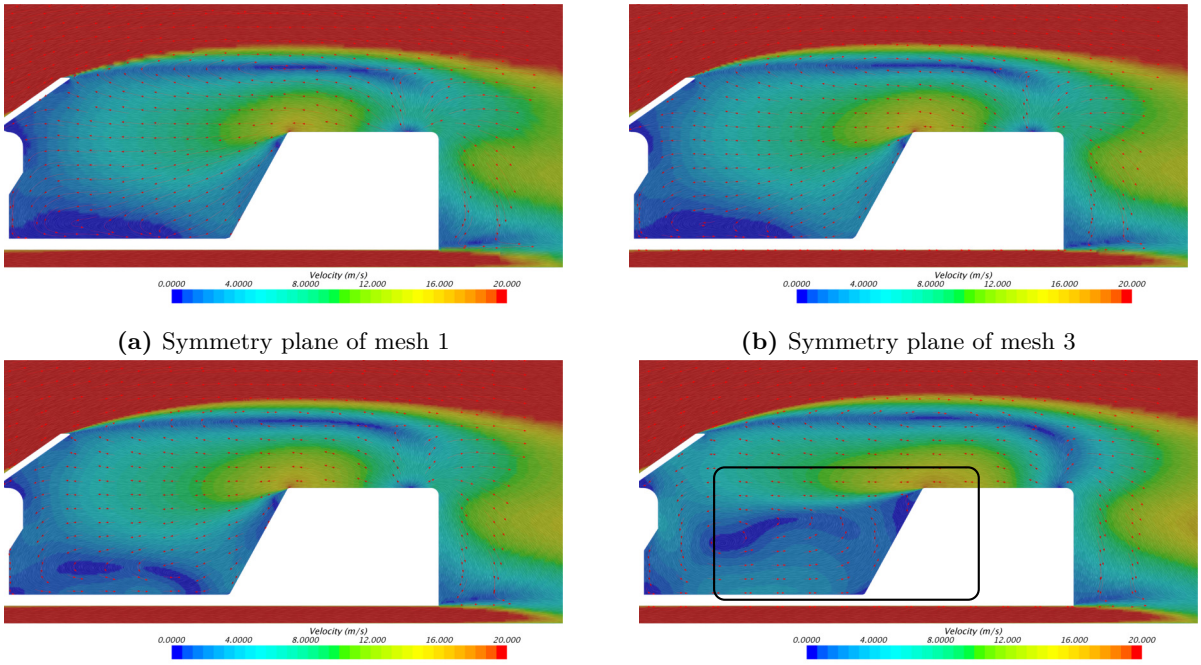

(a) Symmetry plane of mesh 1

(b) Symmetry plane of mesh 3

(c) Symmetry plane of mesh 5

(d) Symmetry plane of mesh 6

Figure 7.5: Symmetry planes indicating the velocity of meshes 1, 3, 5 and 6

- the shear layer between the high velocity flow around the car and the low velocity flow of the passenger cabin,
- the stagnation point and thus low velocity at the trunk,
- the high velocity backflow into the passenger cabin,
- the velocity distribution in the passenger cabin.

Especially the latter agrees with the simulation results of meshes 1, 2, 3 and 5 while mesh 4 and 6 do not agree. Not only are they qualitatively similar, but also the velocity distributions are in accordance with each other.

Additionally, the simulation results can be compared with the conducted measurements, see Section 4.2. Figure 7.7 compares the velocities at the different measurement points, see Figure 5.1, of the conducted measurements of Config B, see Table 5.1, with the same measurement points in the CFD simulations.

Before interpreting this, it must be said, that the velocities obtained from the simulations do not match the results obtained from the conducted measurements. This is due to the fact that the model geometry is different from the test vehicle geometry. However, a similar trend can be observed from position 1 to position 6 with one exception at position 2. A possible explanation for this is, that no interior centre console has been included in the CFD model.

From Figure 7.7 it can be noticed that the resulting velocities from mesh 4 and 6 differ significantly from the simulation results of the other meshes. Especially positions 1,2 and 3, which are located in the identified region of Figure 7.5d, show, that the results obtained from meshes 4 and 6 have significantly lower velocities, while the conducted measurements show higher velocities. The results from meshes 1, 2, 3, and 5 are closer to the results obtained from the measurements.

All in all, the flow phenomena of meshes 1, 2, 3 and 5 are in agreement with the obtained results from [10, 14, 63, 64] as well as with the conducted measurements. Consequently, these meshes are suitable for further analysis. For further analysis mesh 3 has been chosen, as the general flow field

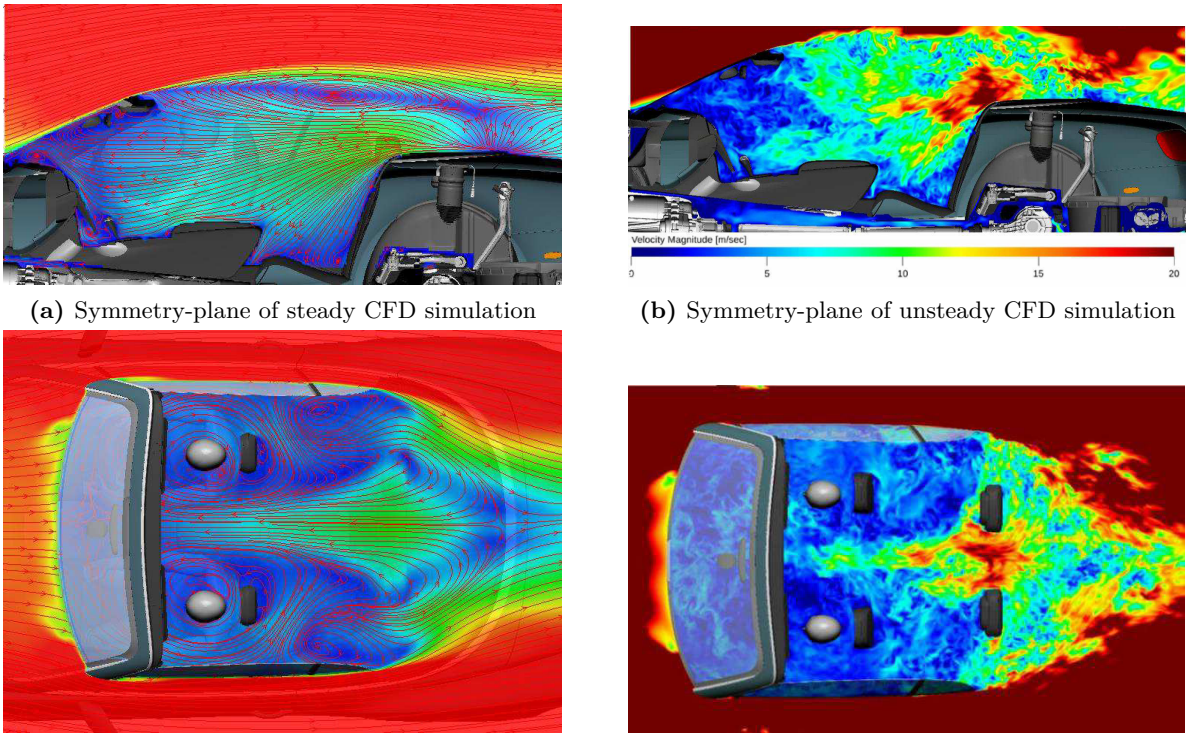

(a) Symmetry-plane of steady CFD simulation

(b) Symmetry-plane of unsteady CFD simulation

(c) XY-plane of steady CFD simulation

(d) XY-plane of unsteady CFD simulation

Figure 7.6: Steady and unsteady CFD results of a Bentley Continental GTC Speed convertible MY 14 [23]

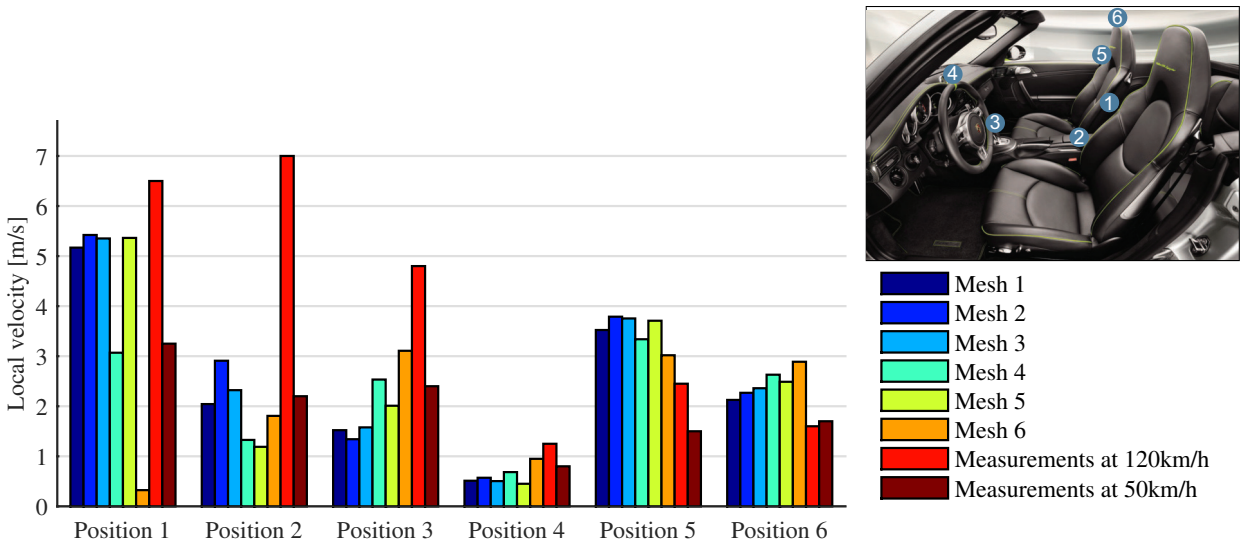

Figure 7.7: CFD results compared with conducted measurement results at different measurement positions

of mesh 5 and 3 are in agreement and to keep computational time low mesh 3 is the better option. As mentioned earlier, the purpose of the analysis is to show that a similar flow field in the reduced region to the complete domain can be replicated in a reduced domain, which will be the case for a physical flow mock up. The reduced domain will only be compared to the reference simulation.

7.4 Analysis of the Target Area

In this section an in depth analysis of the flow field in the passenger cabin is conducted. As a result of Section 7.3, the basis for this analysis is the simulation conducted with mesh 3, with a cell count of $5,854,292$. The goal is to identify the origin of the flow field, which influences the surrounding of the manikin. From this, locations can be identified to impose boundary conditions for the reduced domain and in turn for the physical flow mock-up.

One way to analyse the flow properties, which are present in the passenger compartment, is by taking section cuts, indicating the pressure, the velocity magnitudes and velocity vectors. Next to this two dimensional visualisation of the flow properties, three dimensional streamlines can be created to get a spatial impression of the flow properties. From Section 2.4 it is known, that the separation from the windscreen header as well as from the A-pillar have a major influence on the development of the flow field inside the passenger cabin. To see how the flow propagates from these positions, streamlines emanating from both, the A-pillar and the windscreen header, have been visualized in Figure 7.8.

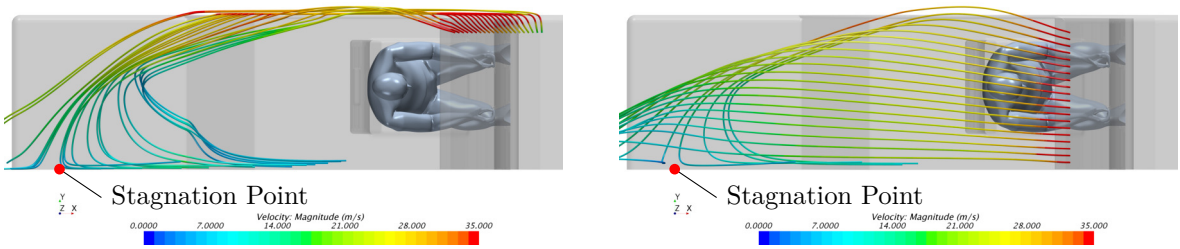

(a) Streamlines over the A-pillar **(b)** Streamlines over the windscreen header

Figure 7.8: Streamlines emanating from the A-pillar and the windscreen header

From these figures it can be seen that the passenger compartment is enclosed by the flow over both, the A-pillar and the windscreen header. While the flow over the windscreen mainly propagates over the passenger cabin and reattaches at the stagnation point, a part of the flow over the A-pillar turns over the side windows to the inside of the vehicle where it is turned near the stagnation point, entering the passenger compartment. Also from Figure 7.8b the latter can be observed. The streamlines emanating from the outboard of the windscreen header, thus closer to the A-pillar, enter the passenger compartment while the streamlines further to the inboard of the windscreen header emerge to the wake of the vehicle. This ingression of the flow drives the fluid inside the passenger compartment to flow from the rear of the vehicle towards the windscreen.

A closer look on how the flow inside the passenger compartment is build up can be made by creating a plane at the inside of the passenger compartment and displaying the streamlines, which emanate backwards from this plane. Figure 7.9 shows these streamlines and it can be observed, that almost all the streamlines originate from the inside of the passenger compartment.

To analyse the flow field in the passenger cabin in more detail, multiple section cuts in the XY- and the XZ-planes for the velocity field as well as for the pressure field have been generated from

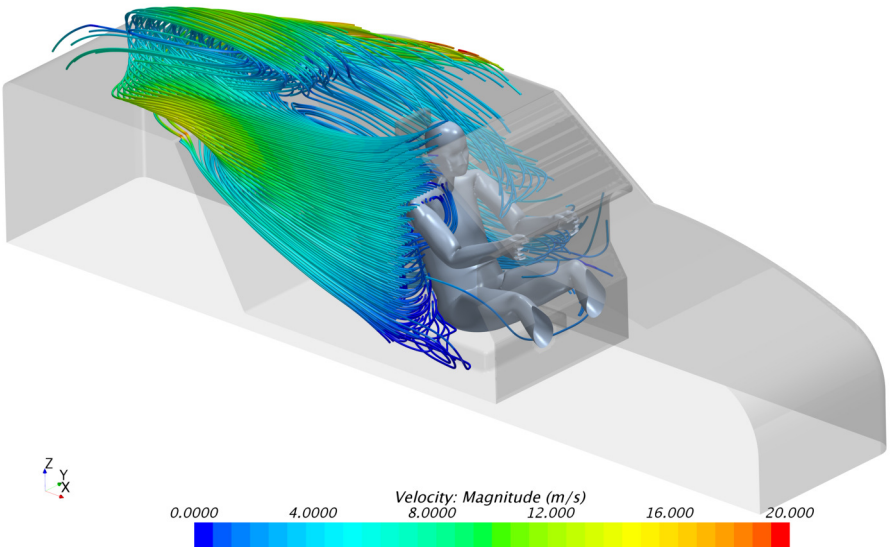

Figure 7.9: Streamlines emanating backwards from a YZ-plane (X = -270mm) at the vehicle inboard

the reference simulation. A selection of these sections cuts can be found in Appendix C. From the XY-planes displaying the velocity vectors it can be noticed, that the flow propagates from the inboard back to the the front, where it turns to the outboard side of the vehicle and flows back to the rear. Thereafter, the flow cannot escape and it start to circulate behind the seat. This flow path is sketched in Figure 7.10.

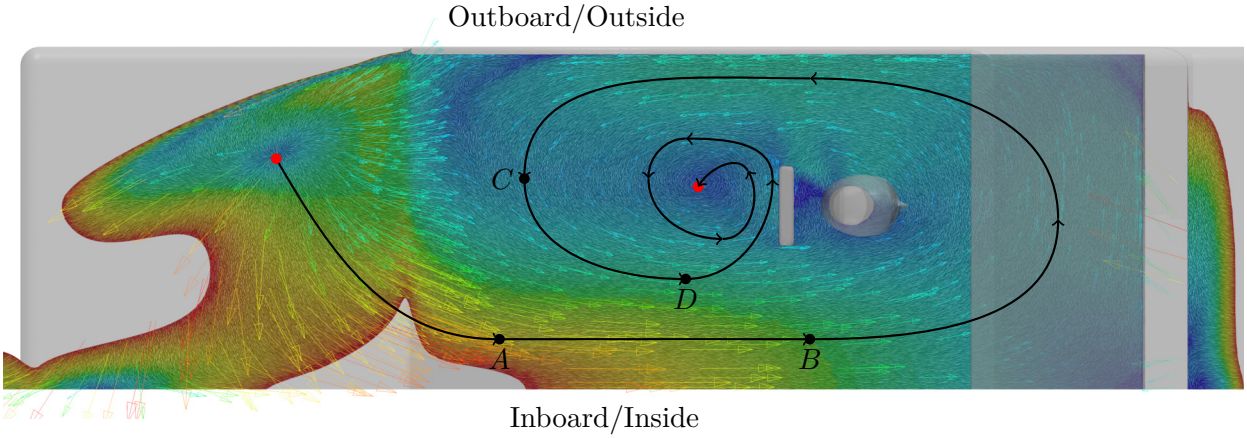

Figure 7.10: Streamlines emanating from the A-pillar and the windscreen header

A clear low velocity circulation region can be identified between the inboard and the outboard of the vehicle. This region separates the backflow at the inboard of the vehicle from the lower velocity flow at the outside. The for this analysis interesting flow starts from point B to Point C. The flow from point B can be identified to be the main source of the backflow, which influences the flow field surrounding the manikin. All XY-planes show that the inboard position of the vehicle is the origin of the flow surrounding the manikin. This can also be visualized by creating a XZ-plane in front of the manikin and visualizing the streamlines, which come together at this plane and which emanate from this plane. This can be seen in Figure 7.11.

Figure 7.11a clearly shows that all the flow originates from the inboard position while the outflow is to the outside position of the vehicle, see Figure 7.11b. Furthermore, these figure show

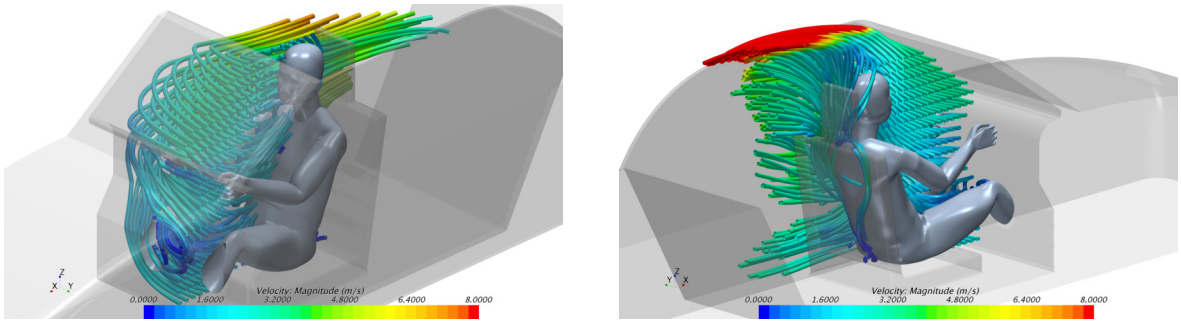

(a) Ending streamlines **(b)** Emanating streamlines

Figure 7.11: Starting and ending streamlines of a XZ plane in front of the manikin

a orderly structure of the streamlines, which go forward and backward of the plane.

7.4.1 Inlet determination

The previous section leads to the conclusion to take a plane at the inboard vehicle behind the seat as a velocity inlet for the reduced domain. The air flows from the rear inside to the front over the inside shoulder of the manikin around the front to the outside shoulder and back. Furthermore, the flow which flows over the outside shoulder to the back recirculates behind the passenger seat and flows back to the front of the inside shoulder. Thus, the flow at the inside shoulder is provided by this circulating flow. By defining the boundary condition as a velocity inlet behind the seat, all the flow which is provided from this circulating flow is included in the mapped velocity. Therefore, it can be assumed, that all the flow phenomena that occur in the space behind the plane are considered and the resulting flow field is passed from the inlet boundary to the flow field surrounding the manikin.

The flow at this plane can be considered to be fully developed from the flow phenomena, which are mainly taken place at the rear. Especially from Figure 7.11, it becomes clear, that all the flow, which influences the flow surrounding the manikin and propagates towards the front part of the passenger cabin, emanates from the cabin inside. Furthermore, this position is also suitable for a realistic set-up, because it is not in the field of view of the test-subject, which would otherwise alter the perception of the test-subject of a cabriolet. Additionally, a cabriolet is either a 2-seater configuration or a 4 seater configuration. To be able to replicate the flow field of both configurations, the most convenient position to place the inlet is the position directly behind the driver. If the position would be further back, the possibility exists that the flow mock-up has to be reconfigured in order to compare two cabriolets with different configurations with each other. This contradicts the requirements, that the flow mock-up should be able to replicate the flow field of different cabriolets instantly without the need of reconfiguration of the set-up.

The contour of the inlet has been set around the seat, because the flow emanating from the plane directly behind the seat has zero velocity and it will not influence the direct flow surrounding the manikin, as it cannot flow through the seat. By visualizing the vectors, which emanate from the XY-plane (Figure 7.12) at this position, and highlighting the determined velocity inlet, it can be seen, that all the vectors to the front are inside the velocity plane, while vectors the vectors behind the seat are pointed to the positive Y-direction and not to the positive X-direction.

Next to the backflow, which mainly influences the flow field around the manikin, the high velocity flow above the passenger cabin has to be considered as well. When analysing the XZ-planes and also from Figure 7.8b, it can be noticed, that the high velocity flow over the cabin encloses the passenger cabin and additionally it reverses the backflow again, see Figure 7.13. If the inlet behind the seat would be the only velocity inlet, the flow at the top would not be reversed

and can escape to the top. By setting an inlet above the windscreen it is assured, that the backflow from the back inlet is constrained as well as reversed. This effect has a major influence on the perception of the velocity field around the head. For example, when sitting in an open cabriolet the hair swirls to the front and upwards instead of just to the front, which would be the case without a front inlet. In that case, the flow emanating from the back inlet is not bounded by the flow from the front inlet. The flow from the back inlet would just flow to the front and it is not redirected to the back again, but it can freely escape to the top. One idea would be to put a wall at the position of the shear layer, however, this wall would direct the flow downwards to the front and not upwards to the back, as a opposing flow would do.

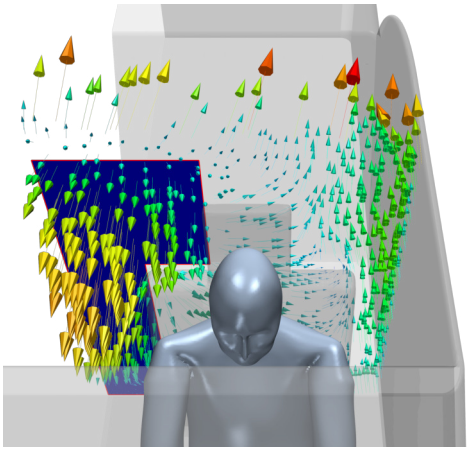

Figure 7.12: Vectors emanating from plane behind seat with inlet plane

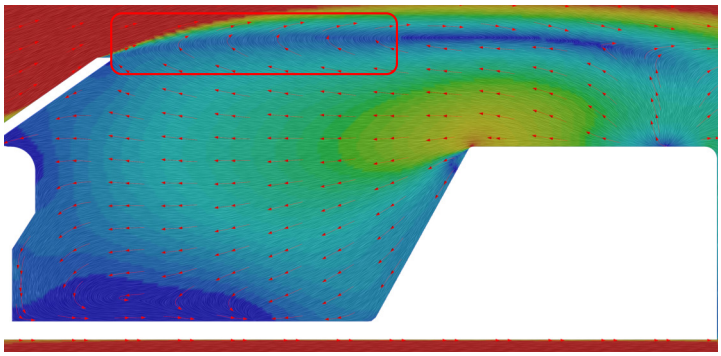

Figure 7.13: Symmetry plane with indication of flow reversal due to high velocity flow over the top of the cabin

The resulting inlets are visualized in Figure 7.14, showing the inlet at the back and the inlet at the front. The front inlet is bounded at the top by the dimension of a garage, as it is defined in Chapter 6.

The outlet of the reduced domain is varied throughout further analysis. However, from the analysis it becomes clear, that the fluid surrounding the manikin only escapes at the outboard of the vehicle. Therefore, a possible outlet can be defined at the same plane of the back inlet.

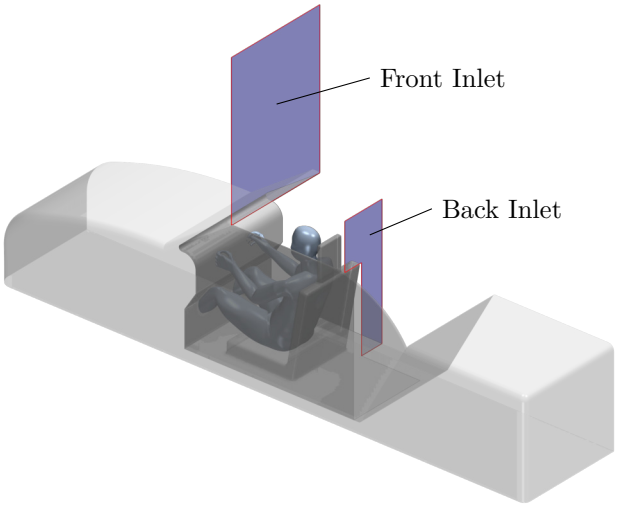

Figure 7.14: Isometric view of the determined inlets at the front and at the back

7.5 Flow Field Replication

With the determination of the inlet positions, a reduced domain can be set-up. StarCCM+ has the option to subtract one geometry from another geometry. A geometry around the manikin has been defined as is indicated in red in Figure 7.15a. With the subtract operation in StarCCM+ this defined geometry is subtracted from the reference domain, obtaining the resulting domain boundaries in Figure 7.15b.

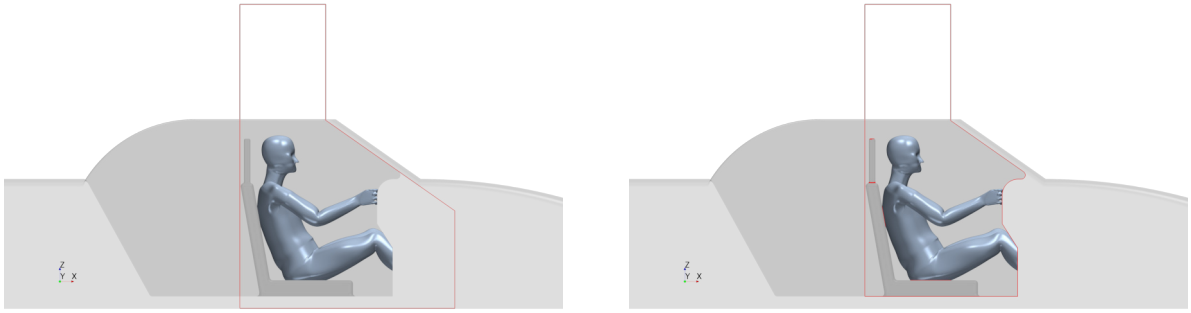

(a) Boundaries from subtract

(b) Resulting region boundaries

Figure 7.15: Defined region to subtract from reference computational domain and resulting reduced region

As already mentioned in Section 7.1, the interior of the car is of importance as it makes the perception of a human comparable with a real cabriolet, consequently the boundaries of the reduced region have an offset of 5 mm from the inside of the windscreen geometry boundary as well as the vehicle side, such that the geometry is included in the created subtract. Furthermore, the boundaries are defined such that geometries like the rear and the front of the vehicle are excluded from the reduced domain, as is defined by the requirement on the flow mock-up to be independent of the vehicle geometry.

This resulting geometry forms the basis of varying reduced regions. Different reduced regions are investigated that converge towards a possible physical set-up of the flow mock-up and the effect of changing the outlet conditions as well as the locations of the outlet is investigated. The inlet boundary at the back however is kept the same throughout the analysis of the different variants of the reduced domain.

The first variant of the reduced region is a highly constrained region, where boundary conditions, obtained from the reference simulation, are imposed onto all the boundaries of the reduced region. Thereafter, the domain is enlarged step by step to a possible physical set-up of a flow mock-up, which is defined in Chapter 6.

The different variants are analysed with respect to the difference to the reference domain by comparing the velocity magnitudes at specific measurement positions. These specific measurement positions are the head and the respective inboard and outboard positions of the forehead, back of the head, cheek, neck and shoulder, which have been determined to be the most sensitive body parts for comfort in a cabriolet [12, 15, 16]. The positions are defined as measurement probes in the CFD program and are visualized in Figure 7.16. The exact coordinates are given in Table B.1. The velocity magnitudes and the pressure coefficients from the reference simulation are plotted in Figure 7.17 and Figure 7.18, respectively.

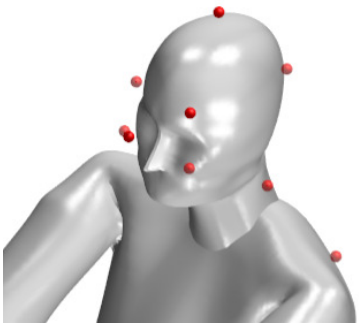

Figure 7.16: Measurements probes around the manikin in the flow domain

In order to impose the correct boundary conditions onto the inlet and outlet of the reduced domain, StarCCM+ has the possibility to extract flow properties from planes. This is done at a

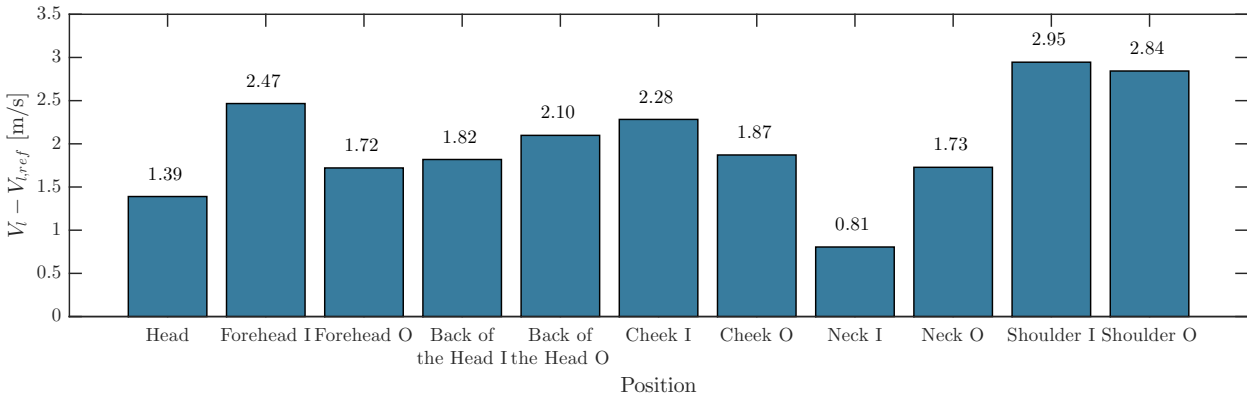

Figure 7.17: Velocity magnitudes at the different measurement position from the reference simulation

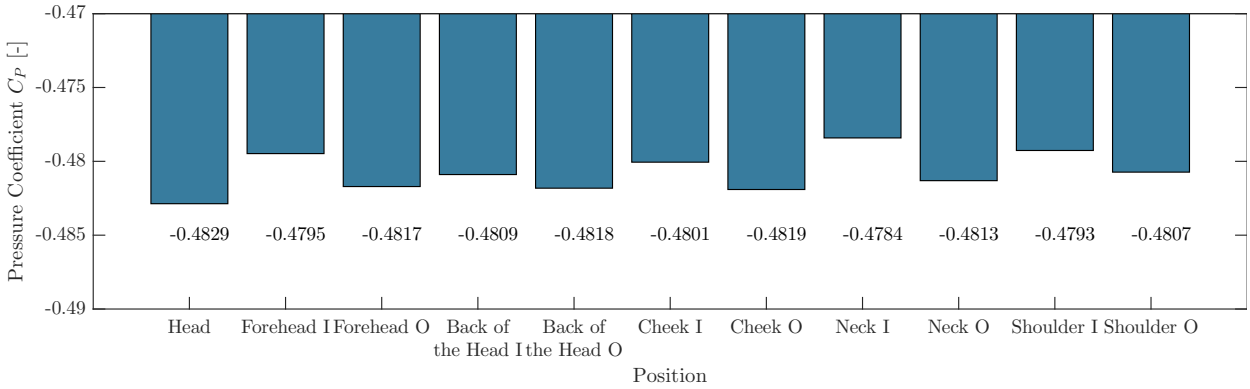

Figure 7.18: Pressure coefficient at the different measurement position from the reference simulation

YZ-plane at $X = 261mm$ (see Appendix B for coordinate system), which is located directly behind the windscreen header, of the reference simulation as well as a YZ-plane directly behind the seat at $X = -270mm$. For the inlets the x-, y- and z-components of the velocity at the respective plane are extracted and for the outlet the pressure. These extracted data can then be mapped onto the boundaries of the new defined domain.

The pressure outlets in CFD are normally in the far field of the model and a constant pressure value is prescribed at the outlet, because in the far field uniform conditions can be assumed. However, throughout this analysis the outlet is set close to the model due to the requirement to place the flow mock-up into a restricted room. One option would be to extract the pressure from the respective plane of the reference simulation and impose this pressure conditions onto the outlet of the reduced region. The subtracted domain in Figure 7.15, however, does not include the rear of the vehicle, because the flow mock-up should be independent of the geometry, and the dimension of the intended space for the flow mock-up exceeds the length of the rear. Therefore, the pressure conditions at the back of the intended space are not known. One way to identify these conditions is by lengthening the reduced domain to the far field, simulate this situation with a constant pressure outlet, extracting the pressure conditions at the respective plane and prescribing these onto the outlet of the reduced domain. But this would imply, that in the development process an additional simulation is needed, which is undesired as the idea is to simulate the total model and to only extract the needed information from this simulation.

The figures of the XY- and XZ-planes which are created during the analysis of the different variants can be found in Appendix D.

7.5.1 Variant 1

The first reduced domain which is investigated is the domain that has been subtracted from the reference domain and can be seen in Figure 7.19. The domain is restricted by the plane directly behind the driver seat, the plane behind the windscreen header, the symmetry plane, the top boundary at $Z = 2000mm$ and the side plane at $Y = 900mm$, middle of the side windows at the outboard of the vehicle. The plane at the back consists of the defined back inlet and a pressure outlet, which is the remaining surface. It is constrained on every boundary by imposing boundary conditions obtained from the reference simulation onto every boundary of the domain. These include the plane at the back, side, front and at the top. The top and side plane are defined as pressure outlet with the mapped pressure from the reference simulation the same for the pressure outlet at the back.

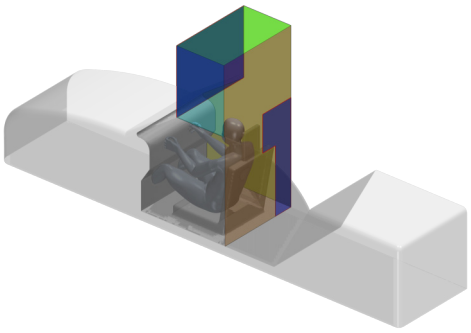

Figure 7.19: Variant 1 of the reduced region

From this simulation it is expected that it matches with results obtained from the reference simulation, as every boundary condition is obtained from the reference simulation.

7.5.1.1 Results of Variant 1

The obtained results are not as expected. The difference between the pressure coefficient at the measurement points is acceptable with 0.01, equivalent to $6.5Pa$. However, visualising the streamlines going in and out of an XZ-plane in front of the manikin, as in Figure 7.11, the streamlines are not as structured as the streamlines of the reference simulation. Furthermore, comparing the velocity magnitudes at the measurement points with the results obtained from the reference simulation, the velocity magnitudes do not match with the reference values either. Figure 7.20 shows the difference between the obtained velocity magnitudes of variant 1 and the reference simulation as well as the percentage with respect to the velocity magnitudes of the reference simulation at the respective measurement point.

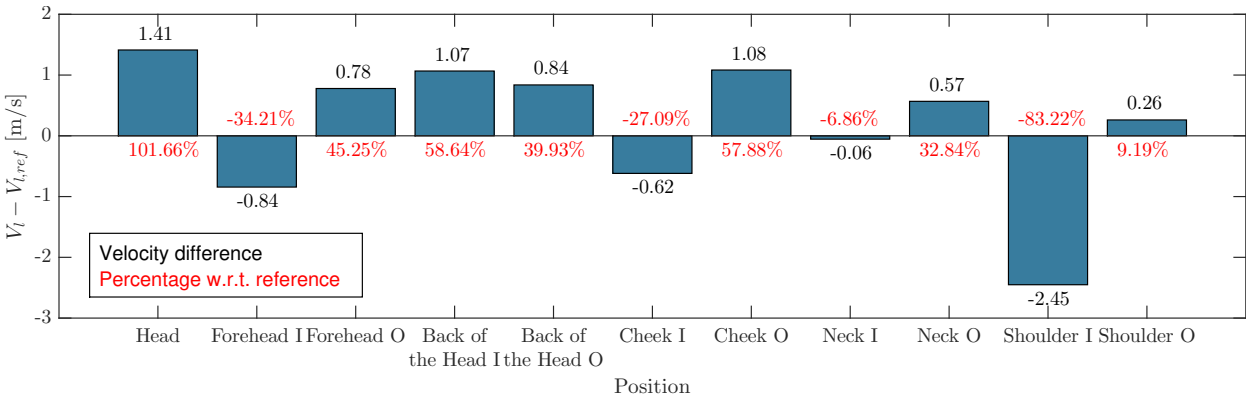

Figure 7.20: Velocity magnitude difference between reference simulation and variant 1

Especially the velocity magnitudes at the head and the inboard shoulder differ significantly from the reference simulation. The latter is totally unexpected, because this position is the closest to the velocity inlet at the back. While the velocity magnitude at the head is double as high as the reference velocity, the velocity at the inboard shoulder is 6-times lower than the reference velocity. Visualizing the flow field on the XY-plane at the y-coordinate of the measurement probe, a vortex

can be identified around the measurement probe of the inboard shoulder, resulting in a velocity magnitude of 0.4941 m/s compared to 2.95 m/s of the reference simulation.

Additionally, when analysing cut planes in the XZ-plane it can be seen, that the velocity field differs from the reference simulation. Evaluating the flow from the inside out, because the velocity field is build up starting from the inboard position of the vehicle, already at the XZ-symmetry-plane a circulation region can be noticed at the front bottom, which is different from the reference simulation. This can be seen in Figure 7.21. This circulation seems to be built up because the

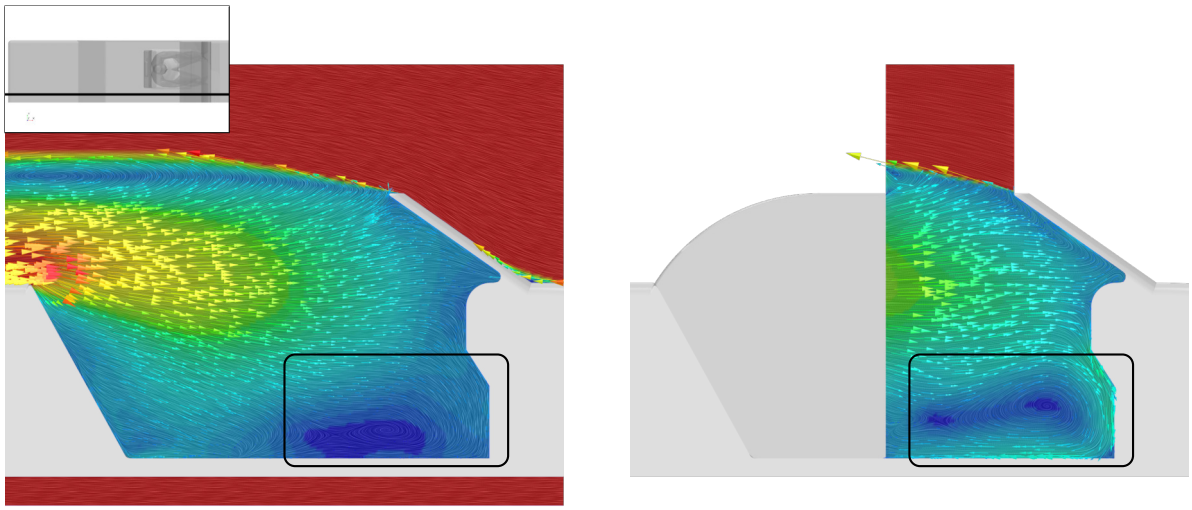

(a) Reference simulation **(b)** Variant 1

Figure 7.21: Comparison between velocity flow fields of the reference simulation and variant 1 at XY-plane. Picture in the top left corner indicates the position of the XY-plane

flow near the bottom back inlet cannot flow away due to the back inlet boundary. Furthermore, this circulation influences the remaining flow field, as the flow propagates from the inboard to the outboard. From this it follows, that the inlet conditions have to be optimized in order to improve the flow field.

7.5.2 Variant 2

As a follow up on the results from the previous variant, the back inlet and outlet are adapted by adding the lower part of the inlet to the outlet. The resulting domain can be seen in Figure 7.22. This alteration should enable the fluid at the bottom to flow away to the outlet at the vehicle inboard side. With this modification it is desired to prevent the build up of the circulation region at the inboard bottom.

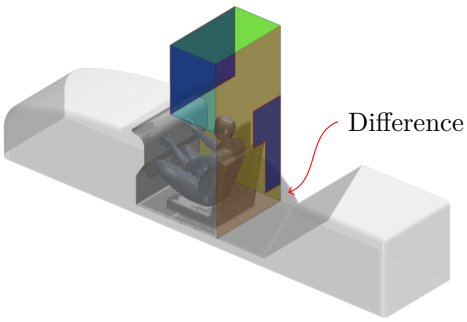

Figure 7.22: Variant 2 of the reduced region with altered back inlet

7.5.2.1 Results of Variant 2

Analysing the results of the velocity magnitudes at the measurement points, see Figure 7.23, a small improvement for the head, inboard forehead, inboard cheek, inboard neck, inboard shoulder and outboard should can be noticed, while he outboard forehead, back of the head outboard, cheek outboard and neck outboard are slightly worse with a maximum difference of 0.17 m/s, which is not very much. From the analysis of the flow field in the XY- and XZ-planes it can be observed, that the circulation at the front bottom is not as big as it was present in the first variant. However, near

the manikin there are still three vortices present, which are not present in the reference simulation. Overall, this inlet and outlet change did not significantly improve the flow field.

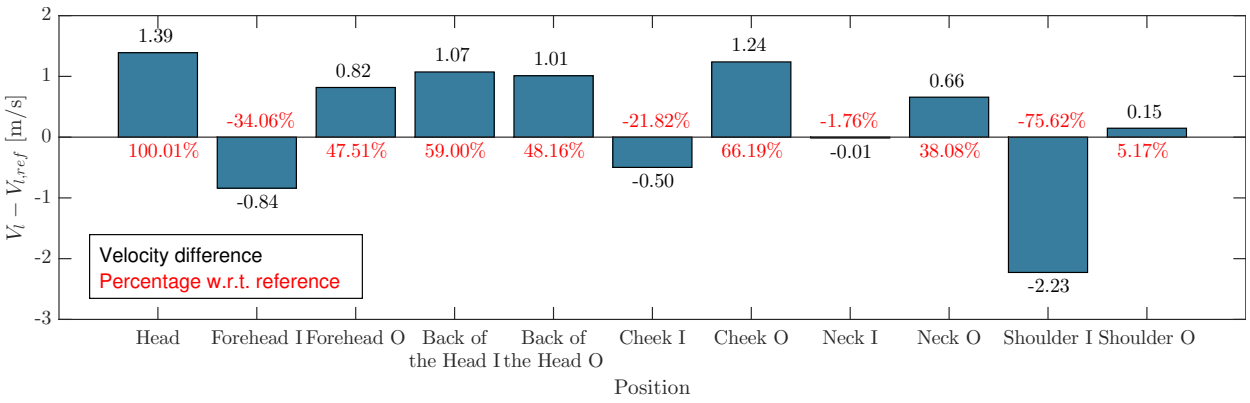

Figure 7.23: Velocity magnitude difference between reference simulation and variant 2

Visualizing the streamlines starting from the inlet, it can be observed, that in contrast to the reference simulation the streamlines are not as structured as in Figure 7.11. Figure 7.24 shows the streamlines emanating from the same plane for variant 2 and the reference simulation.

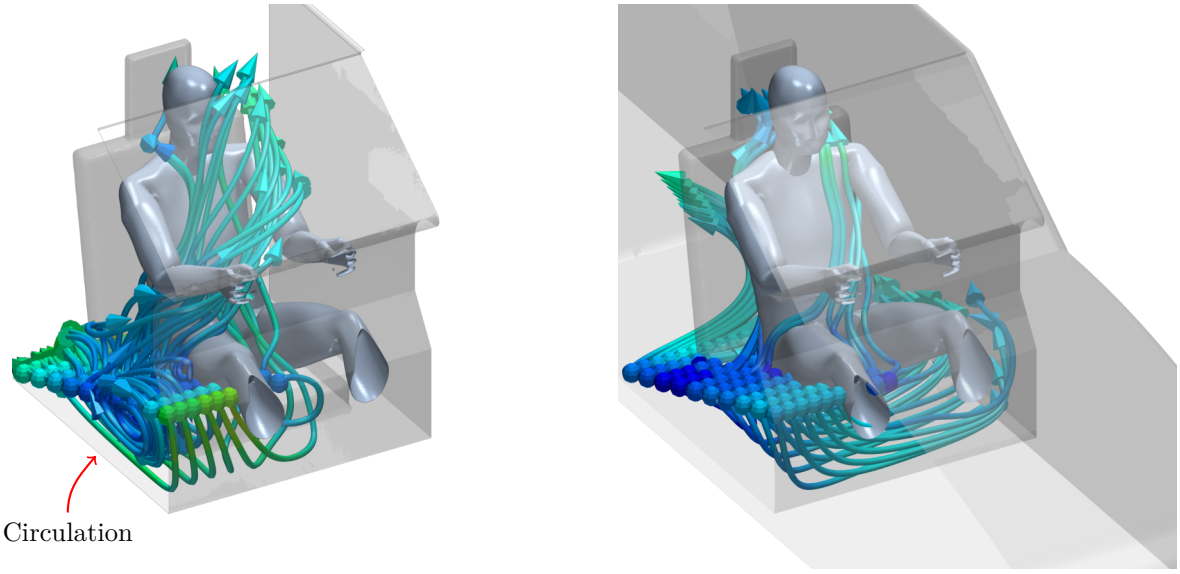

(a) Streamlines of variant 2

(b) Streamlines of the reference simulation

Figure 7.24: Defined region to subtract from reference computational domain and resulting reduced region

It can be clearly noticed, that the majority of the streamlines of the reference simulation are propagating over the bottom to the outboard of the passenger cabin in a structured way while for variant 2 at the inboard a circulation is present from which the streamlines propagate more around the manikin to the positive z-direction. This is a significant difference in the flow field which will probably affect the perception of the subject.

Although it is clear that the inlet conditions are not optimal, further analysis is conducted with these inlet conditions, because this analysis serves as a preliminary investigation of the overall possibility of reproducing the flow field and an evaluation of how the flow field behaves in a constricted room. This was defined as a requirement for the flow mock-up. The optimization can be done as a subsequent step, if the analysis shows there is a overall possibility.

7.5.3 Variant 3

For the third variant the back outlet has been elongated to the actual outlet of the reference simulation and a pressure outlet is defined with a prescribed pressure of $0Pa$. This is done because it is desired to release the restrictions on the boundaries, e.g. viewer prescribed boundary conditions at the outlets. Additionally, as is well known for CFD, the outlet is taken far away from the model, because at these positions the flow can be assumed to be uniform again and it is guaranteed that the flow field is not influenced by the prescribed boundary condition at the outlet. The inlet boundaries at the front and the back are kept the same. Furthermore, the boundaries at the top and at the side have been changed to a wall boundary, as it would be the case for a physical set-up of the flow mock-up.

From this variant it is expected that due to the velocity difference between the high velocity flow over the top and the stagnant fluid in the passenger cabin, a shear layer is created, extracting fluid from the passenger cabin and therefore creating an underpressure in the passenger cabin. Consequently, the shear layer is directed downwards and attaches at the bottom, where a stagnation point divides the flow to a backflow into the created separation region and the wake. This situation is comparable with the flow in the reference simulation, except the rear part of the vehicle is absent. Due to this however, the backflow could have an influence on the flow field around the manikin, influencing its velocity magnitude. The pressure can be expected to be near the value of the reference simulation, as the same extraction of fluid takes place.

Next to this effect, a boundary layer is expected to be build up at the top and at the side due the high velocity flow.

7.5.3.1 Results of Variant 3

Figure 7.25 shows the difference in velocity magnitude between variant 3 and the reference simulation. This variant has lower differences in velocity magnitude to the reference simulation compared to variant 2. The velocity magnitude at the inboard shoulder is still far off from the reference velocity.

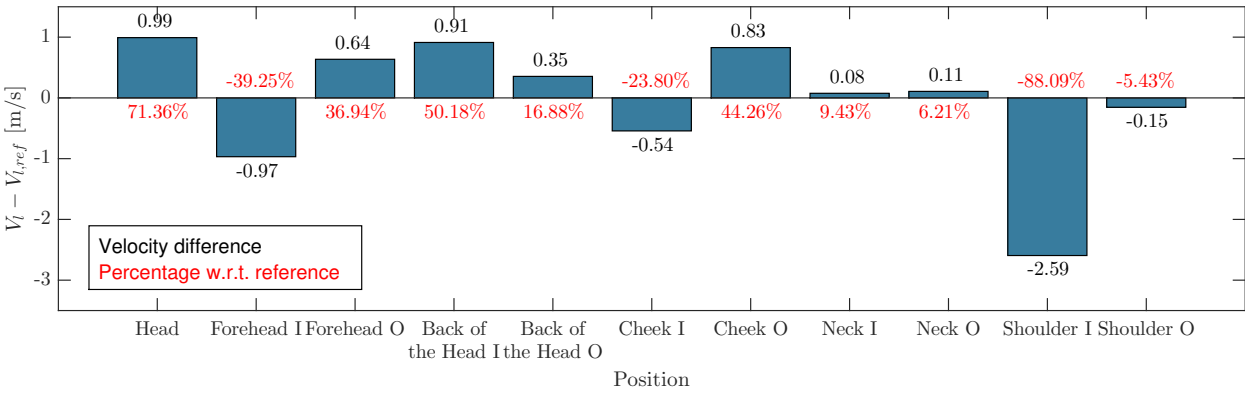

Figure 7.25: Velocity magnitude difference between reference simulation and variant 3

The the velocity flow field at different section cuts indicate the expected separation bubble, which is created by the high velocity flow. Starting from the stagnation point additional backflow is present, influencing the flow field at the front.

The pressure section cuts indicate a much lower pressure coefficient in comparison with the reference and previous variants. At the measurement probes a pressure coefficient of $C_p = -0.6$ is obtained in contrast to -0.48 for the reference simulation. This is due to the created separation bubble and the shear layer, which, as described in Section 2.4, extracts fluid from the separation bubble, consequently creating an underpressure.

From the solution it can be seen, that the creation of the additional backflow influences the flow field surrounding the manikin. Although it decreases the velocity magnitude difference with respect to the reference simulation, the backflow is undesired, because it does not belong to the original flow field.

7.5.4 Variant 4

From variant 3 to variant 4 the back has been restricted to a length of $6m$, as has been defined in Chapter 6. This variant is shown in Figure 7.26 Additionally, the effect of prescribing a constant pressure at the outlet is investigated, because, as already pointed out above, the additional backflow is undesired.

At the measurement probes of the reference simulation a pressure coefficient of -0.48 is measured, which can be used to calculate the pressure difference at the outlet to be equal to

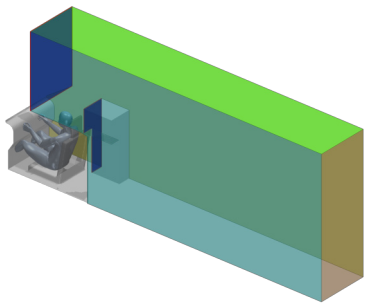

Figure 7.26: Variant 4 of the reduced region with restricted back region

$$\begin{aligned} \Delta P &= C_p \cdot \frac{1}{2}\rho_\infty V_\infty^2 \\ &= -315.77Pa \end{aligned} \tag{7.2}$$

where V_∞ and ρ_∞ are the ambient conditions and can be found in Table 7.4.

This pressure is prescribed at the pressure outlet in order to obtain a C_p-value of -0.48 around the manikin. This prescribed pressure at the outlet will probably affect the flow, as it has to adapt to the outlet condition, especially the high velocity flow over the top

This variant could represent a realistic set-up with a constant suction outlet of $-315.77Pa$.

7.5.4.1 Results of Variant 4

Comparing the obtained results, see Figure 7.27 with the results from variant 3, see Figure 7.25, it can be observed, that these two variants are very similar, with a maximum difference in velocity magnitude of $0.25m/s$ and an average velocity percentage difference with respect to the reference simulation of . The flow field shows a similar back flow as was observed for variant 3 as well. This is due to the adaptation of the flow to the prescribed outlet condition of $-315.77Pa$.

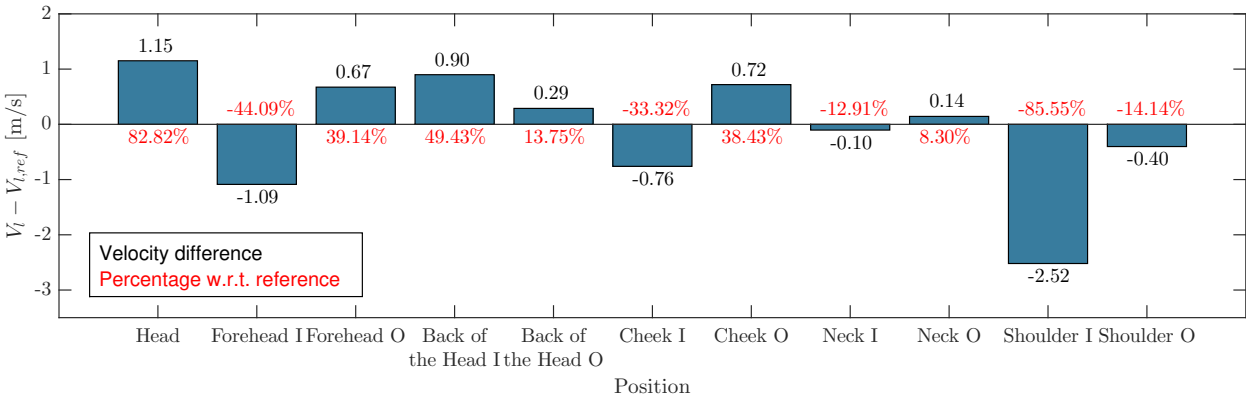

Figure 7.27: Velocity magnitude difference between reference simulation and variant 4

The difference in pressure coefficient of variant 4 and 3 is only $\Delta C_p = -0.0076$. By prescribing the pressure at the outlet to a value of $-315.77Pa$ it was desired to obtain the same pressure coefficient as in the reference simulation. However, due to the back flow of the high velocity flow

and the shear layer between the high and the low velocity flow, the pressure is lower. Furthermore, the pressure in the high velocity region is higher than the pressure in the passenger compartment. By prescribing the pressure, which is present in the passenger compartment, at the outlet the higher pressured flow has to adapt to it, which is why it starts to circulate until it satisfies the pressure condition at the outlet. Therefore in the next step, it would be recommended to distinguish these two fluid flows from each other.

Although the outlet conditions have a constant prescribed pressure condition, the flow behaves very similar to the obtained results from variant 3, which have a prescribed outlet condition of 0 Pa in the far field. The section cuts of the flow field show a very similar flow field as for variant 3, where the creation of the backflow due to the velocity difference between the high velocity flow over the top and the flow in the passenger compartment is present. For this variant the backflow is present because the flow has to adapt to the prescribed pressure conditions. This is an undesired behaviour, the same for variant 3, because it generates a an additional flow field different from the reference simulation.

7.5.5 Variant 5

The results of the previous variants indicate additional backflow due to the high velocity flow over the top, which is not desired, because the main backflow which is generated from the reference simulation is considered in the mapped velocity inlet at the back. The backflow that is generated in variants 3 and 4 is a newly generated flow, which influences the flow field surrounding the manikin. This newly generated flow is not connected with the flow around the vehicle and thus it is undesired. This variant should prevent the generation of a backflow by separating the high velocity from the low velocity flow in the passenger compartment. Therefore, an outlet boundary has been set at $X = -770mm$. The outlet is not positioned at the same x-coordinate as the inlet, as it is the case for variant 1 and 2, in order to give the fluid some room to escape, both the high velocity flow over the top and the flow from the back inlet. At this outlet the pressure from the reference simulation is mapped while at the second outlet at the back the pressure is set to $-315,77Pa$. In this way it is desired to distinguish between two separate regions as it is also the case of the reference simulation. The first region is the region above the vehicle and the second region is the passenger compartment. The regions are distinguished due to the pressure difference between the ambient flow and the passenger compartment.

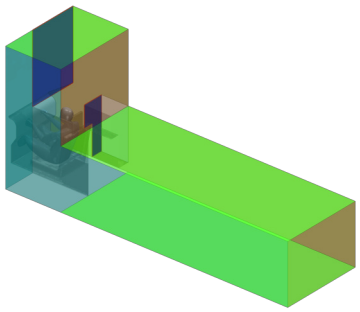

Figure 7.28: Variant 5 of the reduced region with altered back inlet

Additionally, the domain is extended in the y-direction to converge further to a realistic set-up. The boundary is therefore set to $Y = 1500mm$, which is half of the width of the defined space in Chapter 6.

7.5.5.1 Results of Variant 5

The results in Figure 7.29 indicate an improvement in the average percentage of 4.92% in contrast to variant 4.

The section cut planes with the flow field show the desired distinction between the flow over the top and the flow in the passenger compartment. Especially the circulation in the front bottom inboard is reduced and the flow field seems qualitatively more similar to the flow field of the reference simulation. Comparing the symmetry planes with the velocity distribution of variant 4 and 5, shown in Figure 7.30, it can be seen that the backflow in variant 4 flows over the bottom

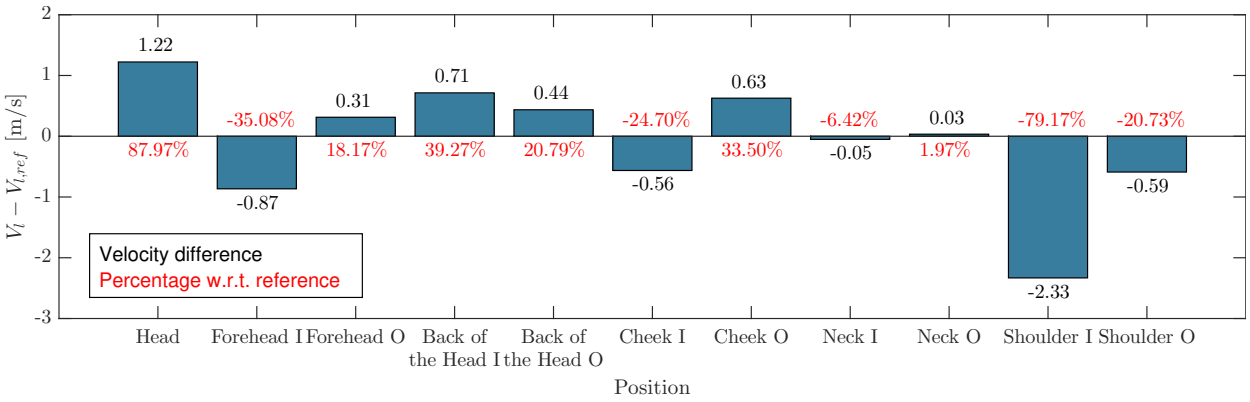

Figure 7.29: Velocity magnitude difference between reference simulation and variant 5

to the front, hindering the circulation flow to escape. Instead the flow field of variant 5 shows that the circulation flow escapes towards the back and thus the circulation is reduced.

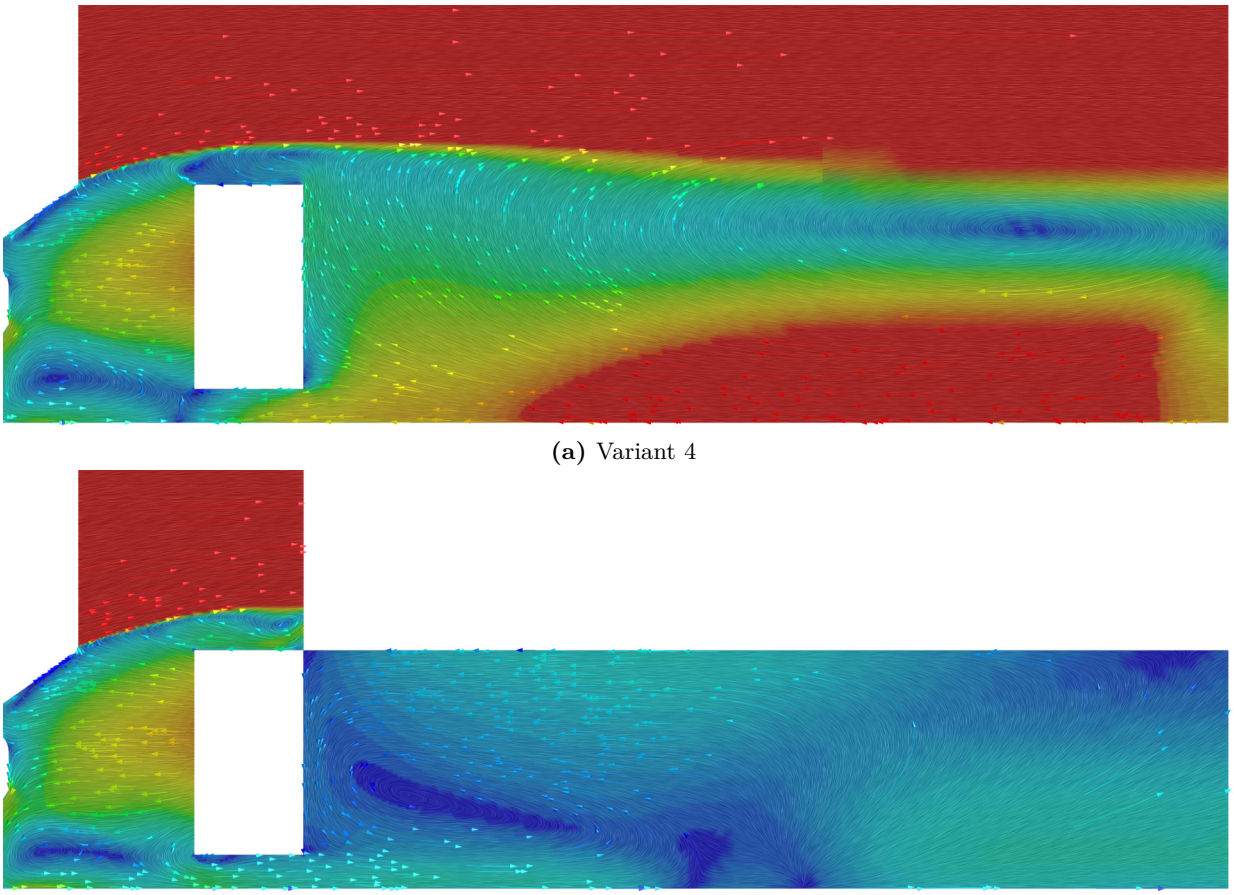

(a) Variant 4

(b) Variant 5

Figure 7.30: Velocity distribution at the symmetry plane of variants 4 and 5

However, there is still a significant flow field in the rear region that influences the flow field in the front. This can be noticed in the XY-planes, see Figure 7.31. Behind the seat at the vehicle outboard the flow can not escape unobstructively. From the XZ-planes the cause for this can be identified to be due to the front pressure outlet. At the lower part flow emanating from the outlet into the domain and propagate to the second outlet at the back.

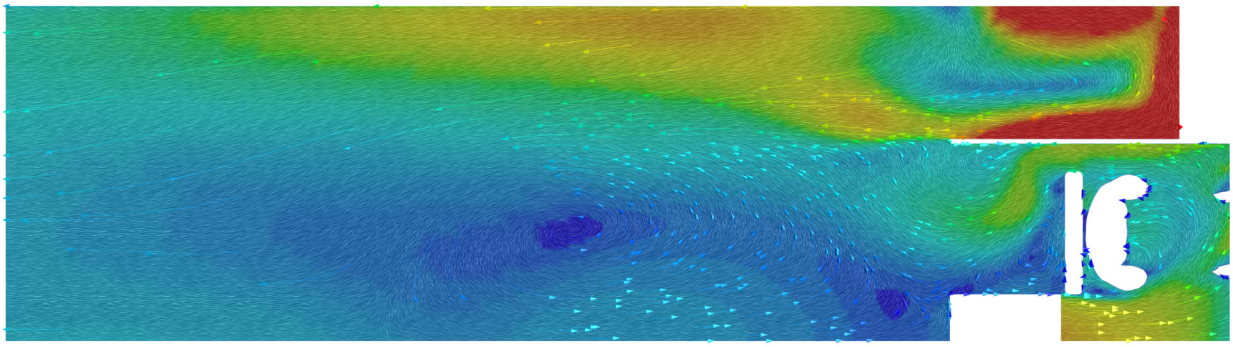

(a) XY-plane at $Z = 800mm$

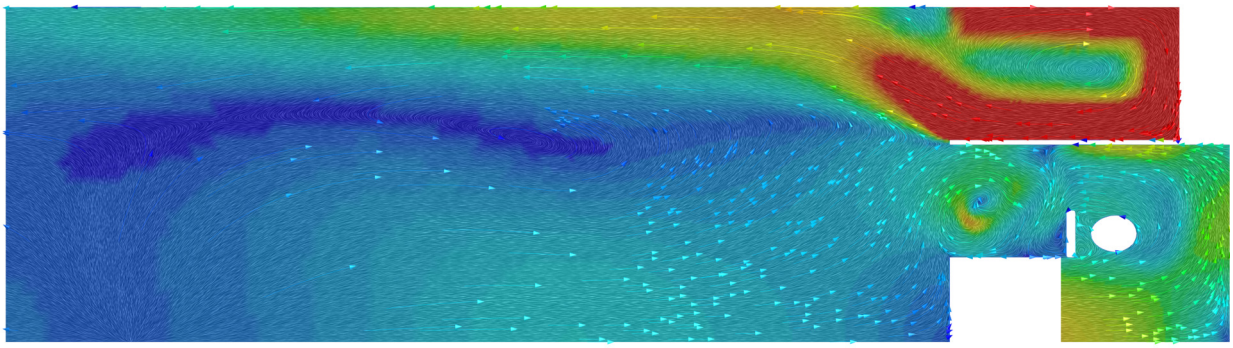

(b) XY-plane at $Z = 1100mm$

Figure 7.31: Velocity distribution at the $Z = 800mm$ and $1100mm$

7.5.6 Variant 6

The domain of variant 6 is not modified with respect to variant 5, but the outlet conditions at the front outlet are also set to a constant pressure of $-315.77\,\text{Pa}$. The results of variant 4 reveal some backflow due to the mapped pressure at the front outlet. Therefore, with this variant the behaviour of the flow under constant pressure conditions is investigated. This also serves as an intermediate step for variant 7, where the front inlet is modified and the pressure conditions at the outlet are not known for the respective situation.

7.5.6.1 Results of Variant 6

The plotted velocity magnitudes in Figure 7.32 show an improvement with respect to variant 5 of 2.99% in the average percentage. The positions head, forehead inboard and cheek outboard still show a velocity magnitude difference of almost 1 m/s, while the difference of the other positions are all below 0.45 m/s, which is can be considered as a good margin without an intensive optimization of the inlet condition. The inboard shoulder position is still far off from the reference value, but this, as was pointed out earlier, is the result of the circulation at the bottom inboard position and can probably only be improved by optimizing the inlet conditions.

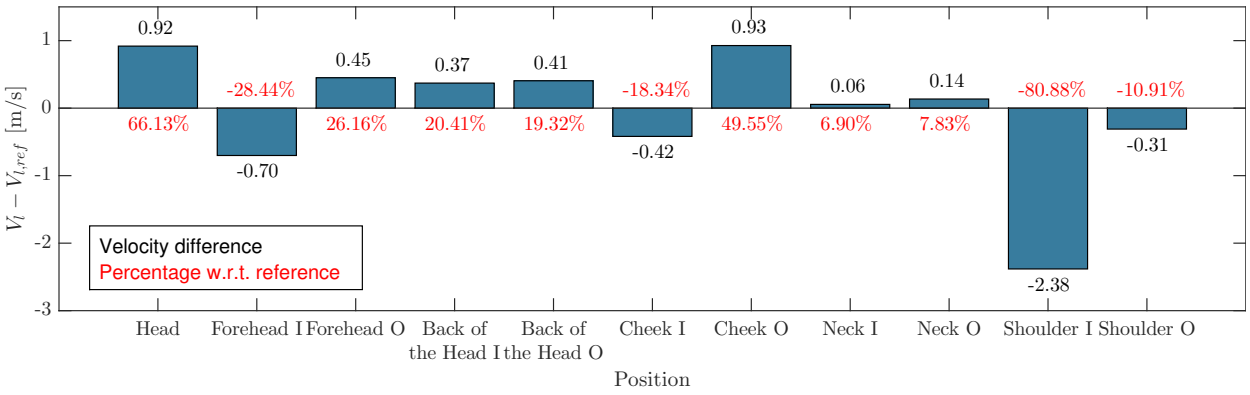

Figure 7.32: Velocity magnitude difference between reference simulation and variant 6

The velocity field distribution at the XY- and XZ-planes also show a better flow distribution in the rear of the domain. This can be considered as an improvement as the flow from the the front can escape to the rear and is less affected by backflow.

7.5.7 Variant 7

With this variant the effect of reducing the front inlet is investigated. A high velocity inlet with a dimension of 904 *mm*x1261 *mm* requires a big fan, which would produce a lot of noise and consequently would irritate the test subject, would be less suited for a physical set-up of a flow mock-up. The reduced flow inlet represents a smaller realistic fan and it keeps the physical set-up of a flow mock-up simple, which is highlighted in blue in Figure 7.33.

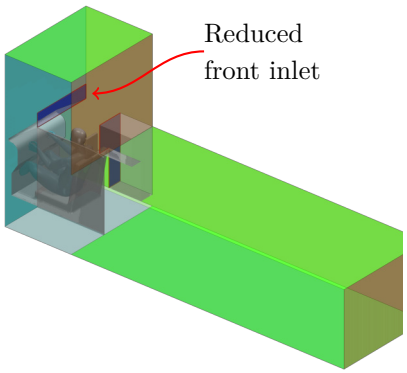

Figure 7.33: Variant 2 of the reduced region with altered back inlet

Due to the reduced front inlet, the fluid at the top of the domain is stagnant as well as the fluid in the passenger compartment. Therefore, it is expected that due to the high velocity flow from the inlet an additional shear layer at the top is created. This will also create an underpressure region as fluid is extracted, which in turn directs the flow upwards, while the underpressure below the high velocity flow will direct the flow downwards. Thus, at the top the pressure will be below ambient pressure and the high velocity flow from the inlet will be more directed upwards compared to the previous variants.

7.5.7.1 Results of Variant 7

At the measurement probes of all outboard positions and the forehead inboard as well as cheek inboard the velocity magnitudes are improved with respect to variant 6, see Figure 7.34. The velocity magnitude of the other positions are slightly increased, especially the neck inside position has increased with 0.12 m/s relative to variant 6, resulting in 49% difference with respect to the reference simulation in contrast to 6.9% for variant 6.

The overall performance of this variant is promising, as due to the reduced velocity inlet no significant disadvantages can be noticed.

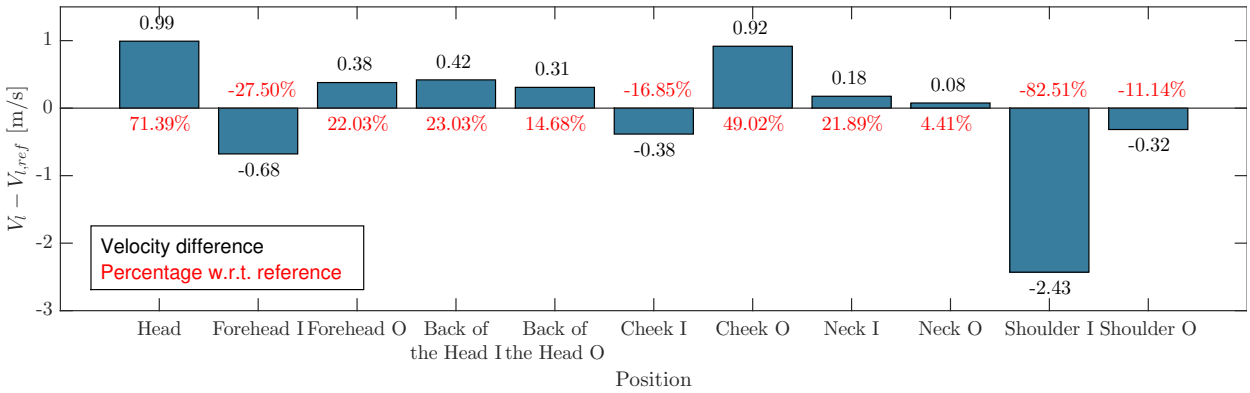

Figure 7.34: Velocity magnitude difference between reference simulation and variant 7

7.5.8 Variant comparison

As a wrap up, Figure 7.35 and Figure 7.36 line up the velocity magnitude and the pressure coefficient of all the variants once again.

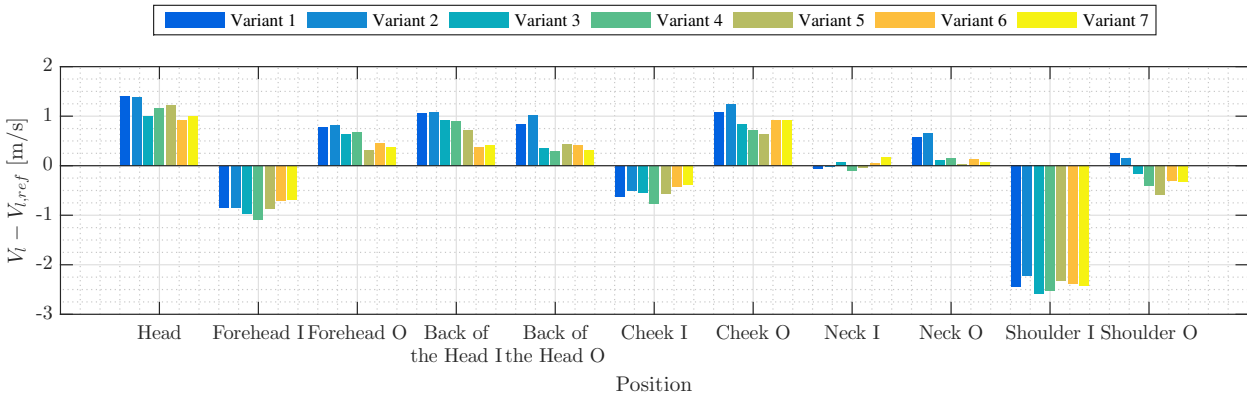

Figure 7.35: Velocity magnitude difference between reference simulation and variant 1

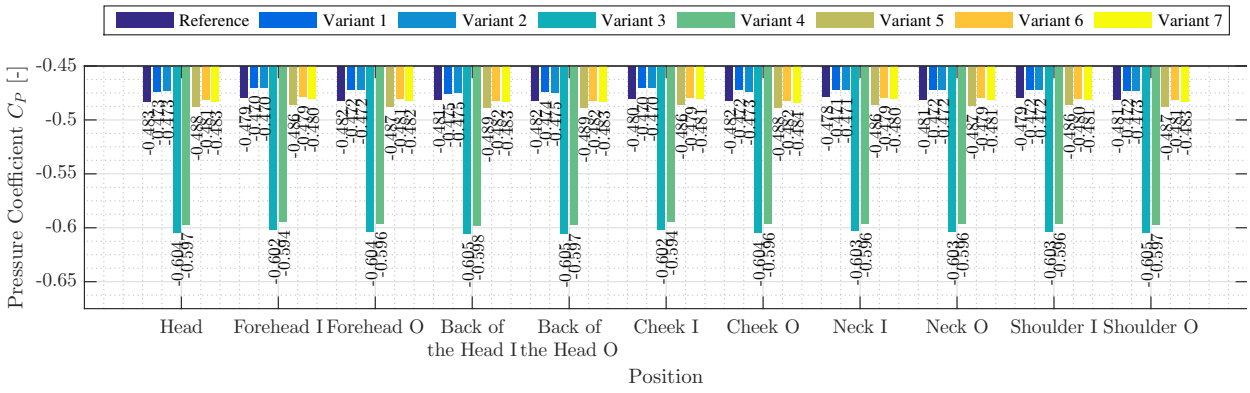

Figure 7.36: Pressure coefficients of the reference simulation and all variants

The comparison of the difference in velocity magnitudes with respect to the reference simulation shows an improving trend from variant 1 to 6. Furthermore, as already pointed out in the results of the variants, the error at the inside shoulder position is recurrent. From Figure 7.35 it can be noticed, that the inlet change of variant 2 has a positive effect on the inboard shoulder position,

while the backflow in variant 3 and 4 on the other hand had a negative effect on the velocity magnitude, as the velocity has been either decreased or increased.

From the comparison of the pressure coefficients in Figure 7.36 especially the effect of the backflow and the associated flow interchange at the shear layer for variants 3 and 4 can be noticed.

7.6 Unsteady Simulation

As a final check of the unsteady phenomena for the reduced domain an unsteady simulation is conducted. The intention is to check whether the fluctuating phenomena, which are considered to be the most influential physical factors on the comfort, are present when the domain is reduced. Because such an unsteady simulation takes a lot of time, this is executed with a different version of variant 6. This version has the front and back inlet as are defined for variant 1, while at both pressure outlets a constant pressure of $-250Pa$ is defined. The settings for this unsteady simulation have been chosen as recommended from [33, 66] and are summarized in Table 7.8.

Table 7.8: Numerical set-up summary of the unsteady simulation

Program	CD-Adapco StarCCM+
Model	Symmetrical
Number of cells	11 million
Smallest cell size	$10mm$
Numerical Equations	DES
Turbulence Model	SST (Menter) $k-\omega$ detached eddy
Flow type	Constant density & incompressible
Time modelling	Implicit unsteady
Time step	3.3×10^{-4} according to a CFL-value of 1
Wall treatment	All y+
Solver	Segregated flow
Simulation speed	33.33 m/s

The obtained result of the C_p-fluctuations can be compared with with CFD simulations from [23]. In [23] experimental measurements are conducted and the pressure coefficients at different positions around a measurement-manikin and for different vehicle configurations are recorded and averaged over a period of 30 seconds. Additionally, the different configurations are simulated under unsteady conditions in CFD, which correlated well with the experimental measurements according to [23]. The paper does not exactly describe, which exact settings were used for the simulations. The stated properties are given in Table 7.9.

The CFD results of the CFD simulation of [23] at the inboard and outboard ear are shown in Figure 7.37b. In contrast to these results Figure 7.37a shows the results of conducted unsteady CFD simulation of variant 6.

The obtained C_p-results of Figure 7.37a have been filtered with the use of a Savitzky-Golay filter in Matlab, as the simulation settings have probably been chosen with too much detail producing very high frequency data compared to the CFD simulations of [23].

The probe values show similar behaviour as has been determined in [23]. The amplitudes of Figure 7.37a are a higher compared to Figure 7.37b, which could be explained by the difference in simulation speed. Overall, the results show that fluctuations are present in the reduced domain, even for boundary conditions at the inlets obtained from the reference simulation under steady conditions. Due to missing information of the CFD settings from [23] as well as due to limited time the simulation settings are not the same.

Table 7.9: Numerical set-up summary of the unsteady simulation in [23]

Program	PowerFLOW 4.5C
Model	Bentley Continental GTC Speed convertible 14MY with side windows up and multiple configurations of passengers and wind breaks
Number of cells	172 million voxels
Smallest cell size	$1.5mm$
Numerical Equations	Lattice-Boltzmann
Turbulence Model	Very Large Eddy Simulation
Flow type	-
Time modelling	-
Time steps	500,000
Wall treatment	-
Solver	-
Simulation speed	27.78 m/s

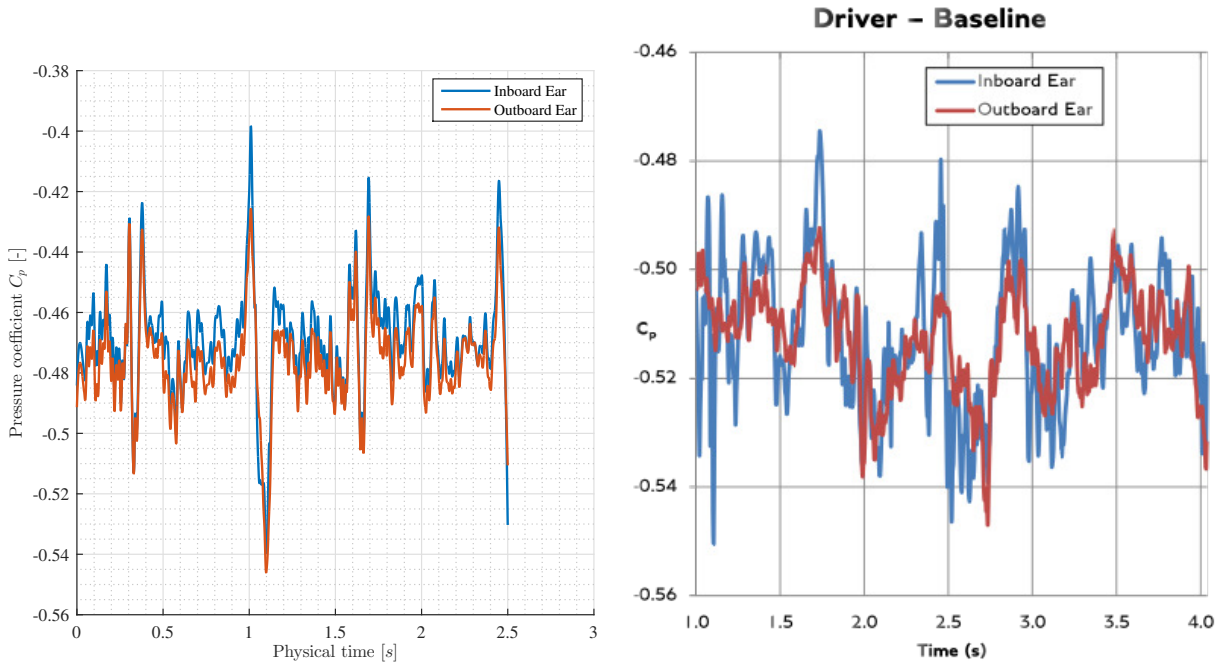

(a) Resulting dynamic C_p probe of variant 6

(b) Dynamic C_p probe from [23]

Figure 7.37: Comparison of pressure coefficient fluctuations for unsteady simulation

7.7 Discussion & Implications of CFD Results on the Physical Flow Mock-Up

Comparing the obtained results with the results of the measurement analysis in Chapter 5, it can be seen, that the velocity differences between the reference simulation and the variants, with the focus on variant 7 in Figure 7.34, are close to within the ±5% margin of sensitivity for the body parts, see Table 5.3. This implies, that the percentage of dissatisfied subjects range inbetween 10% at the most sensitive velocity. In a cabriolet a subject will probably not sense such a low velocity difference. Additionally, due to the fluctuating phenomena, this velocity difference becomes even

less noticeable. However, from the three dimensional flow field visualisation, like Figure 7.24a, a significant difference in the overall flow field can be identified. All the variants indicate a formation of a circulation region at the bottom of the vehicle inboard position, which propagates to the outboard and significantly influences the flow field around the manikin. Although the analysis in Section 7.4 indicates the main flow source of the flow field surrounding the manikin to be at the inboard of the vehicle, other inlet conditions could optimize the overall flow field.

Further practical tests have to reveal whether the perception is similar and comparable. The difference between the CFD simulation and a physical flow mock-up would be the outlet. It is not practical to define a physical outlet with a constant pressure. Instead for the physical flow mock-up, the mass outlet can be regulated as an outlet condition, which is not directly possible with CFD simulations.

Physical Translation Translating variant 7 into a physical set-up would mean that the indicated inlets represent the position of the flow generators. In Figure 7.38 variant 7 is placed into the space of the specified room. In the front the cut-out of the cabriolet can be seen and the possible positions of the flow sources are highlighted in red, while the outlet is highlighted in green.

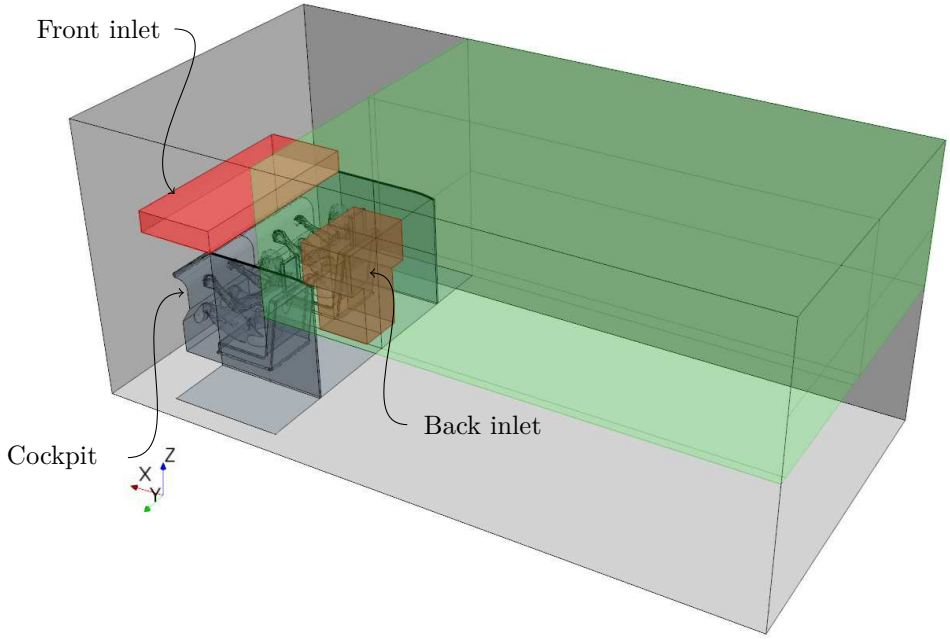

Figure 7.38: Isometric view from the back onto physical translation set-up of variant 7

The air inlets have to be independent of each other because different velocity conditions appear at the inlets. One flow source would have to be placed at the front above the windscreen along the horizontal length of windscreen header. This flow generator would have to produce the high velocity flow up to the desired driving speed equally distributed over the whole inlet, in this case $33.33 m/s$. The fan can be placed outside, while a duct leads the air flow to the desired position. As in the CFD simulation the x-, y-, z-components of the velocity from the reference simulation are mapped onto the inlet this has to be translated in the design as well. This is important in order to account for the windscreen angle, which differs for different models of cabriolets.

The back inlet of this variant has no direct connection with the ground or the wall of the surrounding space. The space between the ground and the inlet is on purpose, for the flow to be able to escape, see Section 7.5.2. Additionally, the flow originating from this air inlet has a specific inlet distribution and therefore it not possible to feed this flow inlet from one flow generator.

This flow generator has to generate a specific velocity distribution which differs from cabriolet to cabriolet. This means that this inlet needs to consists of multiple independent flow generators, which have to generate velocities up to $10m/s$, based on the measured velocities in Chapter 5.

The green area indicates the outlet of variant 7. The purpose of the outlet is to mainly suck away or separate the high velocity flow of the front inlet, such that this flow does not further interfere with the flow inside the passenger when propagating to the back.

Unsteady Simulation The unsteady simulation has shown, that the important unsteady phenomena, which mainly influence the thermal comfort of a passenger, are also present in the reduced set-up for the flow mock-up. However, the conducted unsteady simulation were not the main focus of the analysis. More time is needed for the simulation set-up. Furthermore, no numerical values from experimental data are available at this point, except the plots and information given in [23].

Chapter 8

Conclusion & Recommendations

In the introduction the demand for faster and reliable development processes in the automotive sector is stated. One possibility to achieve this is, by the idea of a flow mock-up. The aim of this thesis was to concretise this idea by answering the following research question:

Which factors influence the possibility to experimentally replicate the flow field of a cabriolet in a flow mock-up in the early development phase, addressing thermal comfort, especially draught phenomena and how can this flow around a cabriolet passenger be replicated?

The first part of the research question has been answered by identifying what the flow mock-up should fulfil in order be beneficial for the project development process as well as what characteristic factors influence the human perception while driving an open cabriolet. How the flow around a cabriolet passenger can be replicated has been investigated with a preliminary CFD analysis showing the possibility of replicating the flow field, which is present inside the passenger cabin of an open cabriolet, in a closed space and without the dependency on the vehicle geometry.

Development Process The actual development process regarding thermal comfort development of open cabriolets has been analysed to identify how a flow mock-up can be implemented and how it will improve the development process. Additionally, this has been done to determine the project related requirements on the flow mock-up. Therefore, a modified cabriolet development process has been proposed, showing how the development process would look like when a flow mock-up is used. In contrast to the actual development process, the modified development process has no need for experimental testing with modified predecessors or prototypes in the windtunnel, which is linked to high development costs. The flow mock-up in combination with CFD simulations enable the assessment of thermal comfort throughout the development process. Furthermore, in the actual process experimental testing can only be done after the packaging has been determined. The package freeze milestone is considered as an important milestone, which can be influenced to implement measures to improve the thermal comfort of cabriolets. As CFD simulations as well as the flow mock-up are not dependent on physical models, the subjective assessment can be initiated in the early development phase of the project. The results of the subjective evaluation of thermal comfort in the flow mock-up can be used to influence the packaging of the base model in order to steer the development and implement measures for the improvement of thermal comfort in open cabriolets. Another advantage of the independency on physical models is the flexibility CFD simulations offer, which can be directly replicated in the flow mock-up.

In order to identify further requirements from the project two scenarios have been proposed, which specify the application of the flow mock-up in the development process. The first scenario includes the possibility of an instant before and after comparison of flow fields. With this comparison the direct influence of measures to improve thermal comfort can be evaluated. Therefore, the flow mock-up is required to be able to replicate the flow field independent of the vehicle's geometry because it is an instant change of flow field can be compared the best. If it is independent, no

reconstructions are needed to replicate the flow field of a different vehicle, different component or different configuration. This feature would increase the flexibility even further.

The second scenario picks up the idea of reverse engineering. Starting with a replicated reference simulation in the flow mock-up, a subject evaluates the flow field and identifies the locations, which are most uncomfortable. With the feedback from the subject, the flow field is modified, such that an improvement of thermal comfort is obtained. The modifications are translated back to the CAD-model, from which an optimized component is obtained. To realize this scenario, the flow mock-up needs to have the possibility to individually control the flow field such that velocities at specific positions can be adjusted. Furthermore, a tool would have to be developed, which can reverses the changes from the flow field to the digital model.

Influence factors An intensive literature research has been conducted, to identify the factors, which influence the perception of a human, when driving in an open cabriolet. All the factors have been stated and their properties in an open cabriolet ride have been identified. The influence factors have been split into the human and the physical influence factors. The human factors include the factors, which influence how the human subjective perception is formed, while the physical influence factors identify the physical phenomena a human is exposed to when driving in an open cabriolet.

The most essential conclusion from the human influence factors for the flow mock-up is, that the subject should be able to associate the experience in flow mock-up with an open cabriolet ride. Therefore, the appearance of the flow mock-up should be very similar to the appearance of a real cabriolet. This can be either done by taking a cut-out of a cabriolet cockpit in combination with the use of a screen showing a road simulation or by the use of virtual reality in combination with a simplified set-up consisting of the components that a passenger needs to control when driving a cabriolet.

The main task of the flow mock-up will be to replicate the physical factors, including the air velocity, especially their fluctuations, pressure fluctuations, temperature, air humidity and solar radiation. The most characterizing physical factor are the velocity fluctuations, which will also be the most challenging factor to be replicated by the flow mock-up. In the passenger compartment velocities of 3% to 40% of the driving velocity, depending on the location at the body, are present. The velocity fluctuations at the different body parts are not known, except at the head, which fluctuated between 4% to 12% of the driving velocity. In the passenger compartment of an open cabriolet an underpressure is present due to the shear layer. The pressure fluctuations are a consequence of the velocity fluctuations. The temperature, air humidity and solar radiation directly influence the impact of the velocity fluctuations and depend on the desired climate conditions to be replicated.

The accuracy of the flow mock-up to replicate a flow field such, that it can be recognized as a specific flow field, has been determined with the use of measurement data obtained from [12, 15, 16]. The available measurement data for every upper body locations, which are the most sensitive to draught phenomena in open cabriolets, has been used to generate curves, which indicate the sensitivity for every body position. These curves indicate, what flow velocity accuracy a flow mock-up needs to have to be within a certain range of predicted percentage dissatisfied. Every curve has a inflation point, at which the slope is the highest, and thus indicates the highest point of sensitivity. For the most sensitive body part, which is the neck, the flow mock-up should be within a velocity of $\pm 0.14\ m/s$ from the average velocity in order to be within a $\pm 5\%$ confident bound of predicted percentage dissatisfied.

CFD Analysis The technical feasibility of the flow mock-up has been investigated by a CFD analysis. The aim was to investigate the possibility of replicating the flow field inside the pas-

senger compartment in a constrained environment and without the dependency of the vehicle's geometry. From the results obtained from a reference simulation with a simplified cabriolet model with windows-up and no wind-break configuration, boundary conditions have been imposed on constrained computational domains. Seven variants of the constrained environment have been investigated, which started from an domain with imposed boundary conditions on every boundary of the domain and converged to a realistic set-up of physical flow mock-up, with boundary conditions imposed on only two inlet boundaries and two distinct.

The CFD analysis has shown promising results as a similar flow field has been replicated as well as fluctuating phenomena without the use of the vehicle geometry. With inlet conditions without optimization a configuration has been generated, which obtained local velocities deviating from 0.08 m/s to 0.68 m/s from the velocities of the reference simulations, except near the inside shoulder and the head. At these locations, an important difference in the flow field has been identified, which propagates through the flow field and introduces differences in the overall flow field.

Conclusion

In order enable the possibility to replicate the flow field of a cabriolet in a flow mock-up in the early development, from the point of view of the project it is required that the flow mock-up improves the development process by reducing the costs as well as improving the thermal comfort when driving a cabriolet with an open roof. To achieve this, CFD simulations have to be conducted soon after the milestone of the project mission, which then have to be replicated in the flow mock-up. This enables the possibility to assess the thermal comfort of the vehicle under development before the milestone of the package freeze, which can therefore be influenced with the obtained results. The combination of no experimental testing, early assessment of thermal comfort with the help of CFD simulation and the flow mock-up lead to the conclusion that the use of a flow mock-up offers to make the development process more cost efficient as well as more flexible. Furthermore, the possibility to experimentally replicate the flow field of a cabriolet in a flow mock-up is conditioned by the influence factors, which affect the human perception in psychological and physical manner. From these influence factors it can be concluded that the flow mock-up is required to be suggestive for a cabriolet in its appearance. Additionally, the physical perception of the flow field is primarily influenced by the fluctuating phenomena of the velocity and the pressure, which have to be reproduced in the flow mock-up.

The CFD analysis has shown the theoretical possibility to replicate the flow field obtained from a reference simulation in a reduced closed space without the dependency of the vehicle geometry. To replicate this flow field around the passenger of an open cabriolet two main velocity inlets have been localized, one constant velocity inlet at the front above the theoretical windscreen and one inlet at the inboard back behind the front passenger, which has to produced variable velocity flow. This CFD analysis has been produced in a short amount of time and certainly needs optimization to achieve better results. All in all, the research has shown results, which can be used as a basis to further elaborate on the development of a flow mock-up.

Recommendations

This research serves as a starting point of the development of a flow mock-up, but it is far from finished and several recommendations have emerged from this research.

Until the day of writing, measurements on cabriolets have been mainly conducted with the goal to generate an analytic thermal comfort model. One of the next steps should be to investigate a cabriolet with the specific goal in mind to build a flow mock-up. Therefore, measurements of the

exact physical conditions, which are present in a cabriolet, have to be conducted, i.e. no averaged measurements. The physical conditions should definitely include the frequency and magnitude of the velocity and pressure fluctuations for all body parts. Additionally, CFD simulations should be conducted and verified with these measurements. This should also reveal, what resolution is needed for the CFD simulation to get similar results.

The CFD analysis has shown many points of investigations. This analysis was a preliminary investigation and was done for a cabriolet without a wind-break and with side windows up only. However, the flow mock up should be able to replicate multiple configurations in order to be advantageous for the development. Thus, it is recommended to simulate other cabriolets configurations in order to find a common flow source, such that the flow mock up does not has to be reconfigured. This would also include the optimization of the inlets, as the CFD analysis has identified a circulation region that influences the flow field significantly.

Furthermore, it needs to be investigated, how dependent the flow is on the design of the cabriolet interior. For this, CFD simulations of different cabriolets have to be generated from which boundary conditions can be imposed onto the optimized inlets of a general cockpit design, representing the flow mock-up.

The unsteady simulation has shown, that fluctuating phenomena have been produced even with boundary conditions obtained from a steady simulation. A point of investigation follows from this, whether the reference simulation, which has to be performed to *feed* the flow mock-up with information regarding the velocities which have to be reproduced, has to be conducted in unsteady conditions or can be performed in steady conditions to obtain an unsteady physical flow field in the flow mock-up. This would save computational time in the early development phase.

Last but not least, it has to be investigated, which components can be used to generate the flow field, especially the fluctuations. While the front inlet, generating the high velocity flow over the cabriolet, has no special requirements, the flow from the back inlet is not constant. The flow has to be regulated with respect to velocity magnitude as well as direction.

Bibliography

[1] Oden, J. et al. "Simulation-based engineering science". In: *National Science Foundation* (2006).

[2] Wiedemann, D. B. *Prozesse und Trends in der Nutzfahrzeugindustrie*. 2006.

[3] Bubb, H. et al. "Produktentstehungsprozess". In: *Automobilergonomie*. Springer, 2015, pp. 1134–1213.

[4] Bubb, H. et al. *Automobilergonomie*. Springer, 2015. Chap. Der Mensch als Fahrer, pp. 67–162.

[5] American Society of Heating, Refrigerating, and Air-Conditioning Engineers, Inc., Atlanta, Ga. *Standard 55-2004, Thermal Environmental Conditions for Human Occupancy*. Tech. rep. ANSI, 2004.

[6] Wang, Y., Lian, Z., and Lan, L. "The effect of turbulence intensity on local skin temperature and subjective responses to draft". In: *Energy and Buildings* 43.10 (2011), pp. 2678–2683.

[7] Alahmer, A. et al. "Vehicular thermal comfort models; a comprehensive review". In: *Applied Thermal Engineering* 31.6 (2011), pp. 995–1002.

[8] Fanger, P. O. et al. "Thermal comfort. Analysis and applications in environmental engineering." In: *Thermal comfort. Analysis and applications in environmental engineering.* (1970).

[9] Fuchslocher, G. *Mercedes-Benz: Der Zugluft im Cabrio auf der Spur*. Ed. by Automobil Produktion. Retrieved: 04/11/2016. Nov. 4, 2016. URL: `https://www.automobil-produktion.de/technik-produktion/forschung-entwicklung/mercedes-benz-der-zugluft-auf-der-spur-281.html`.

[10] Currle, J. and Moos, O. "Numerical Analysis of the Flow Over Convertibles". In: *SAE Technical Paper*. SAE International, May 2001.

[11] Fanger, P. and Christensen, N. "Perception of draught in ventilated spaces". In: *Ergonomics* 29.2 (1986), pp. 215–235.

[12] Meder, J. "Erstellen eines neuen analytischen Modells zur Bewertung und Optimierung des subjektiv empfundenen Klimakomforts in offenen Fahrzeugkabinen". Master thesis. RWTH Aachen, June 2004.

[13] Cogotti, A. *Experimental Techniques for the Aerodynamic Development of Convertible Cars*. Tech. rep. SAE Technical Paper, 1992.

[14] Moos, O. and Currle, J. "Evaluation of Thermal Comfort in Convertibles". In: *SAE Technical Paper*. SAE International, Mar. 2002.

[15] Wetzlich, B. *Aufbau und Validierung eines Messsystems zur objektiven Bewertung und Optimierung des Klimakomforts in offenen Fahrzeugkabinen*. Porsche AG. 2006.

[16] Behre, L. *Bewertungsmodell für Zugfreihaltung (Evaluation model for draught phenomena)*. Tech. rep. RWTH Aachen, Feb. 2012.

[17] Weber, J. *Automotive development processes*. Springer, 2009.

[18] Kennings, P. R. et al. "A Novel Use of Acoustic and Vibration Simulation Techniques to Develop Better Ride Comfort for a Luxury Cabriolet Car". In: *SAE Technical Paper*. SAE International, May 2013.

[19] Anderson Jr, J. D. *Fundamentals of aerodynamics*. Ed. by s. Tata McGraw-Hill Education, 2010.

[20] Schütz, T. *Hucho-Aerodynamik des Automobils: Strömungsmechanik, Wärmetechnik, Fahrdynamik, Komfort*. Springer-Verlag, 2013.

[21] Heisler, H. "Vehicle body aerodynamics". In: *Advanced Vehicle Technology*. Elsevier, 2002, pp. 584–634.

[22] Raemdonck, G. M. V. "Design of Low Drag Bluff Road Vehicles". PhD thesis. TU Delft, 2012.

[23] Hesmondhalgh, M. and Waskett, M. *Convertible Cabin Comfort*. EG/P2 Aerodynamics. June 2015.

[24] Barnard, R. H. "Aerodynamic problems and solutions in open cabriolet vehicles". In: *Royal Aeronautical Society Conference on Vehicle Aerodynamics* Loughborough, UK (1994), pp. 2.1–2.7.

[25] Dannhäuser, P. et al. "Wirkprinzip und Realisierung des Mercedes-Benz Aircap". In: *ATZ-Automobiltechnische Zeitschrift* 112.10 (2010), pp. 722–728.

[26] Ruijter, R. de. "Turbulence structures affecting stone stability in backward-facing step flow: Experiments by means of Particle Image Velocimetry". Master thesis. TU Delft, June 2004.

[27] Schäfer, F., Breuer, M., and Durst, F. "The dynamics of the transitional flow over a backward-facing step". In: *Journal of Fluid Mechanics* 623 (2009), pp. 85–119.

[28] Armaly, B. F. et al. "Experimental and theoretical investigation of backward-facing step flow". In: *Journal of Fluid Mechanics* 127 (1983), pp. 473–496.

[29] Ho, C.-M. "Three-dimensional recirculation flow in a backward facing step". In: *J. fluids Eng* 116 (1994), pp. 228–232.

[30] Lanfrit, M. *Best practice guidelines for handling Automotive External Aerodynamics with FLUENT*. 2005.

[31] ANSYS. *Fluent User Guide Version 6.1*. 2003.

[32] Pope, S. *Turbulent Flows*. Cambridge University Press, 2000.

[33] CD-Adapco. *Star-CCM+ User Guide Version 11.04*. 2016.

[34] Ariff, M., Salim, S. M., and Cheah, S. C. "Wall y+ approach for dealing with turbulent flow over a surface mounted cube: part 1—low Reynolds number". In: *Proceedings of the 7th International Conference on CFD in the Minerals and Process Industries, Melbourne, Australia*. 2009, pp. 9–11.

[35] Braess, H.-H. and Seiffert, U. *Vieweg Handbuch Kraftfahrzeugtechnik*. Vol. 7. Springer-Verlag, 2013.

[36] Hirz, M. et al. "Automotive Development Processes". In: *Integrated computer-aided design in automotive development*. Springer, 2013, pp. 1–23.

[37] Liebl, J., Kerschbaum, H., and Pfannkuchen, E. "Die Aerodynamik des neuen BMW X5". In: *ATZ-Automobiltechnische Zeitschrift* 110.4 (2008), pp. 302–311.

[38] Prenner, M. "Abschätzung des aerodynamischen Verhaltens in der konzeptionellen Fahrzeugentwicklung". Master thesis. Institut für Fahrzeugtechnik Member of Frank Stronach Institute, 2011.

[39] Burk, A. "Aerodynamik in der frühen Fahrzeugentwicklung". PhD thesis. Technischen Universität Berlin, 2014.

[40] Othmer, C. "CFD Topology and shape optimization with adjoint methods". In: *Verkehrstechnik, VDI Fahrzeug-und* (2006).

[41] Georgios K, K. et al. "Adjoint Optimization for Vehicle External Aerodynamics". In: *International Journal of Automotive Engineering* 7.1 (2016), pp. 1–7.

[42] Krist, R. "Modellierung des Sitzkomforts: Eine Experimentelle Studie (Modelling sit comfort: an experimental study)". PhD thesis. Ph. D. Thesis, IfE, Munich (in German), 1994.

[43] Knauer, P. et al. "Objektivierung des Schwingungskomforts bei instationärer Fahrbahnanregung". PhD thesis. Technische Universität München, 2010.

[44] Bubb, H. et al. "Gestaltung der Konditionssicherheit". In: *Automobilergonomie*. Springer, 2015, pp. 471–524.

[45] Mikulec, A. A. et al. "Noise exposure in convertible automobiles". In: *The Journal of Laryngology & Otology* 125.2 (Feb. 2011), pp. 121–125. url: https://www-cambridge-org.tudelft.idm.oclc.org/core/article/noise-exposure-in-convertible-automobiles/1C34842FC2977A8AACEA2B868BC9136A.

[46] Michael, P., Opie, N., and Smith, M. "Noise exposure and convertible cars". In: *Otolaryngology-Head and Neck Surgery* 143.2 (2010), pp. 219–222.

[47] *DIN 33402 Ergonomics - Human body dimensions – Part 2: Values*. 2005.

[48] *ISO 7250 – Basic human body measurements for technological design*. 2010.

[49] Hensen, J. "Literature review on thermal comfort in transient conditions". In: *Building and Environment* 25.4 (1990), pp. 309–316.

[50] Griefahn, B., Künemund, C., and Gehring, U. "The impact of draught related to air velocity, air temperature and workload". In: *Applied Ergonomics* 32.4 (2001), pp. 407–417.

[51] Griefahn, B. and Künemund, C. "The effects of gender, age, and fatigue on susceptibility to draft discomfort". In: *Journal of Thermal Biology* 26.4 (2001), pp. 395–400.

[52] Fanger, P. O. et al. "Air turbulence and sensation of draught". In: *Energy and buildings* 12.1 (1988), pp. 21–39.

[53] Fanger, P. and Pedersen, C. "Discomfort due to air velocities in spaces". In: *Proceedings of the Meeting of Commission B*. Vol. 1. 1977, B2.

[54] Huang, L., Ouyang, Q., and Zhu, Y. "Perceptible airflow fluctuation frequency and human thermal response". In: *Building and Environment* 54 (2012), pp. 14–19.

[55] Xia, Y. et al. "Effects of turbulent air on human thermal sensations in a warm isothermal environment". In: *Indoor Air* 10.4 (2000), pp. 289–296.

[56] Toftum, J. and Nielsen, R. "Draught sensitivity is influenced by general thermal sensation". In: *International Journal of Industrial Ergonomics* 18.4 (1996), pp. 295–305.

[57] Mayer, E. "Ist die bisherige Zuordnung von PMV und PPD noch richtig?" In: *KI. Luft-und Kältetechnik* 34.12 (1998), pp. 575–577.

[58] Melikov, A. "Quantifying draught risk". In: *Bruel & Kjaer Technical Review* 2 (1988).

[59] Toftum, J. "Air movement – good or bad?" In: *Indoor Air* 14 (2004), pp. 40–45.

[60] Danca, P., Vartires, A., and Dogeanu, A. "An Overview of Current Methods for Thermal Comfort Assessment in Vehicle Cabin". In: *Energy Procedia* 85 (2016), pp. 162–169.

[61] Newell, J. *New platform for advanced auto engineering simulation*. Ed. by TrafficSafe. Retrieved: 04/11/2016. May 31, 2016. URL: http://trafficsafe.org/index.php/new-platform-advanced-auto-engineering-simulation-12141/.

[62] Dr. Ing. h.c. F. Porsche AG. *911-Katalog*. Oct. 2015.

[63] Palin, R. B., Gaylard, A. P., and Cook, R. G. A. "CFD Investigation of Unsteady Flow Features in and Around the Passenger Compartment of an Open-top Coupe". In: *3rd MIRA International Conference on Vehicle Aerodynamics*. Dunchurch, Oct. 2000.

[64] Regin, F. et al. "Aerodynamic Analysis of Cabriolet Passenger Car: A Design Approach". In: *SAE Technical Paper*. http://dx.doi.org/10.4271/2013-01-0037. SAE International, Mar. 2013.

[65] Wang, D. and Yang, S. Z. "Research on Factors Leading to Variant Aerodynamic Drag Coefficient of Different Cabriolets". In: *Proceedings of SAE-China Congress 2015: Selected Papers*. Springer. 2016, pp. 445–455.

[66] Ross, F. J. *Unsteady Vehicle Simulation*. Ed. by CD-Adapco. Internet Presentation. Retrieved: 08/2016. URL: http://www3.cd-adapco.com/pdfs/presentations/jsw11/11-01-UnsteadyAerodynamics_R02.pdf.

Appendix A

Measurement Analysis

This appendix contains an overview of the tested vehicles from [12, 15, 16], Table A.1 and the plots created with the measurement data. This is further elaborated on in Chapter 5.

Table A.1: Overview of vehicles used for experimental measurements in [12, 15, 16]

Vehicle	Model year	Source
Mercedes E-Class	2010	[16]
BMW 1-Series	2008	[16]
Peugeot 308 CC	2009 (probably)	[16]
Audi TT Roadster	2008	[16]
Porsche 911	2009	[16]
BMW Z4	2003 (probably)	[12, 15]
Mercedes SLK	2003 (probably)	[12, 15]
Porsche Carrera	Type 996	[12, 15]

A.1 Sensitivity Analysis

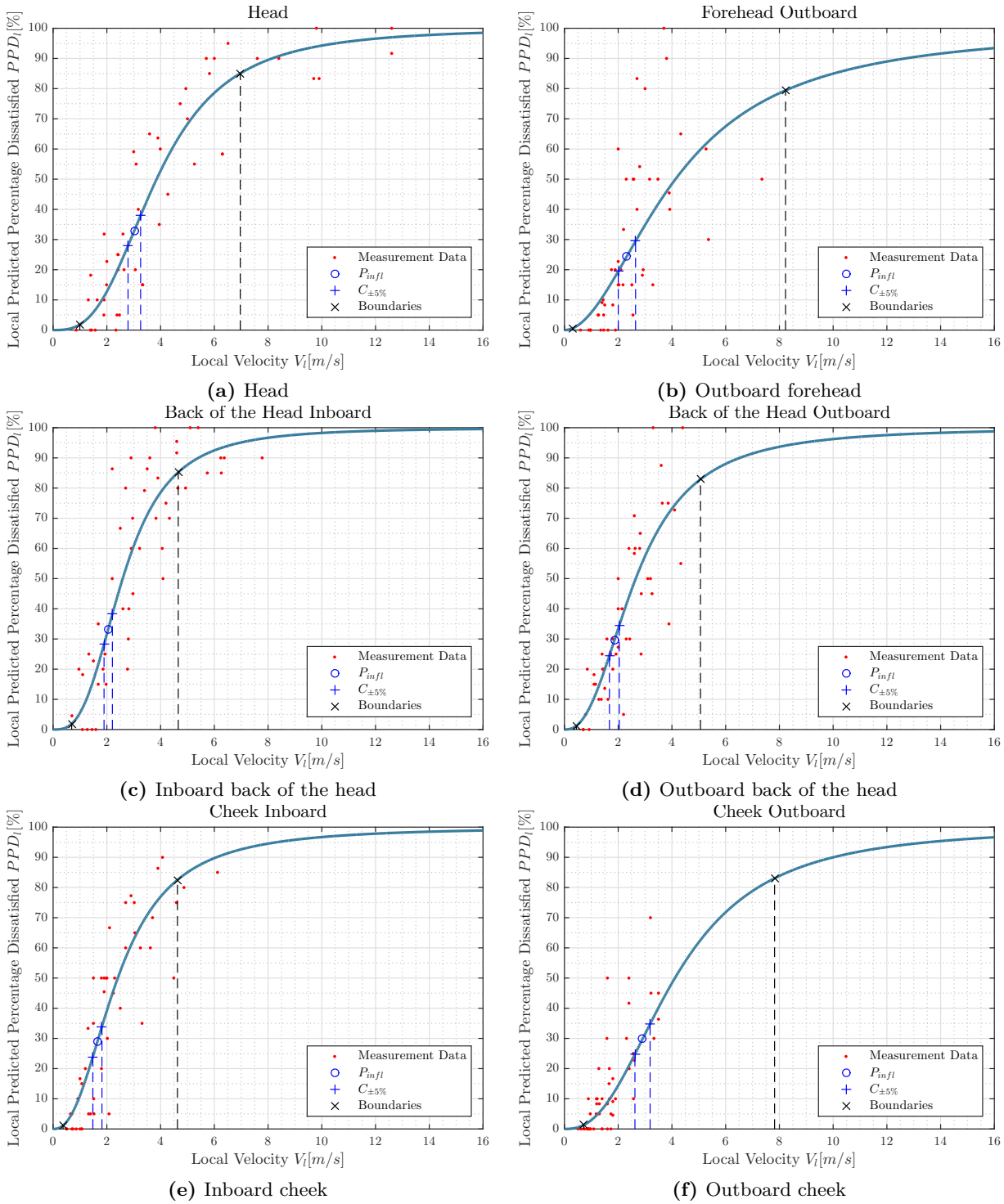

(a) Head

(b) Outboard forehead

(c) Inboard back of the head

(d) Outboard back of the head

(e) Inboard cheek

(f) Outboard cheek

Figure A.1: Averaged measured velocity for every PPD_l at different body parts

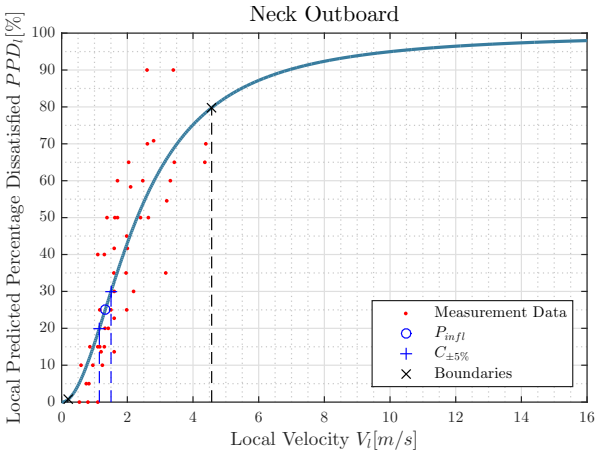

(a) Outboard neck

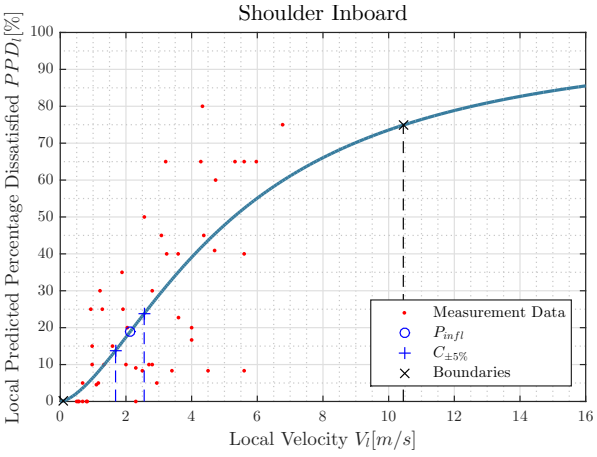

(b) Inboard shoulder

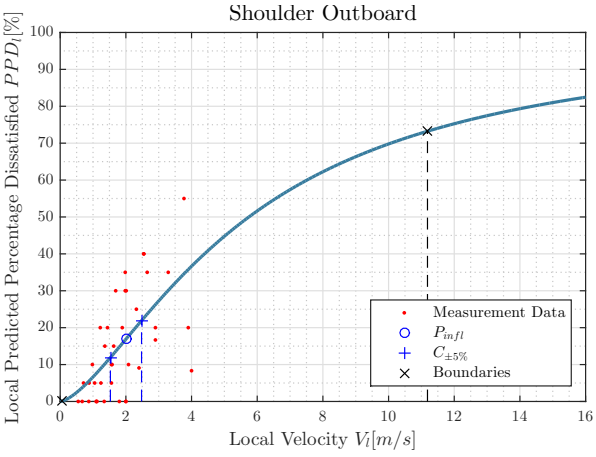

(c) Outboard shoulder

Figure A.2: Averaged measured velocity for every PPD_l at different body parts

A.2 Vehicle Margins

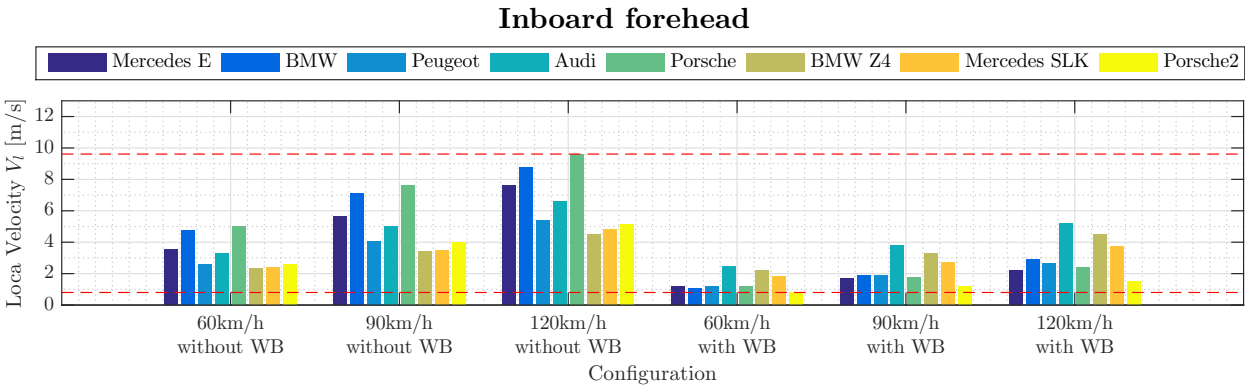

Figure A.3: Velocity measurement data of the inboard forehead of all tested vehicles

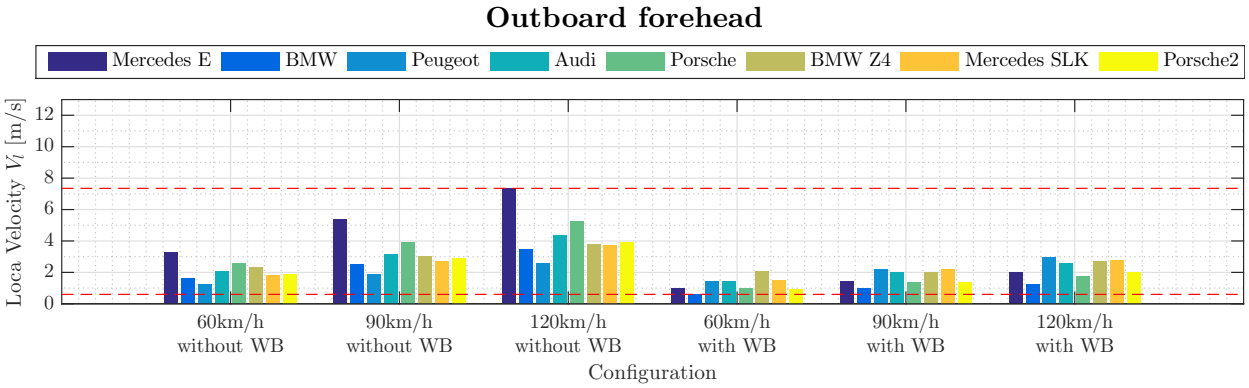

Figure A.4: Velocity measurement data of the outboard forehead of all tested vehicles

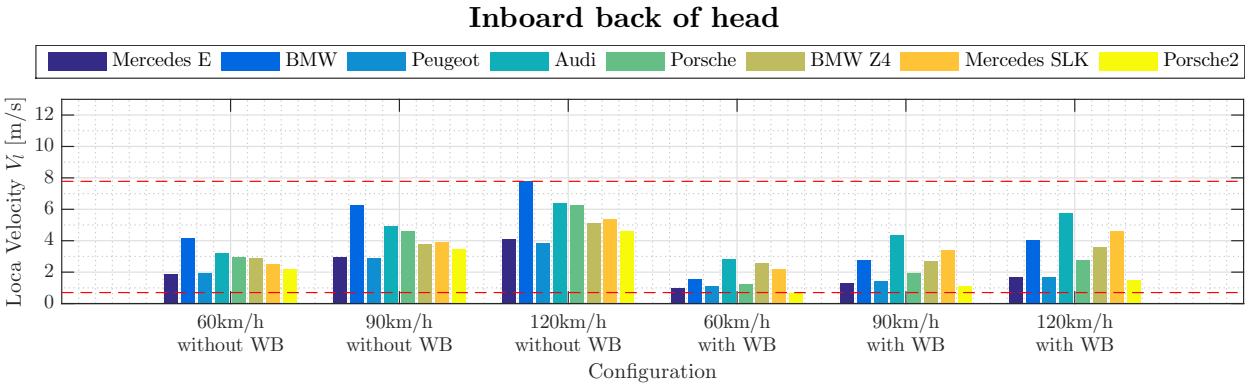

Figure A.5: Velocity measurement data of the inboard back of the head of all tested vehicles

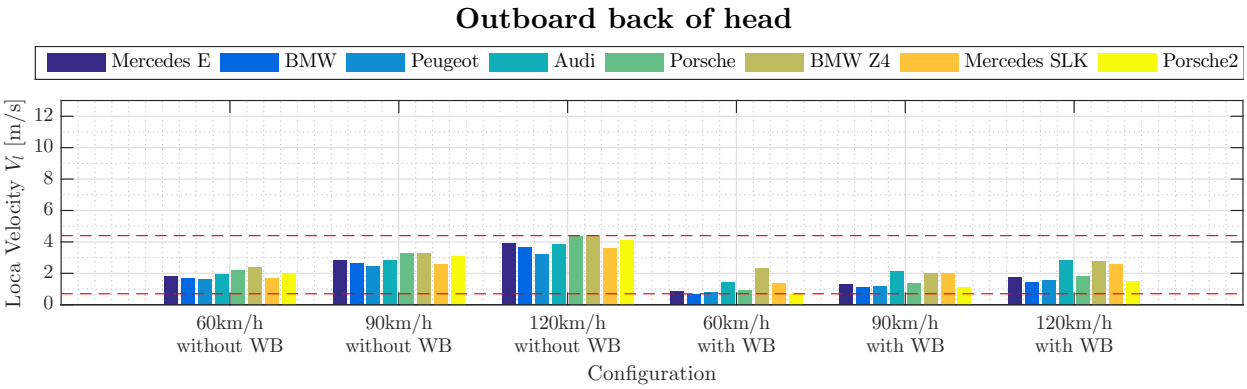

Figure A.6: Velocity measurement data of the outboard back of the head of all tested vehicles

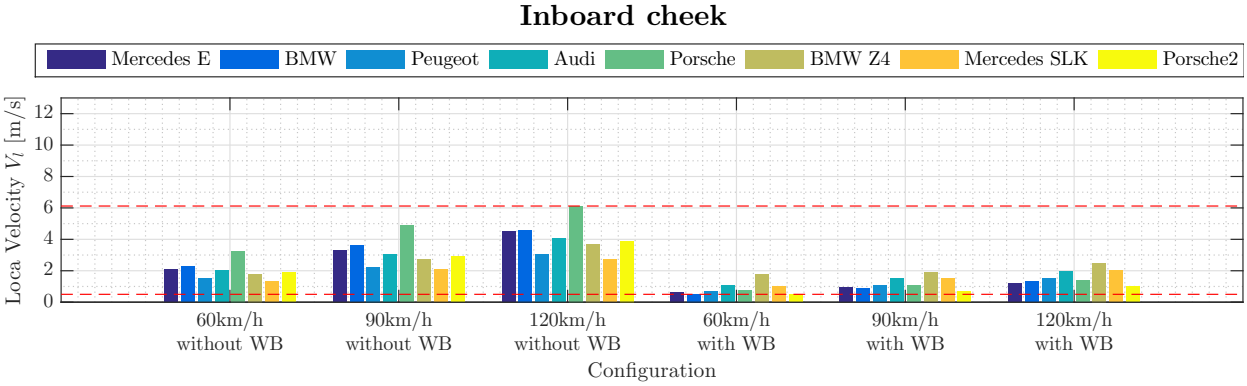

Figure A.7: Velocity measurement data of the inboard cheek of all tested vehicles

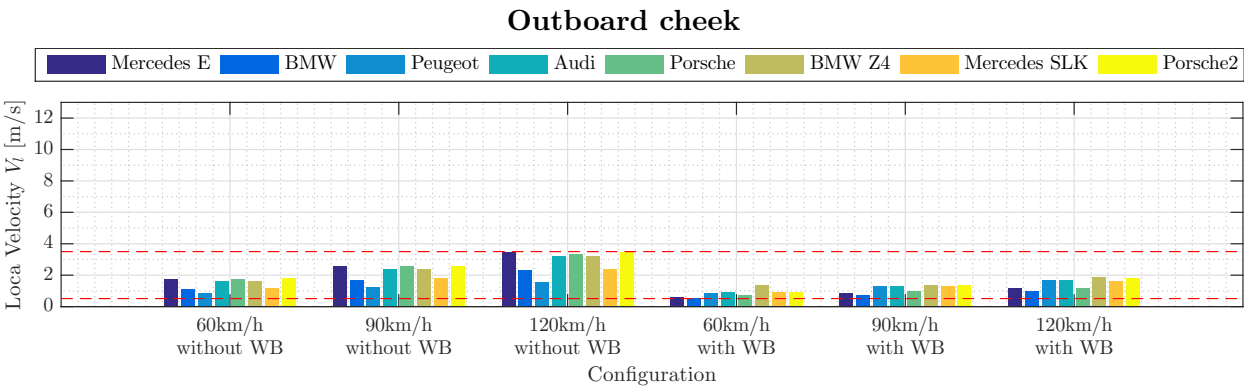

Figure A.8: Velocity measurement data of the outboard cheek of all tested vehicles

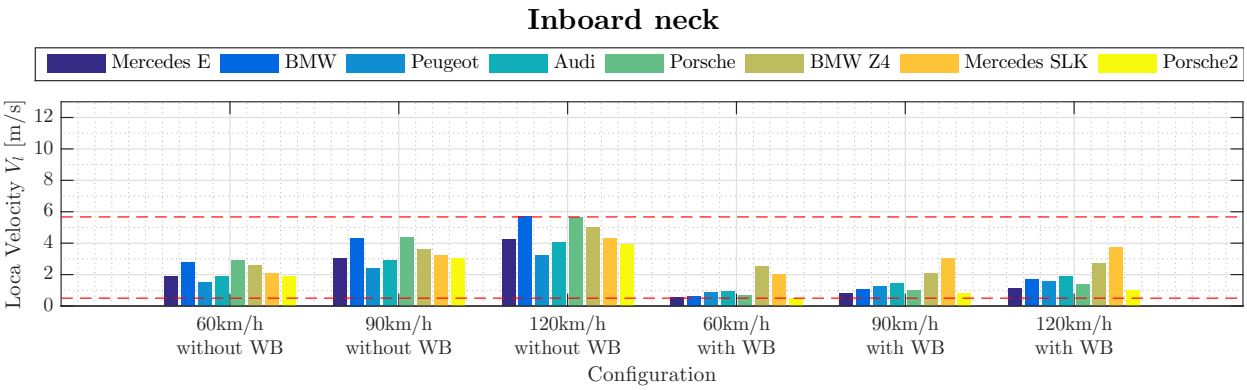

Figure A.9: Velocity measurement data of the inboard neck of all tested vehicles

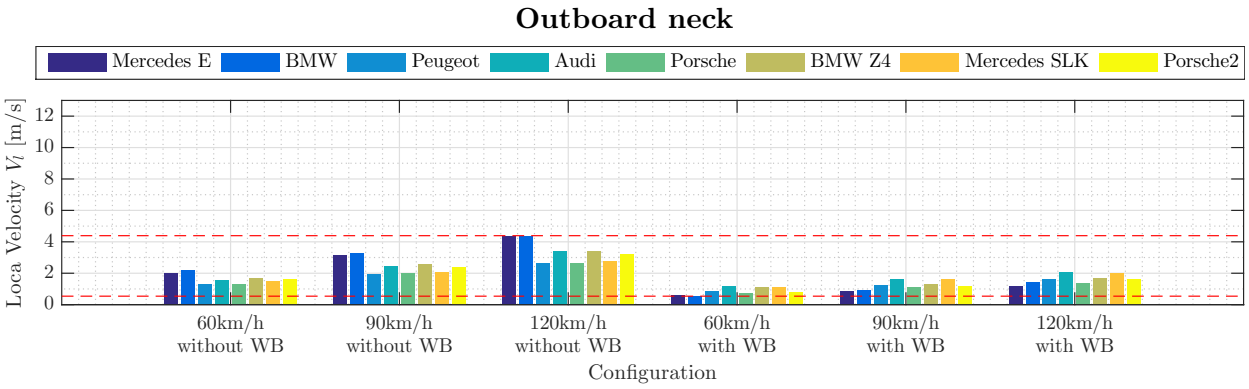

Figure A.10: Velocity measurement data of the outboard neck of all tested vehicles

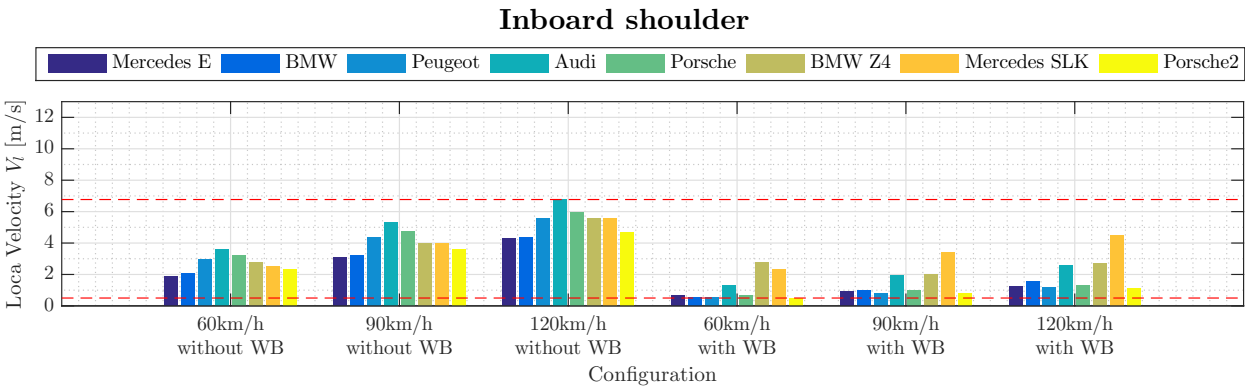

Figure A.11: Velocity measurement data of the inboard shoulder of all tested vehicles

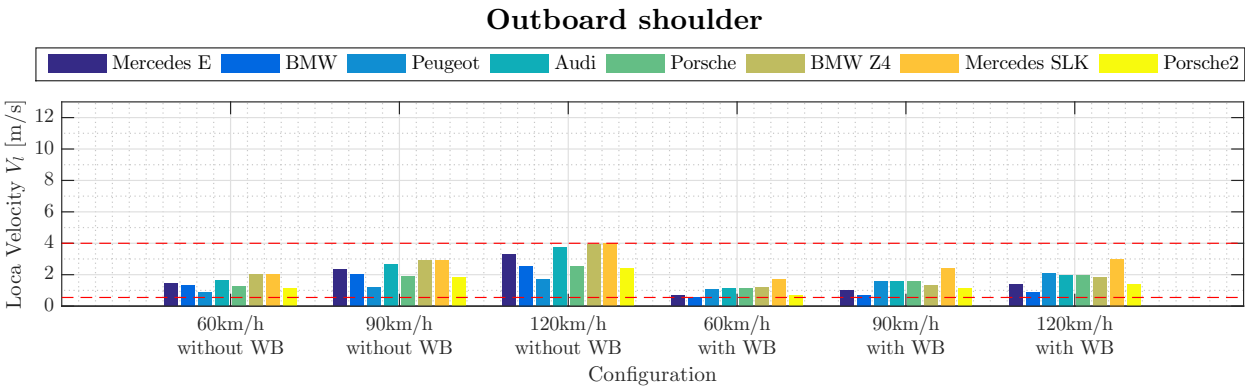

Figure A.12: Velocity measurement data of the outboard shoulder of all tested vehicles

A.3 Inboard-Outboard Comparison

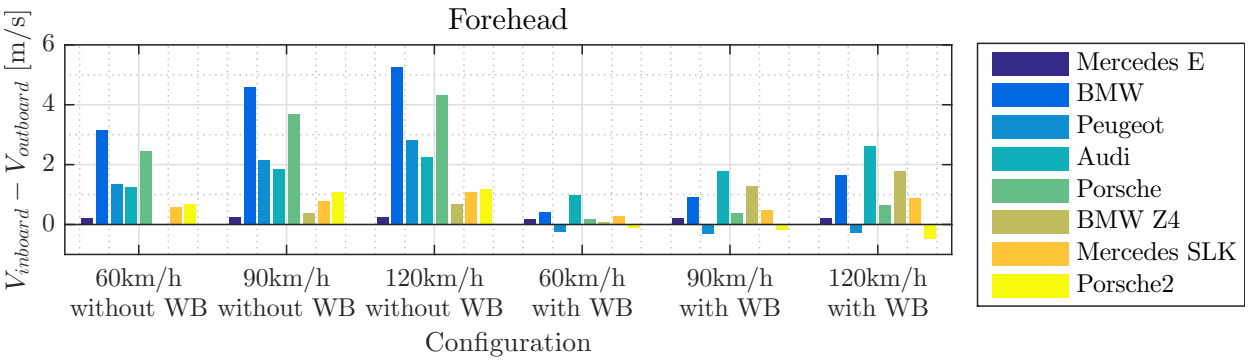

Figure A.13: Velocity difference between inboard and outboard at the forehead for every tested vehicles

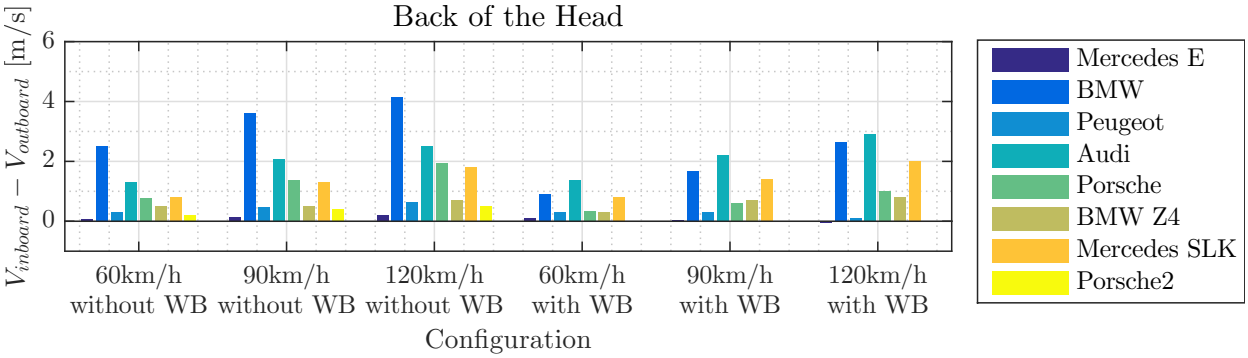

Figure A.14: Velocity difference between inboard and outboard at the back of the head for every tested vehicles

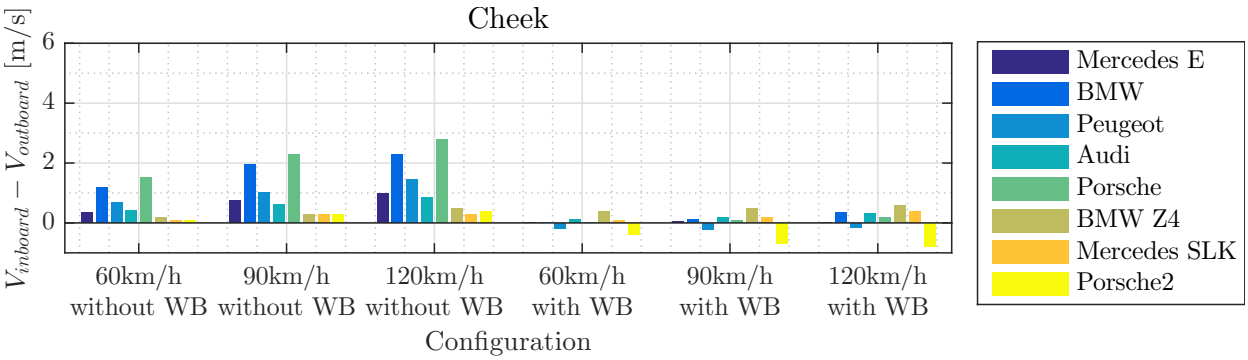

Figure A.15: Velocity difference between inboard and outboard at the cheek for every tested vehicles

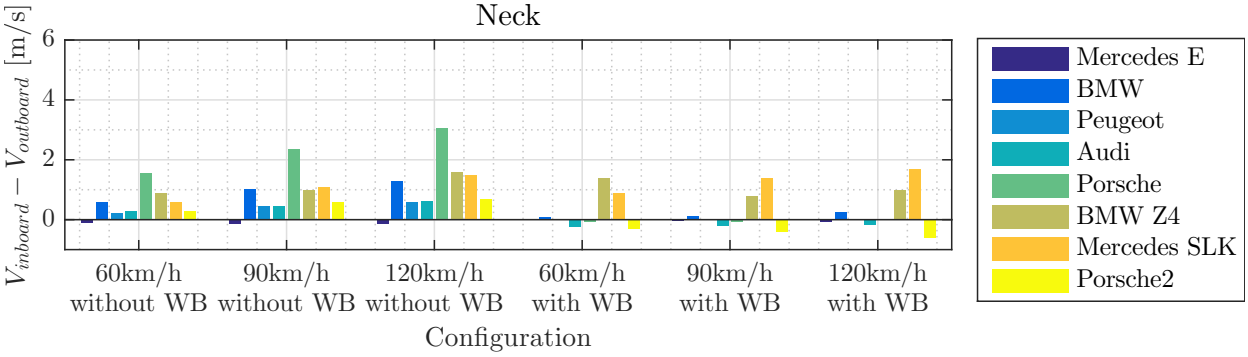

Figure A.16: Velocity difference between inboard and outboard at the neck for every tested vehicles

Appendix B

Model Coordinate System

The reference frame that has been created with the model is visualized in Figure B.1.

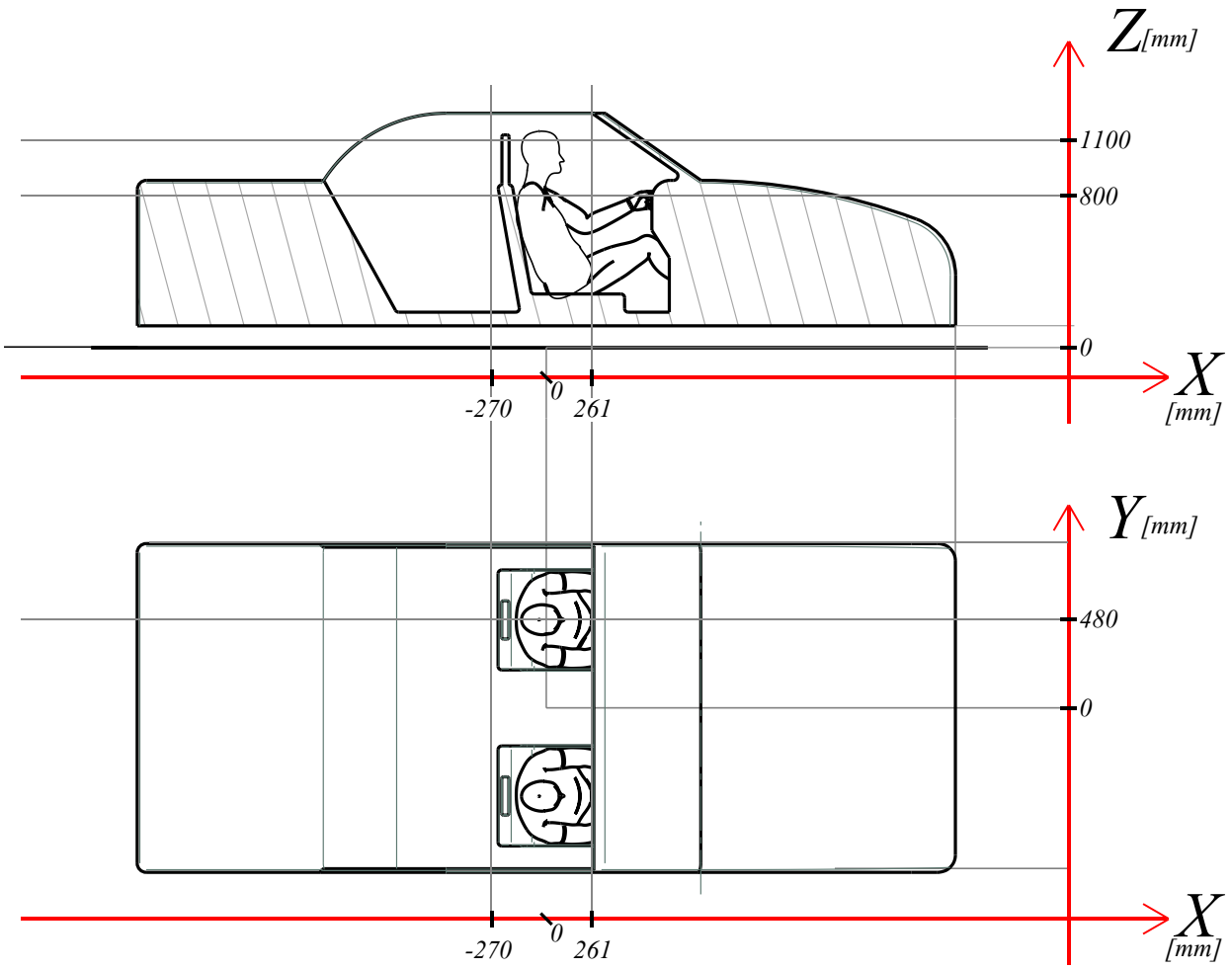

Figure B.1: Model with coordinate system and important coordinates

Table B.1: Coordinates of the measurement points

Name	X	Y	Z
Head	-43	484	1230
Forehead inside	80	414	1125
Forehead outside	80	554	1125
Back of the head inside	-120	408	1125
Back of the head outside	-120	563	1125
Cheek inside	70	422	1045
Cheek outside	70	542	1045
Neck inside	-95	414	950
Neck outside	-95	557	950
Shoulder inside	-70	290	920
Shoulder outside	-70	674	920

Appendix C

Flow Field Analysis

C.1 XZ Planes

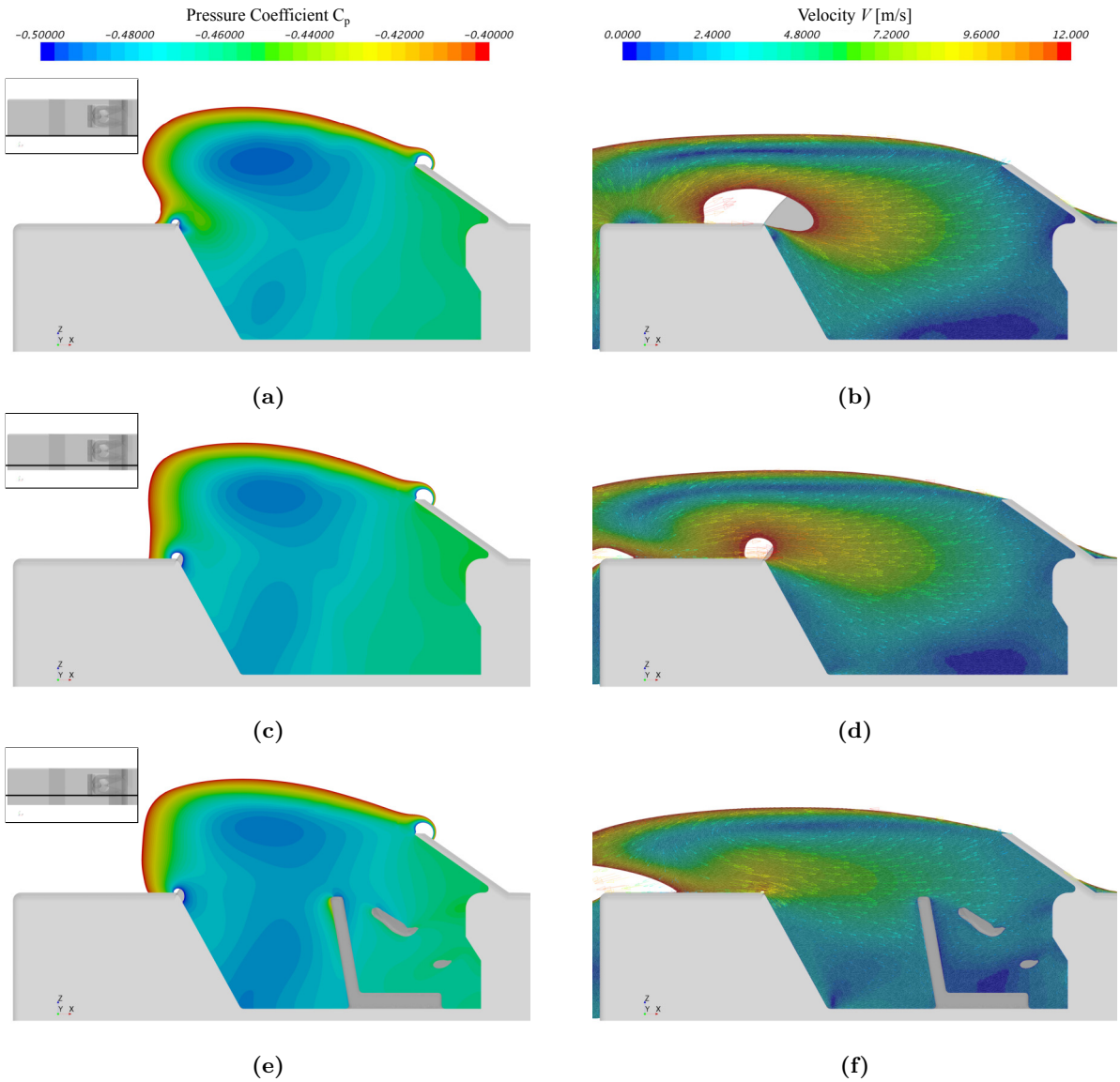

Figure C.1: XZ-Planes for varying y-coordinate

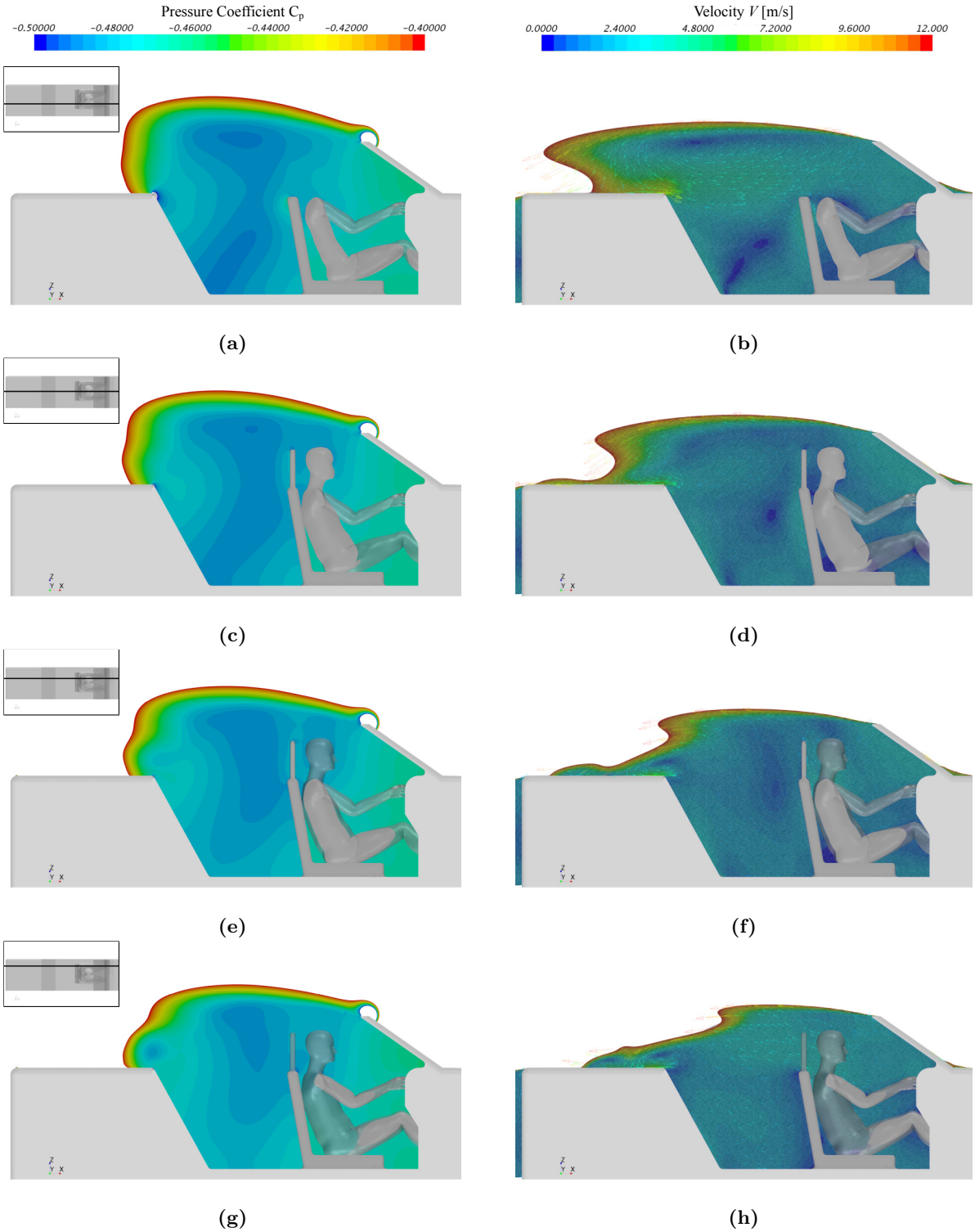

Figure C.2: XZ-Planes for varying y-coordinate

C.2 XY Planes

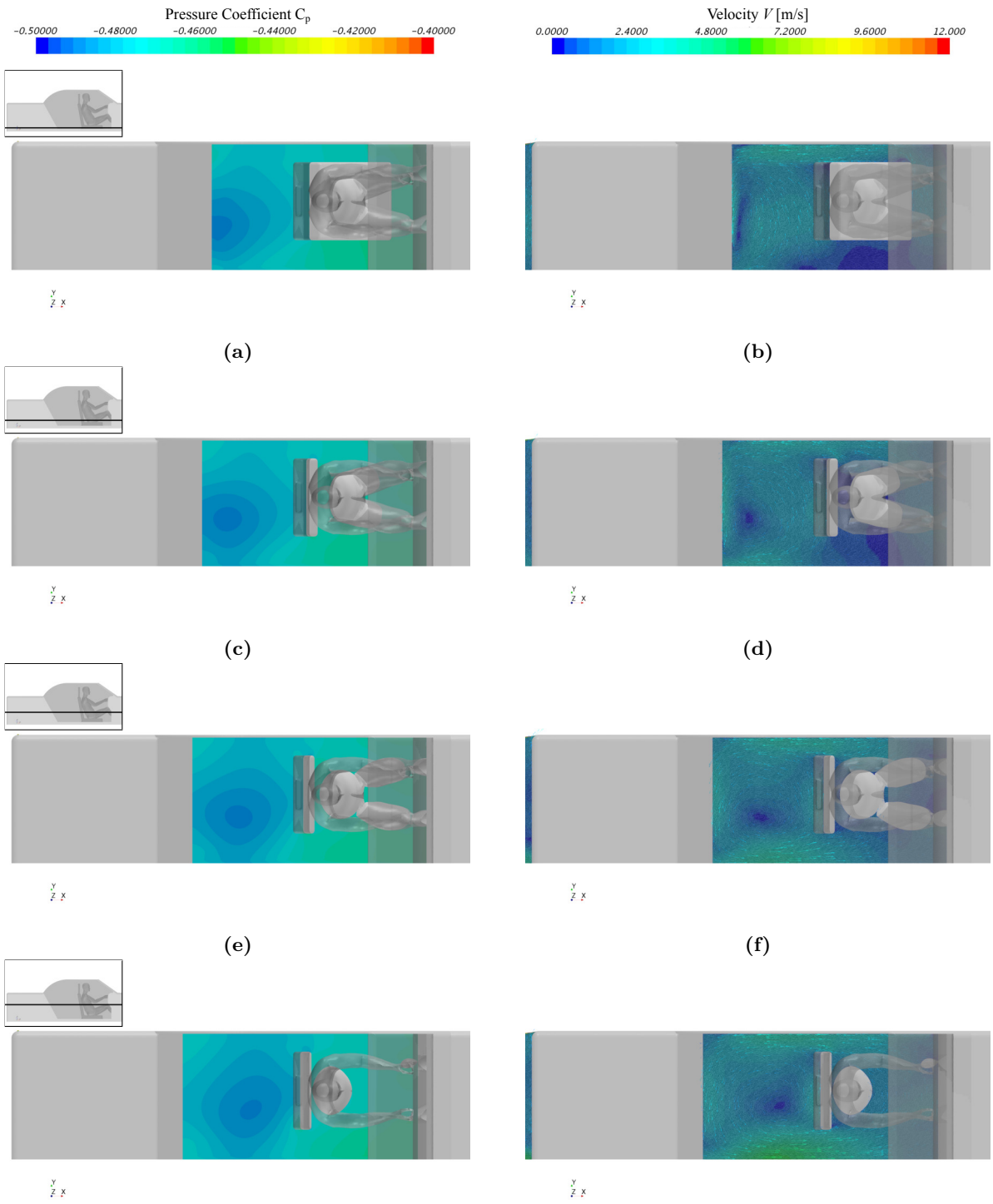

Figure C.3: XY-Planes for varying z-coordinate

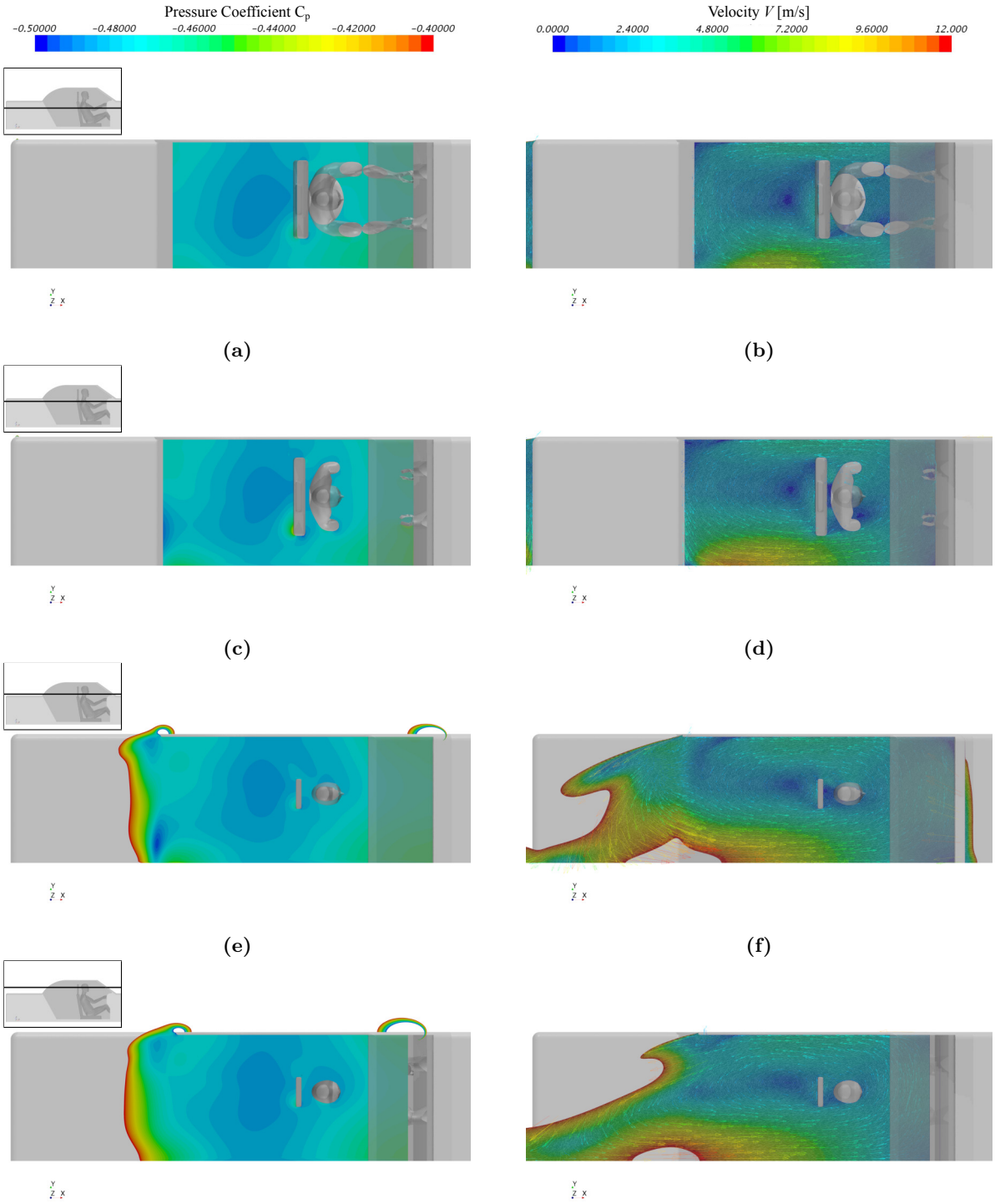

Figure C.4: XY-Planes for varying z-coordinate

Appendix D

Flow Field Replication

This appendix contains the figures which are created during the CFD analysis of the flow field replication in a constrained domain, see Section 7.5.

D.1 Symmetry Planes

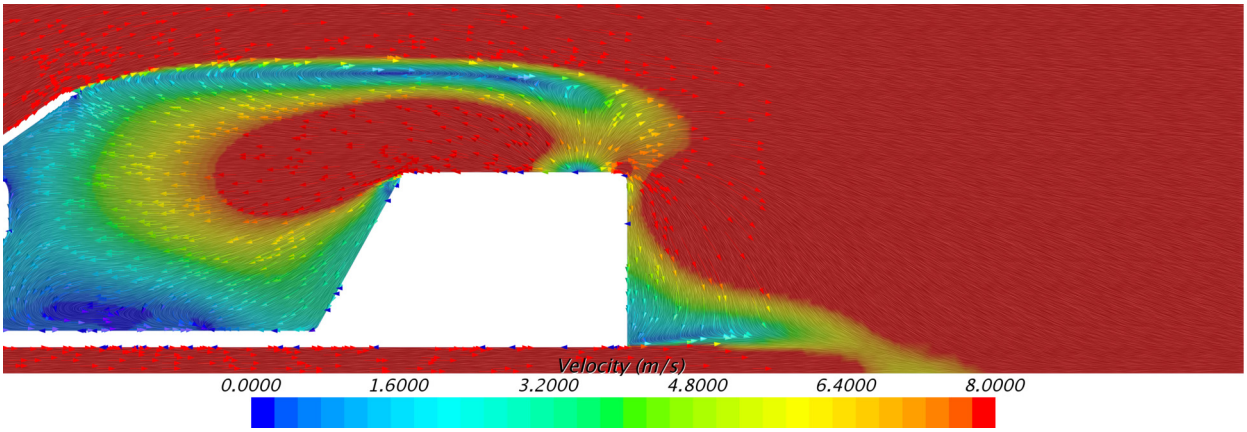

(a) Reference simulation

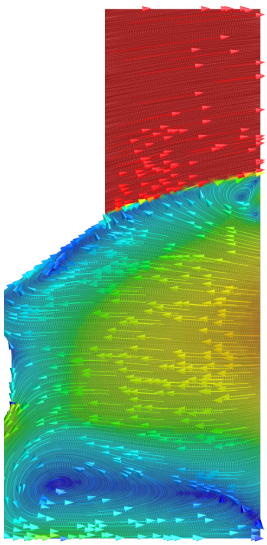

(b) Variant 1

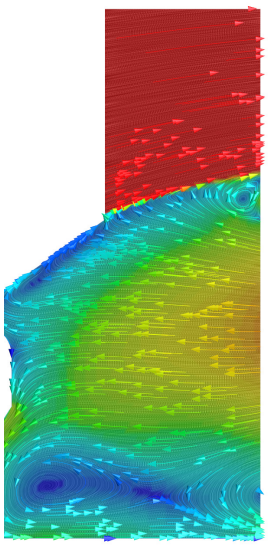

(c) Variant 2

Figure D.1: Velocity distribution in the symmetry plane of the reference simulation and variants 1 & 2

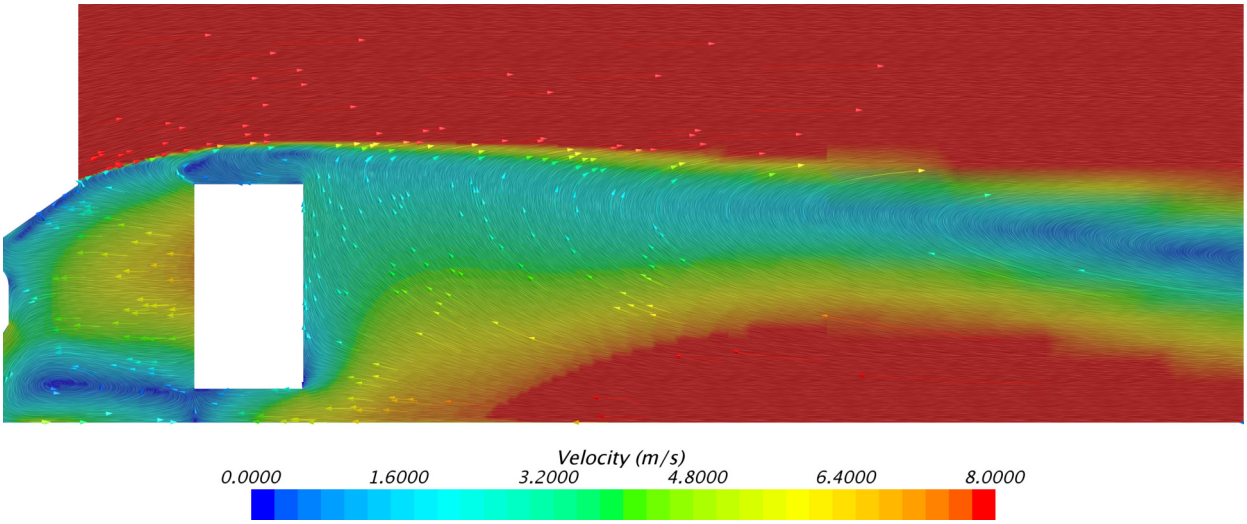

(a) Variant 3

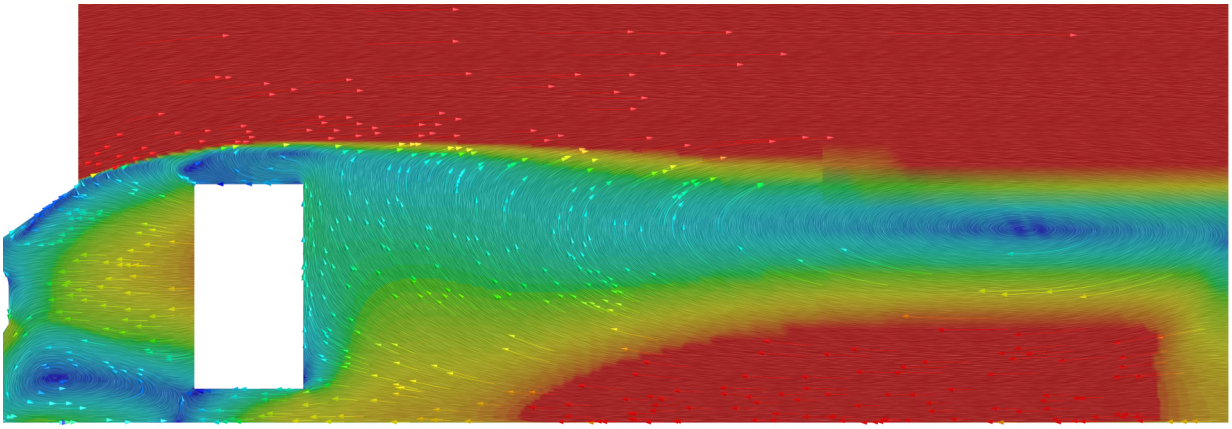

(b) Variant 4

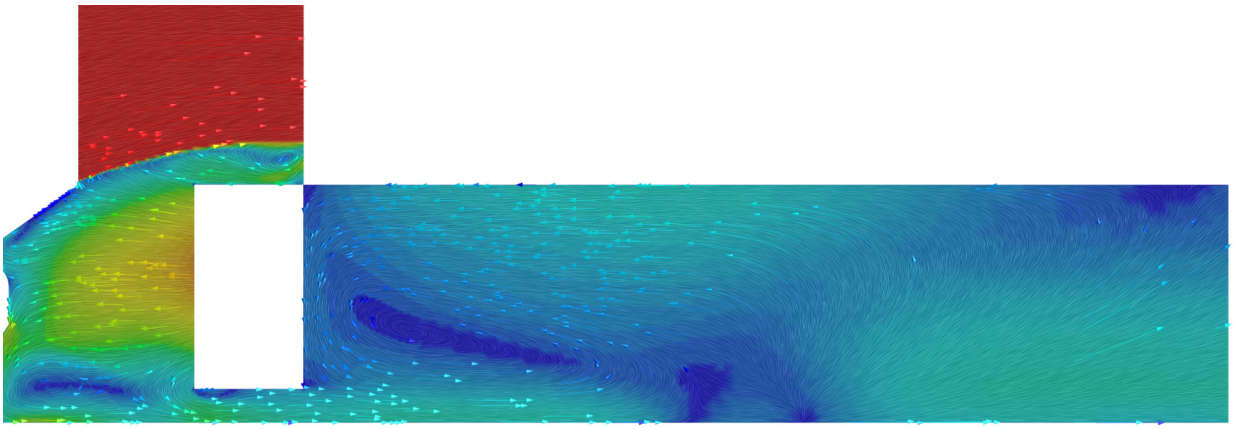

(c) Variant 5

Figure D.2: Velocity distribution in the symmetry plane of variants 3 and 4

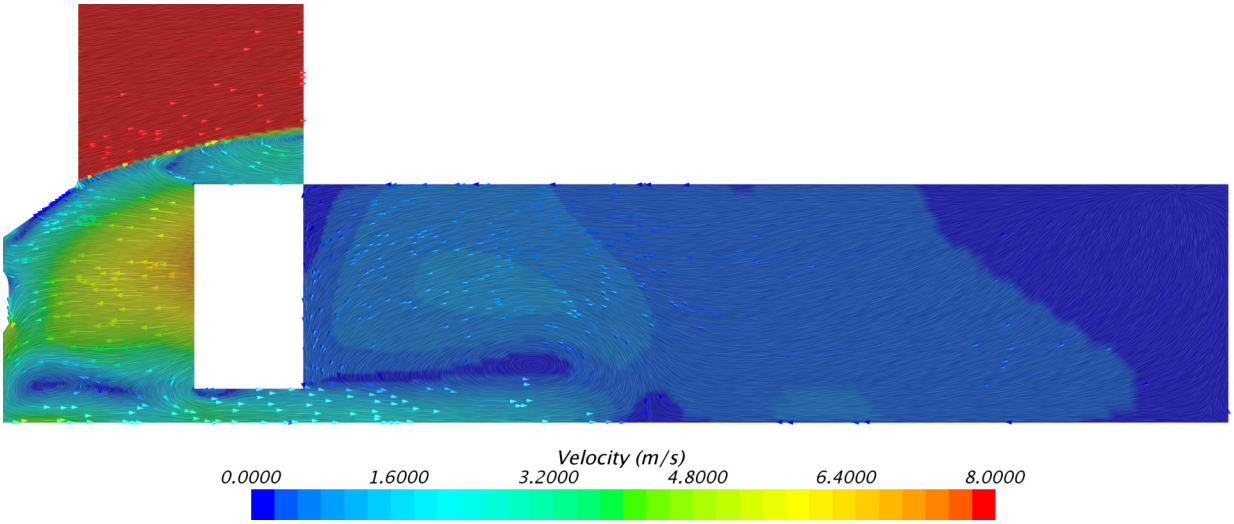

(a) Variant 6

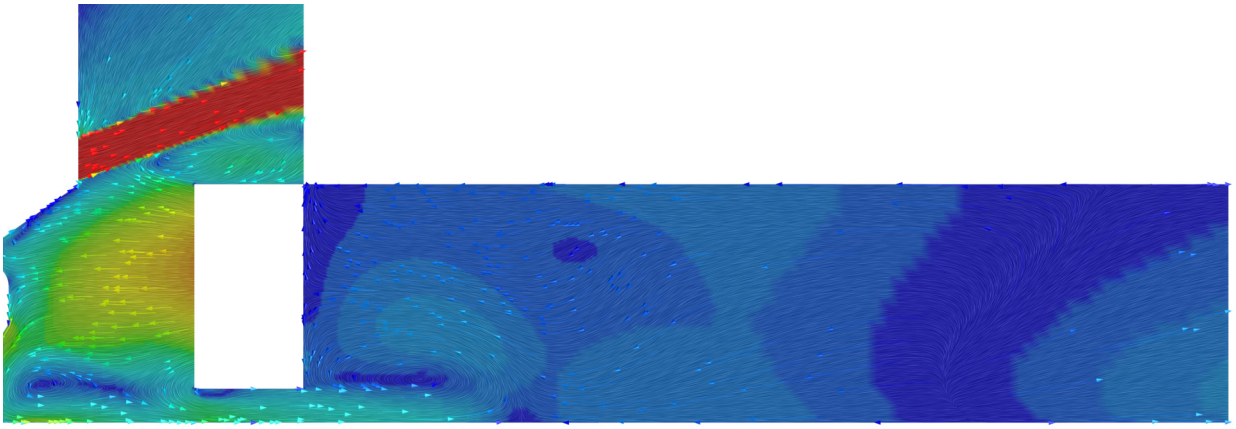

(b) Variant 7

Figure D.3: Velocity distribution in the symmetry plane for different variants

D.2 XZ Planes at Y = 480mm

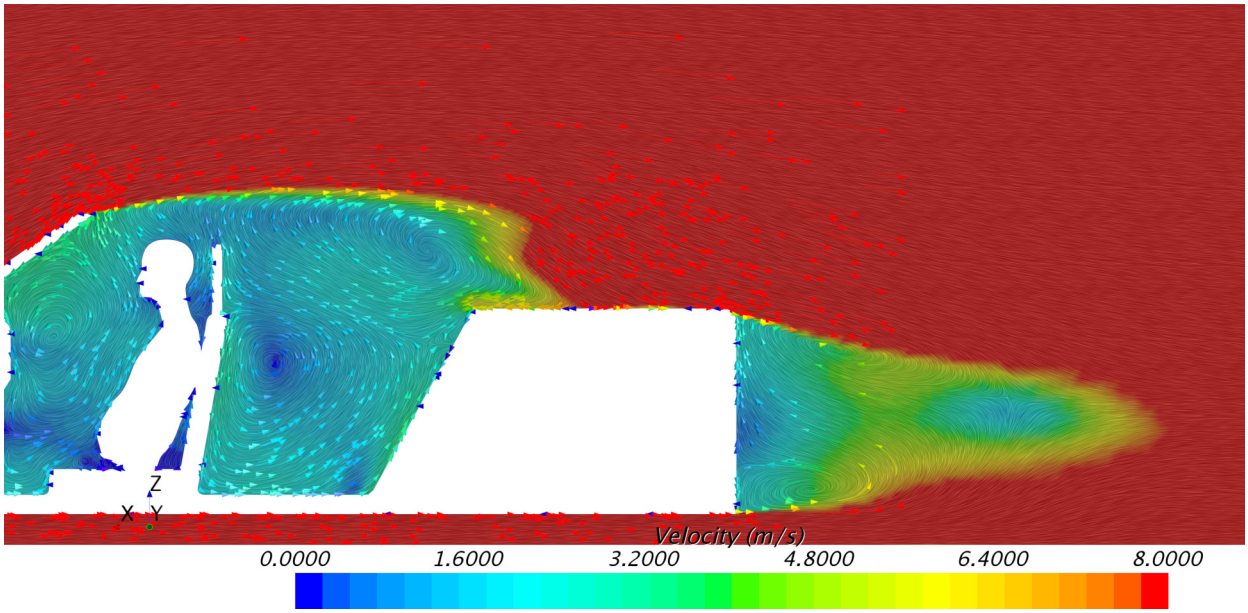

(a) Reference simulation

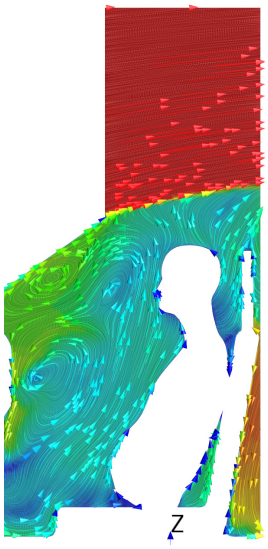

(b) Variant 1

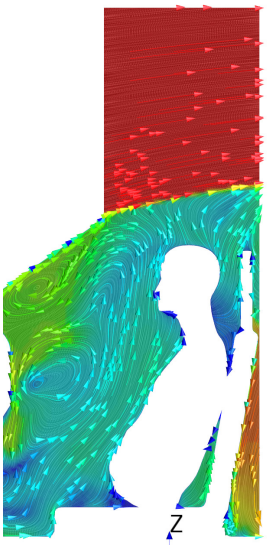

(c) Variant 2

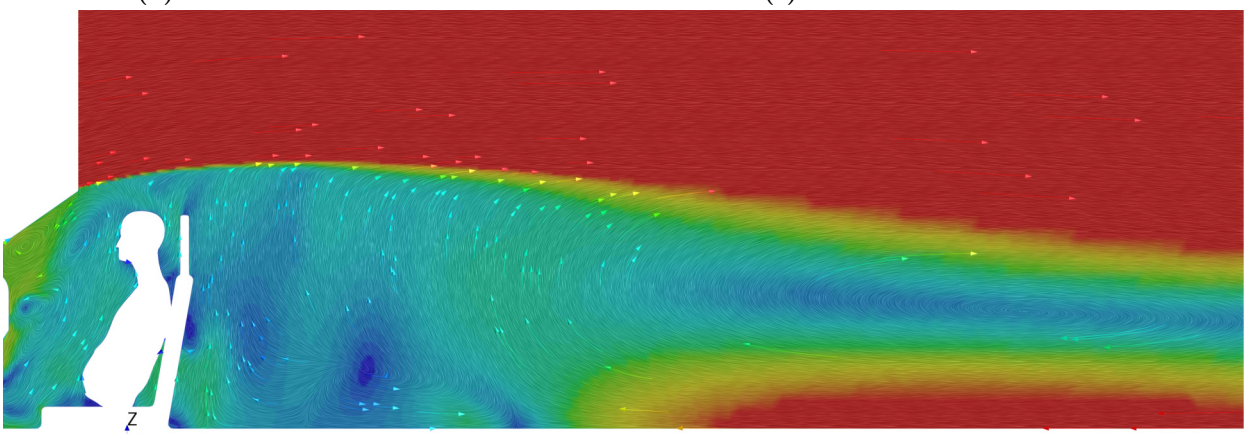

(d) Variant 3

Figure D.4: Velocity distribution in the XZ-plane at Y = 480mm of the reference simulation and the different variants

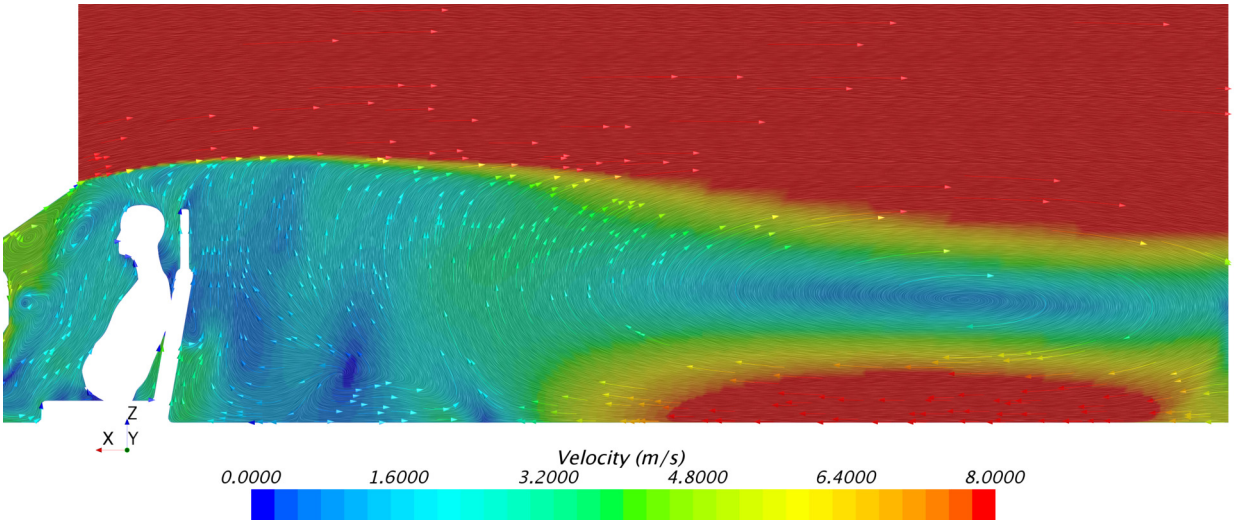

(a) Variant 4

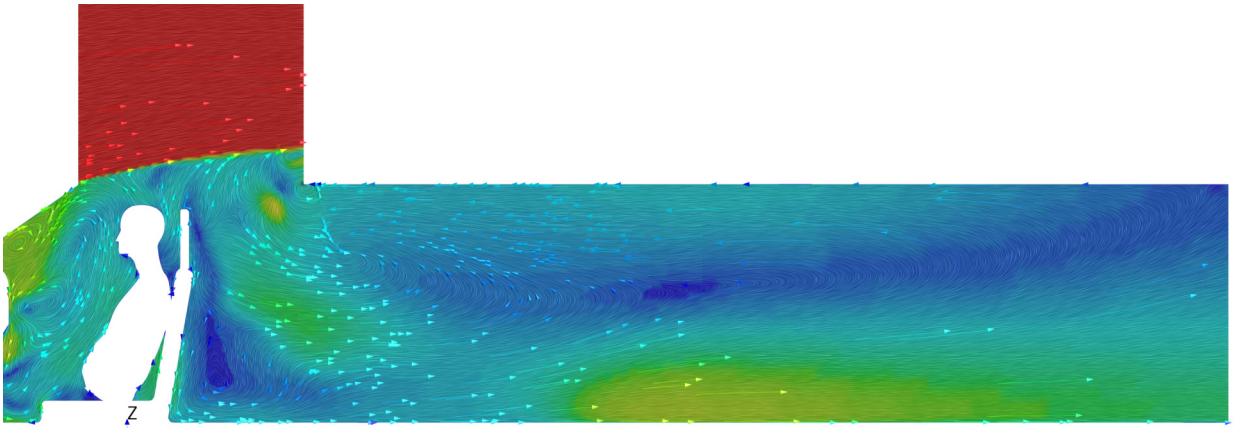

(b) Variant 5

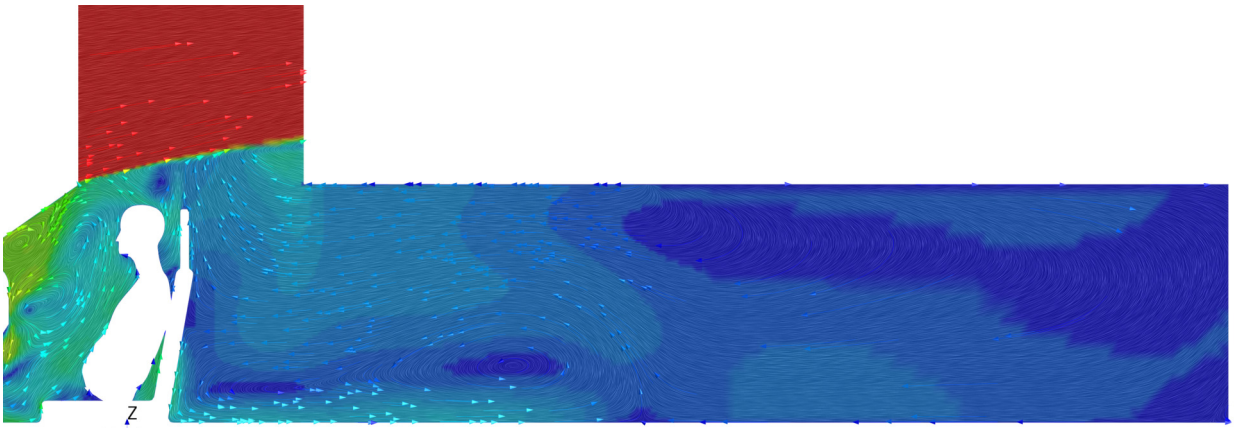

(c) Variant 6

Figure D.5: Y480 plane of the reference simulation and the different variants

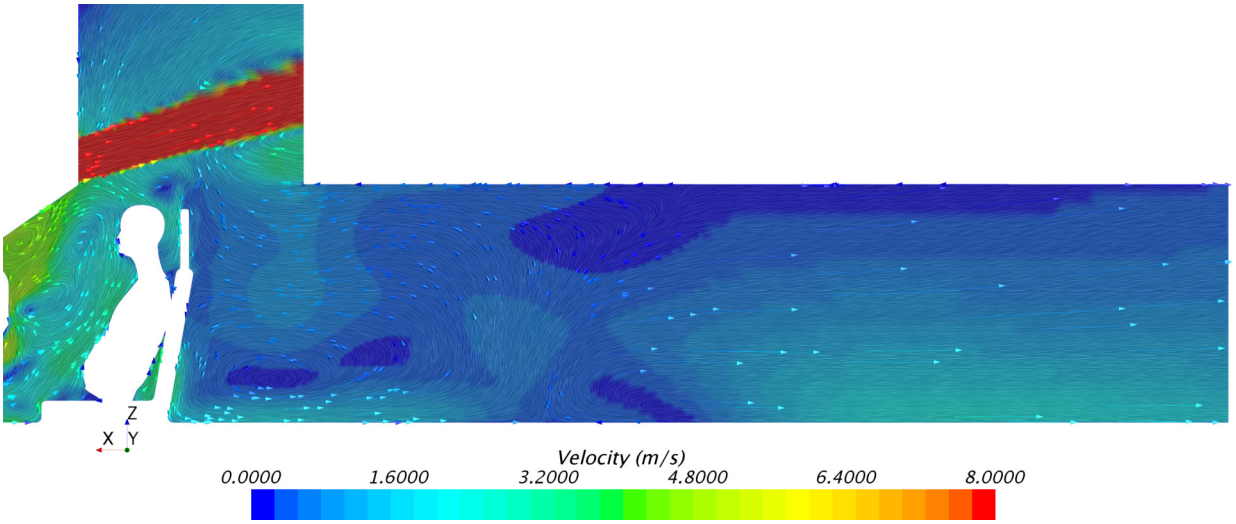

(a) Variant 7

Figure D.6: Y480 plane of the reference simulation and the different variants

D.3 Pressure Symmetry Planes

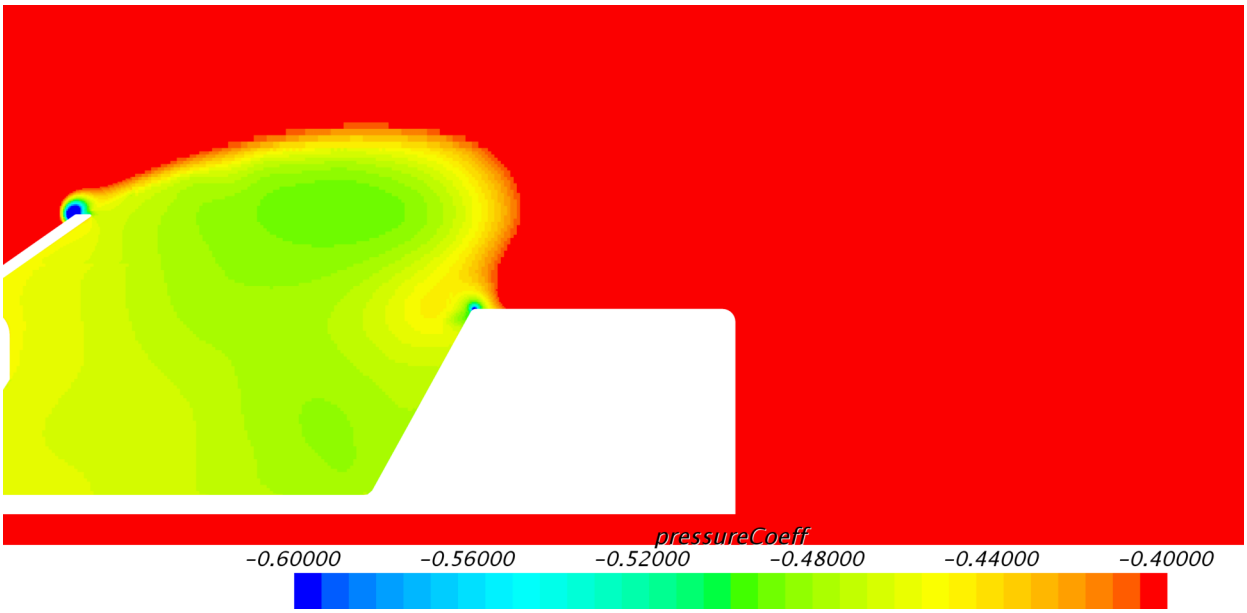

(a) Reference simulation

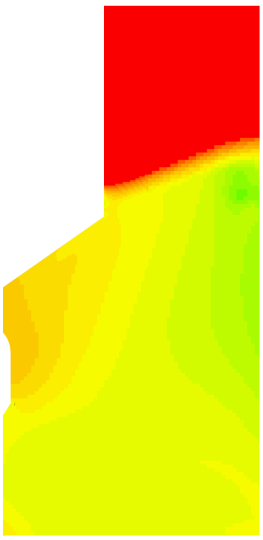

(b) Variant 1

(c) Variant 2

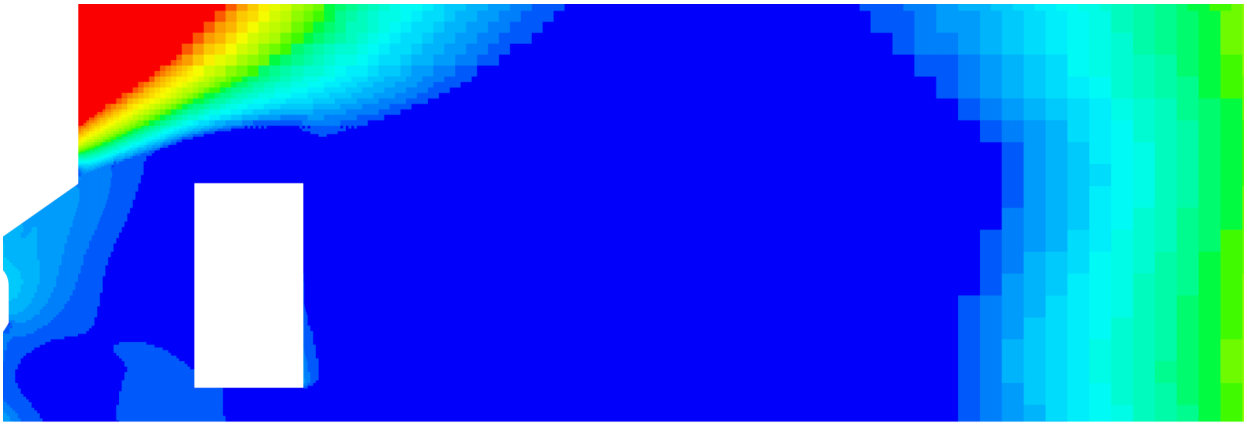

(d) Variant 3

Figure D.7: SymmetryP plane of the reference simulation and the different variants

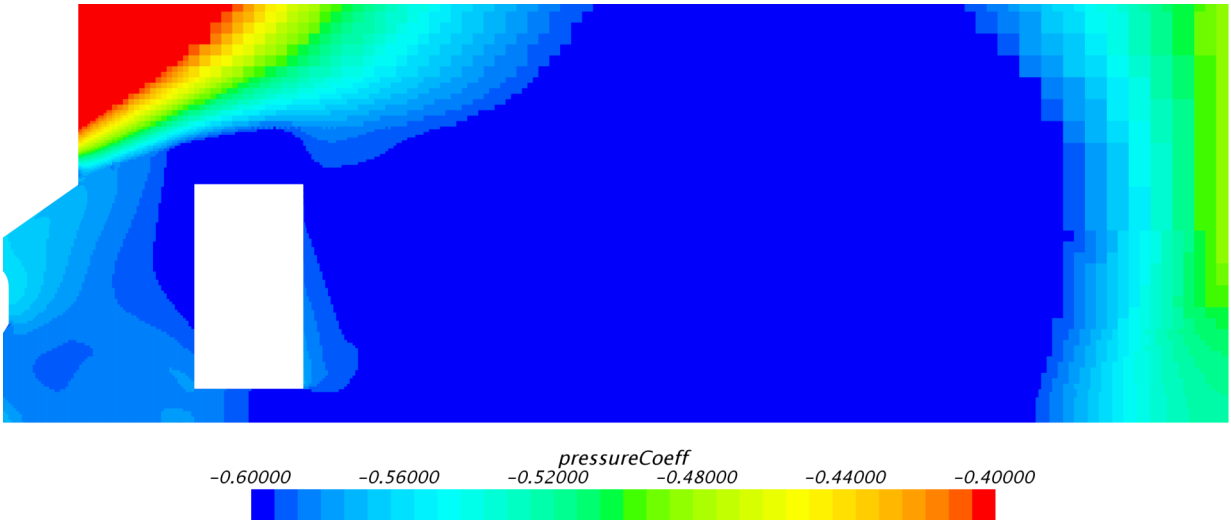

(a) Variant 4

(b) Variant 5

(c) Variant 6

Figure D.8: SymmetryP plane of the reference simulation and the different variants

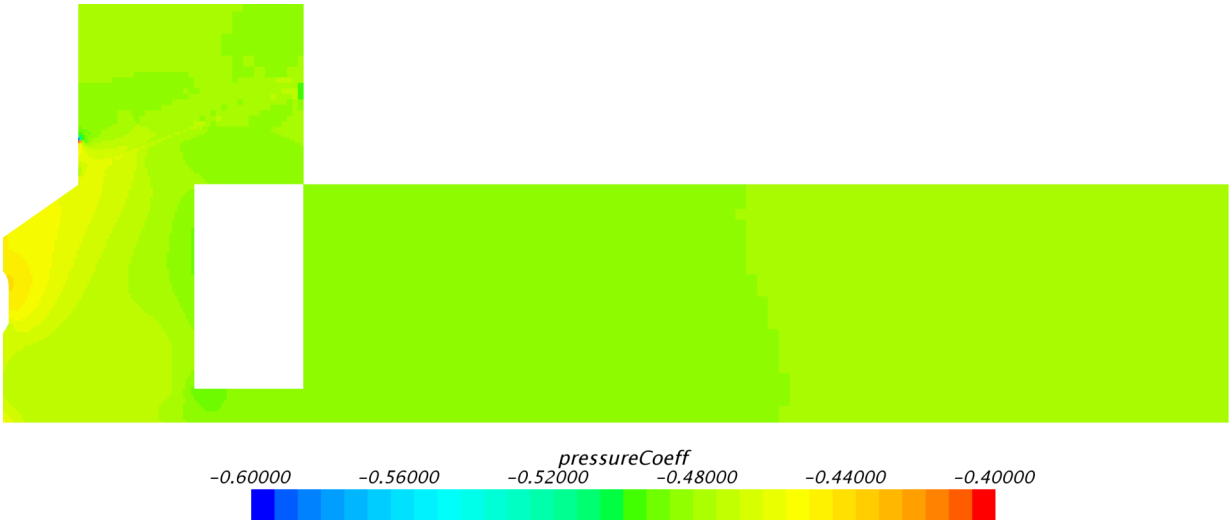

(a) Variant 7

Figure D.9: SymmetryP plane of the reference simulation and the different variants

D.4 Pressure XZ Planes at Y = 480mm

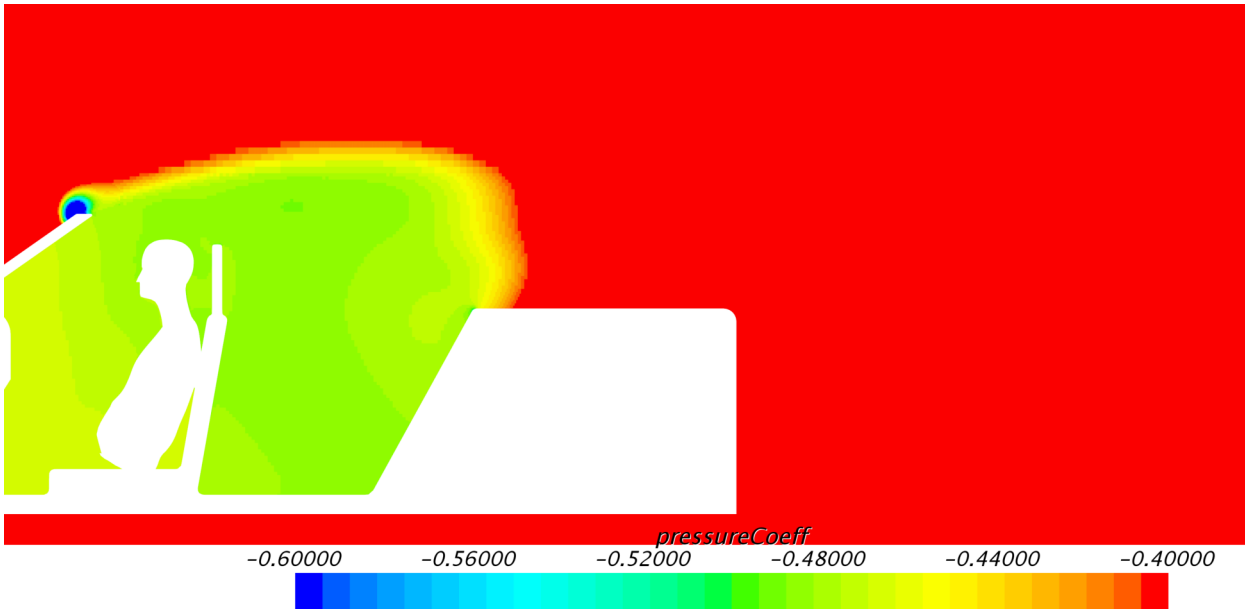

(a) Reference simulation

(b) Variant 1

(c) Variant 2

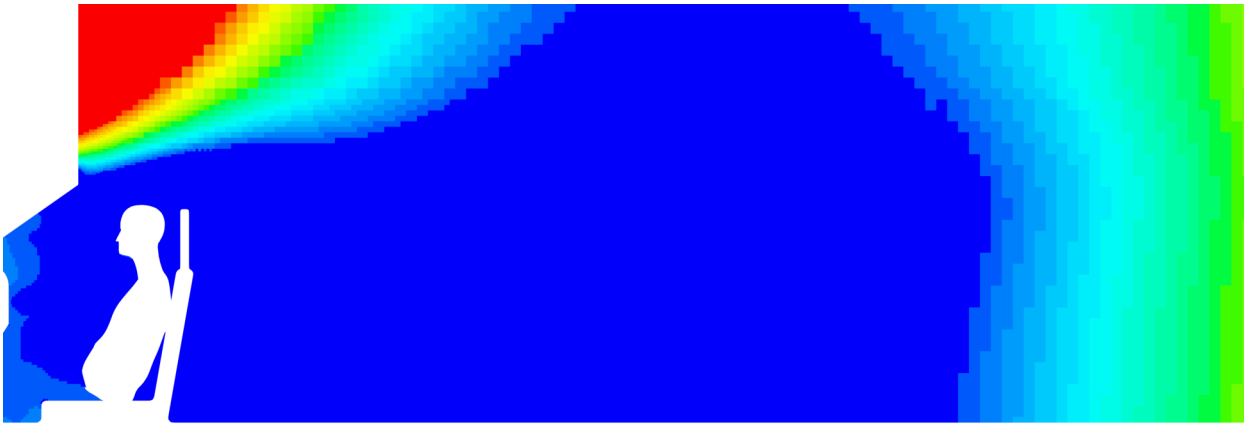

(d) Variant 3

Figure D.10: Y480P plane of the reference simulation and the different variants

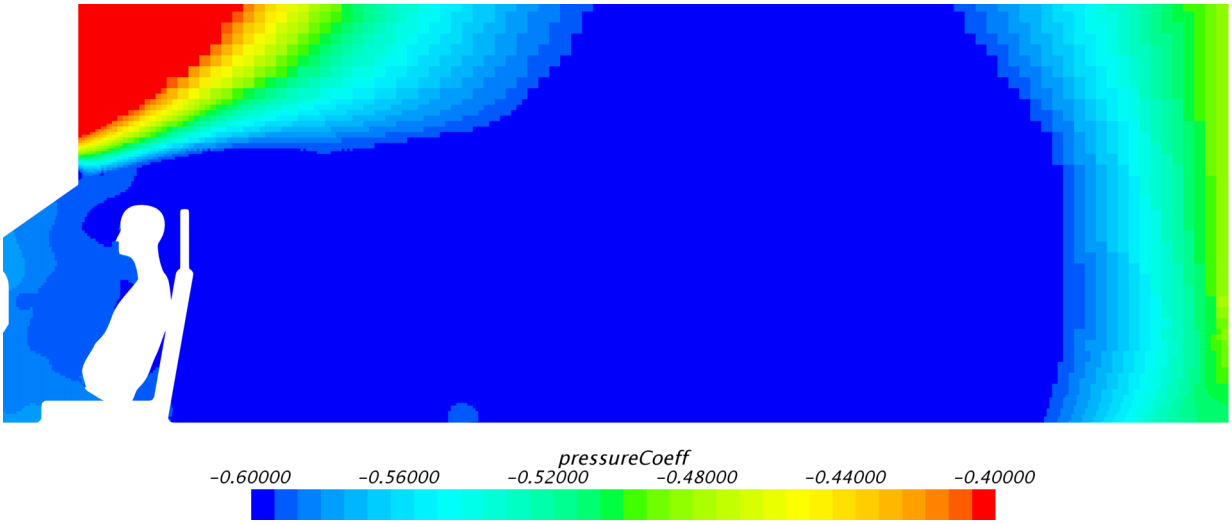

(a) Variant 4

(b) Variant 5

(c) Variant 6

Figure D.11: Y480P plane of the reference simulation and the different variants

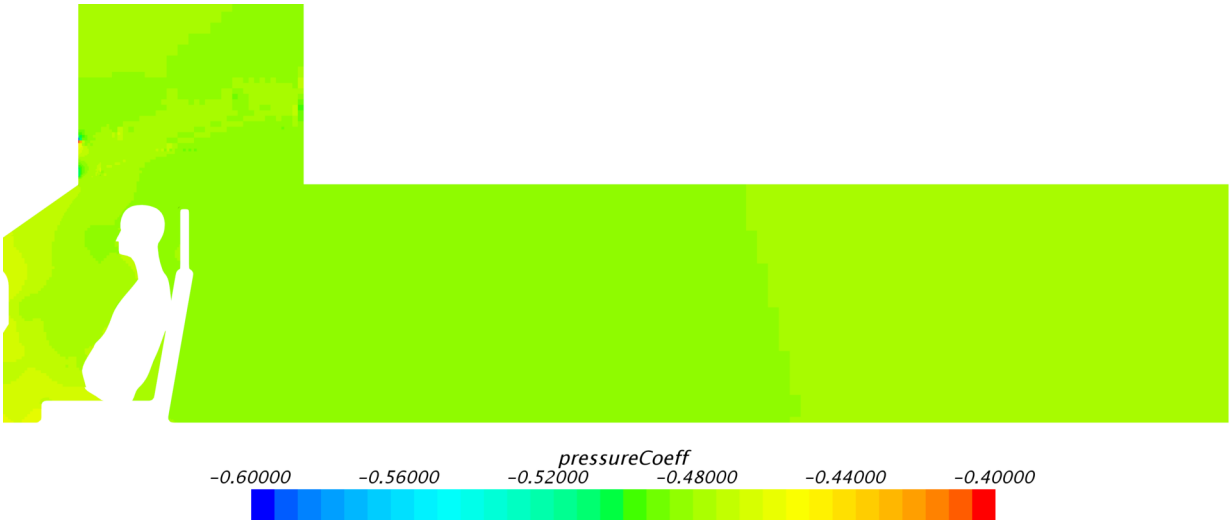

(a) Variant 7

Figure D.12: Y480P plane of the reference simulation and the different variants

D.5 Velocity XY Planes at Z = 800mm

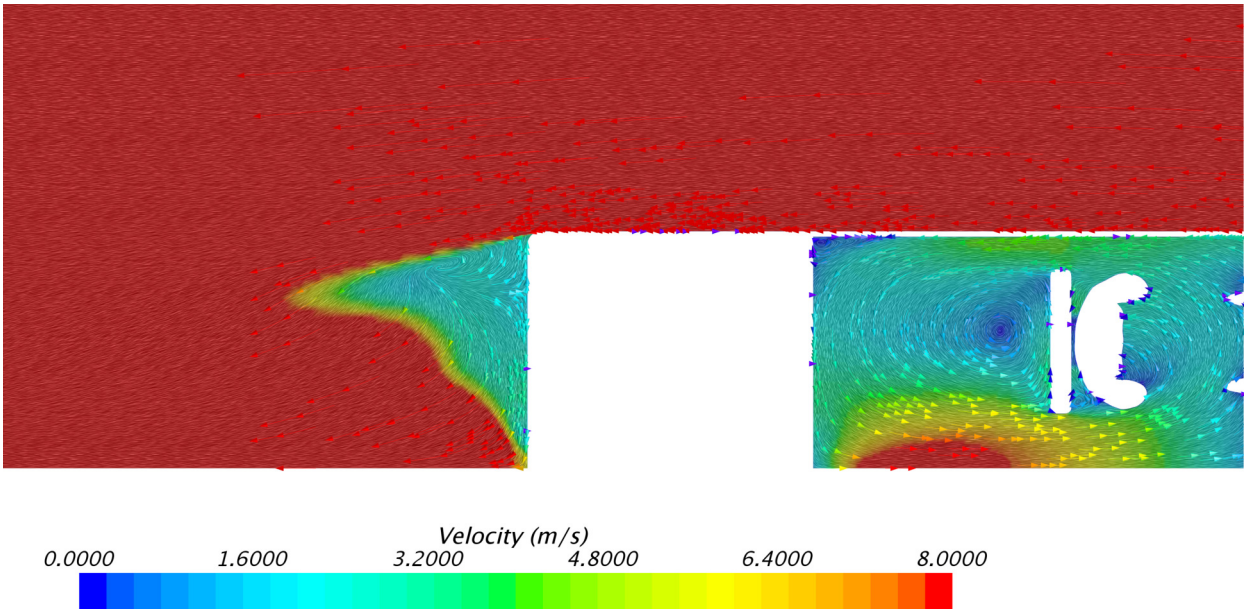

(a) Reference simulation

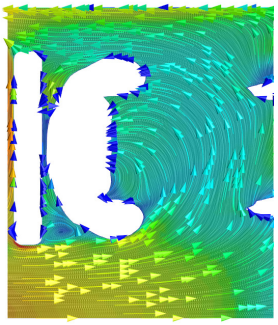

(b) Variant 1

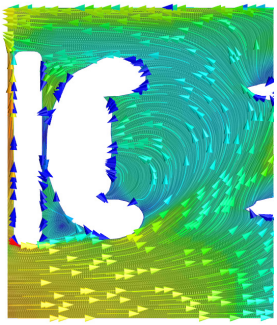

(c) Variant 2

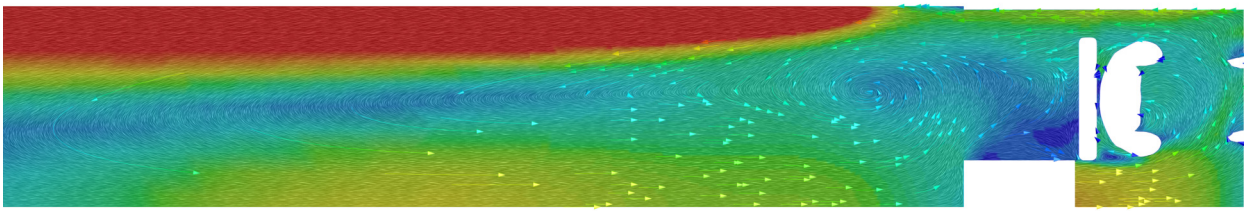

(d) Variant 3

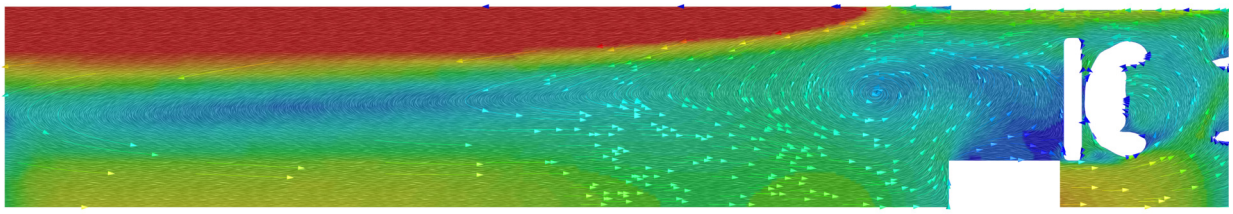

(e) Variant 4

Figure D.13: Z800 plane of the reference simulation and the different variants

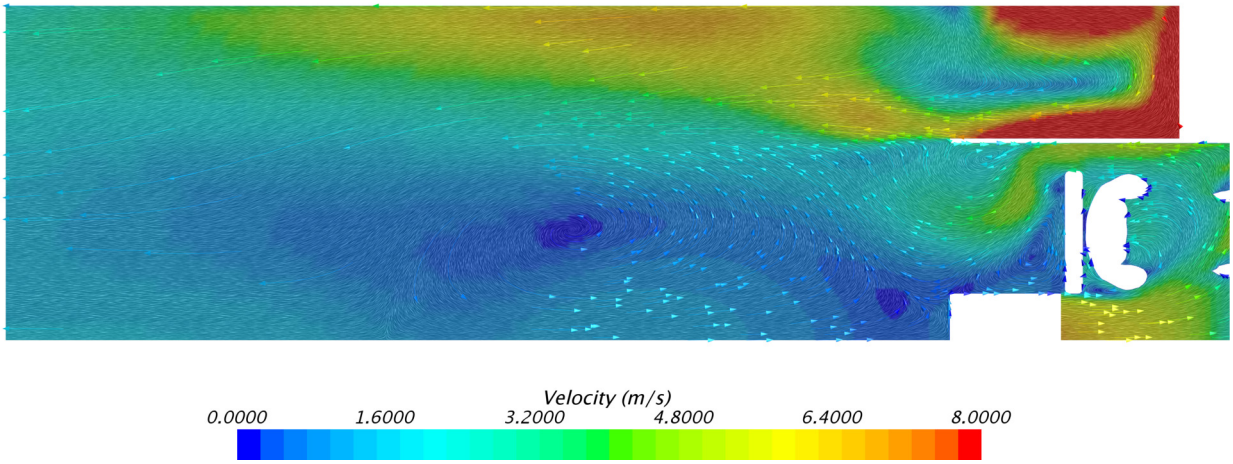

(a) Variant 5

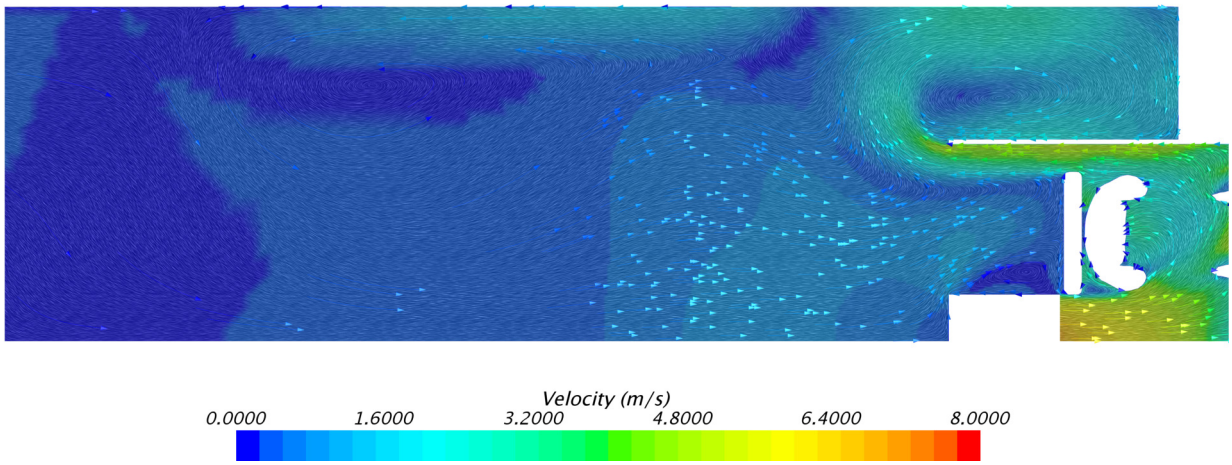

(b) Variant 6

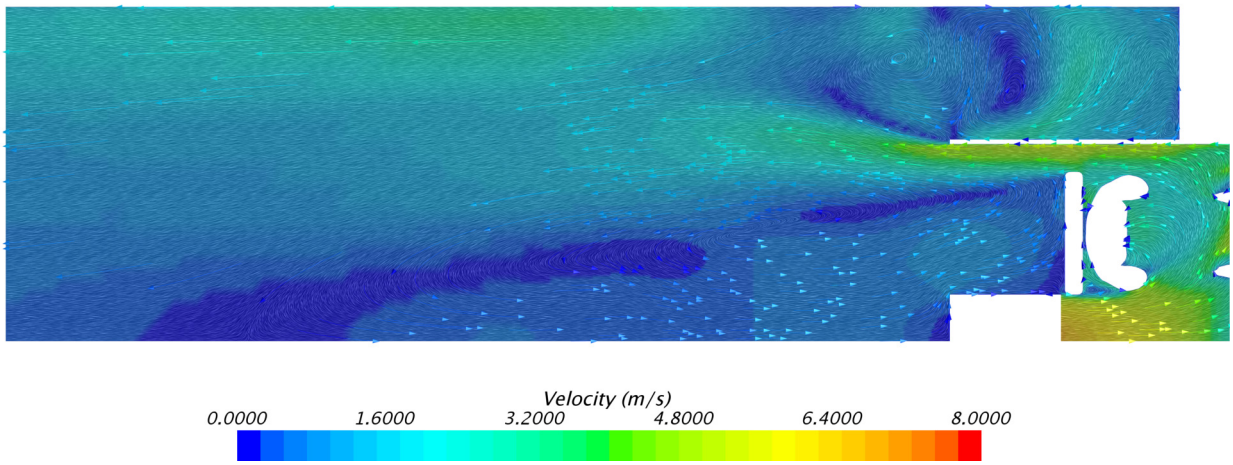

(c) Variant 7

Figure D.14: Z800 plane of the reference simulation and the different variants

D.6 Velocity XY Planes at Z = 1100mm

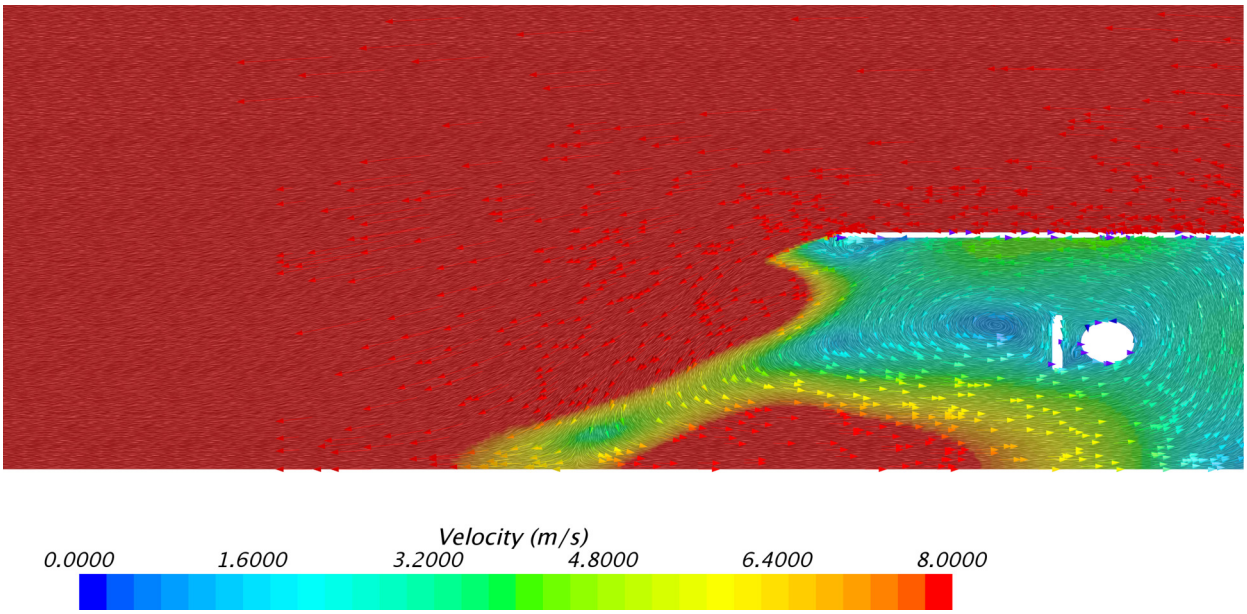

(a) Reference simulation

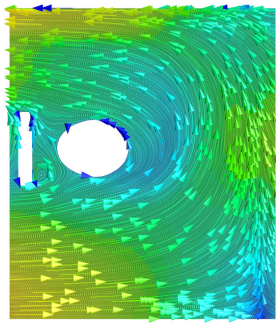

(b) Variant 1

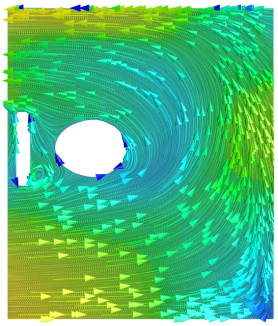

(c) Variant 2

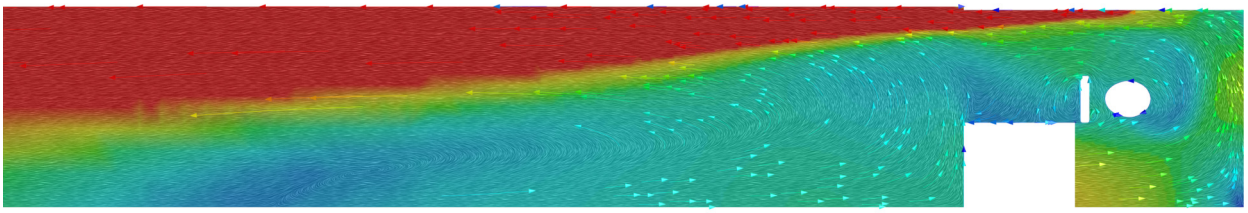

(d) Variant 3

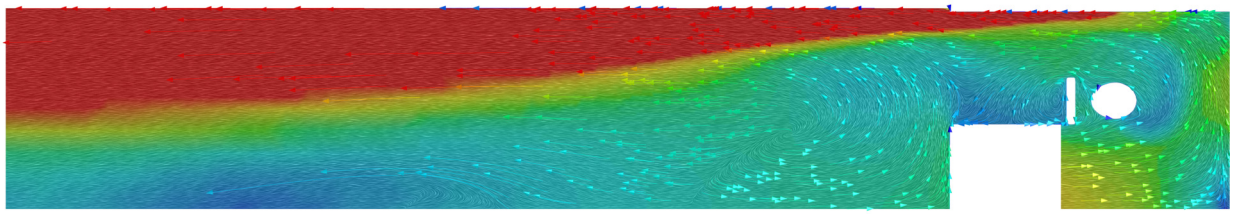

(e) Variant 4

Figure D.15: Z1100 plane of the reference simulation and the different variants

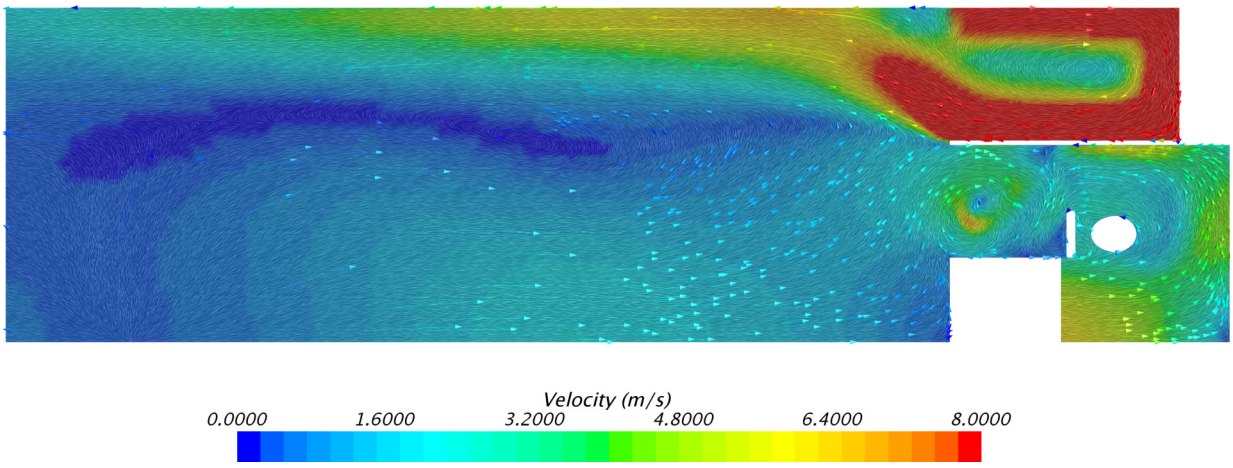

(a) Variant 5

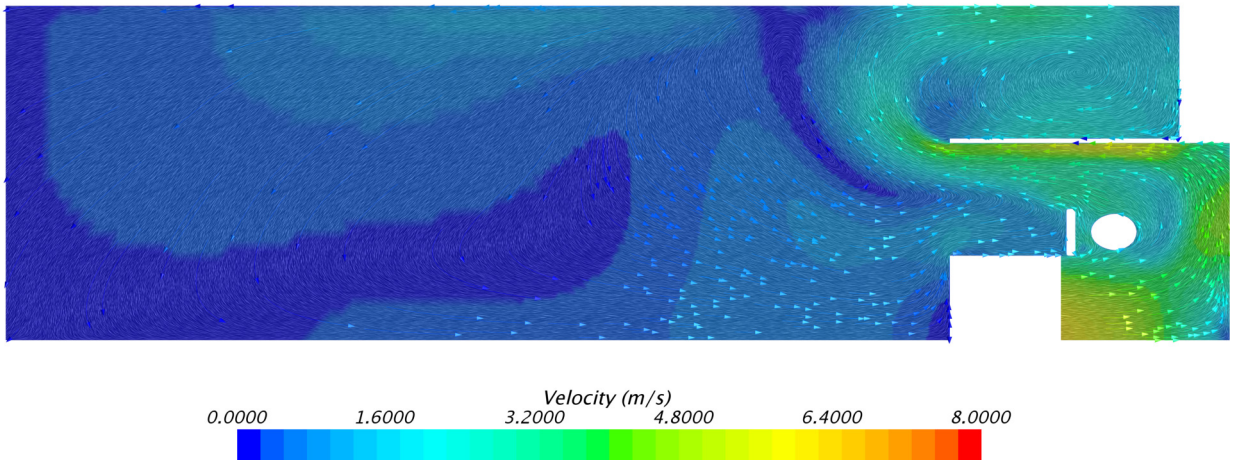

(b) Variant 6

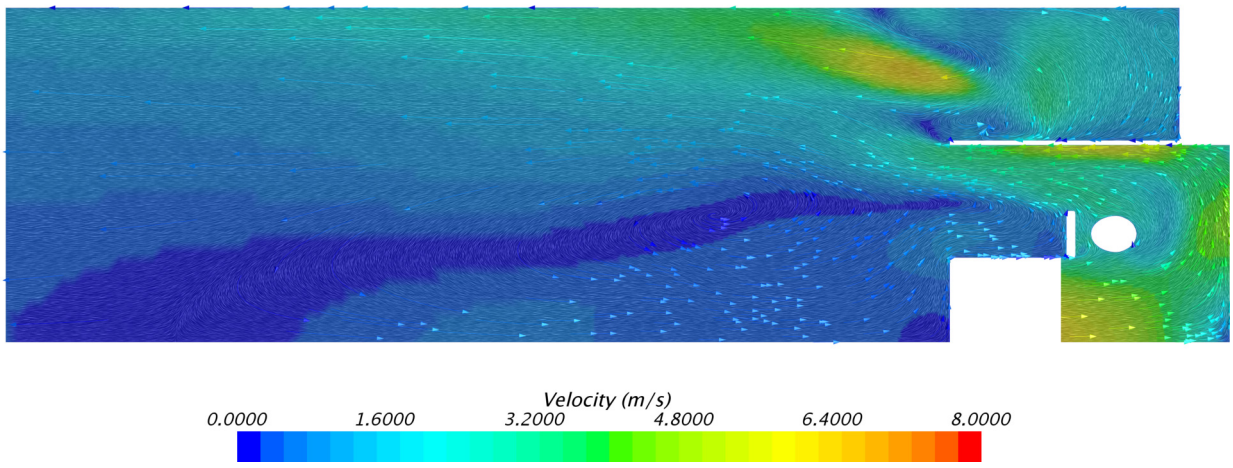

(c) Variant 7

Figure D.16: Z1100 plane of the reference simulation and the different variants